UNIVERSITÀ
DI PAVIA

IUSS

UNIVERSITY OF PAVIA
FACULTY OF ENGINEERING

UNIVERSITY SCHOOL OF ADVANCED STUDIES - IUSS PAVIA

Assessment of the European Ground Motion Service for Landslide Monitoring in the Piemonte Region: A Comparative Analysis with In Situ Monitoring and Multi-Temporal InSAR Datasets

A Thesis Submitted in Partial Fulfilment of the Requirements
for the Degree of Master of Science (Laurea Magistrale) in

Civil Engineering for the Mitigation of Risk from Natural Hazards

by

Mohammad Mahmoodi
Supervisor: Professor Claudia Meisina
Co-supervisor: Laura Pedretti
Co-supervisor: Fraiba Ghalenavi

April, 2026

ABSTRACT

Landslide monitoring plays a crucial role in hazard assessment and risk management, especially in regions like Piemonte, where slope instability is common and affects many different geomorphological environments. In recent years, satellite-based Interferometric Synthetic Aperture Radar (InSAR) has emerged as a valuable method for detecting and measuring small ground deformation across large areas. In this context, the European Ground Motion Service (EGMS) offers a consistent and standardised dataset that creates new possibilities for landslide studies at the regional scale. This thesis evaluates the usefulness of EGMS for slow-moving landslide monitoring in the Piemonte Region by comparing it with in situ monitoring data and historical multi-temporal InSAR datasets.

The research combines landslide inventories, EGMS Calibrated products covering the 2019–2023 period, historical InSAR datasets from earlier satellite missions, and data from GNSS monitoring stations. The analysis first examines how EGMS measurement points are spatially distributed within mapped landslides, with particular focus on landslide type and state of activity. It then explores the kinematic information provided by EGMS through the assessment of mean velocity and measurement point density. To evaluate the reliability of the dataset, EGMS-derived motion is compared with GNSS observations, considering both average velocity and time-series behaviour. An additional comparison with historical InSAR datasets is also performed to assess how consistent the detected deformation patterns remain over time.

The results indicate that EGMS is a valuable source of information for regional landslide analysis, particularly for recognising deformation patterns and supporting the interpretation of ground motion across broad areas. At the same time, its effectiveness is affected by factors such as slope geometry, landslide features, and measurement visibility. Overall, the comparison with in situ monitoring data and historical satellite datasets highlights both the strengths and the limitations of EGMS, confirming its role as a complementary tool for landslide monitoring and regional hazard assessment.

ACKNOWLEDGEMENTS

I would like to express my sincere gratitude to my supervisor, Professor Claudia Meisina, for her invaluable support, guidance, and continuous encouragement throughout my research project. Her constant motivation to think critically and approach challenges with creativity has been deeply appreciated and will remain a lasting source of inspiration.

I would also like to extend my heartfelt thanks to Laura Pedretti for her expertise and thoughtful suggestions. Her knowledge, insightful observations, and patient guidance have played an important role in shaping the direction of this research.

My deepest gratitude goes to my family for their love, prayers, unwavering support, and encouragement throughout my studies. I am equally thankful to my friends, whose enthusiasm and positive feedback have been essential in keeping me motivated along the way.

I sincerely appreciate everyone who supported me throughout this journey.

TABLE OF CONTENTS

ABSTRACT iii
ACKNOWLEDGEMENTS v
TABLE OF CONTENTS vii
LIST OF FIGURES ix
LIST OF TABLES xiii
LIST OF SYMBOLS xvii
1. INTRODUCTION 19
1.1 BACKGROUND 19
1.2 OBJECTIVES 20
1.3 THESIS DESCRIPTION 20
1.4 DATA SOURCE DESCRIPTION 21
2. LITERATURE REVIEW 37
2.1 THE EGMS PRODUCTS AND THEIR CURRENT USE 37
2.2 INSAR DATASET FOR LANDSLIDE INVESTIGATIONS 38
2.3 MULTI-TEMPORAL INSAR FOR REGIONAL-SCALE INTERPRETATION 39
2.4 INTEGRATION WITH IN SITU MONITORING AND INDEPENDENT DATASETS 40
2.5 TIME-SERIES ANALYSIS AND COMPARISON WITH GROUND-BASED MONITORING 40
3. STUDY AREA: PIEMONTE 44
3.1 GENERAL DESCRIPTION 44
3.2 GEOLOGICAL DESCRIPTION 46
3.3 HAZARD DESCRIPTION 46
4. METHODOLOGY 48
4.1 PREPROCESSING 49
4.2 EGMS COVERAGE WITHIN THE LANDSLIDE INVENTORIES 50
4.3 REGIONAL KINEMATIC CHARACTERIZATION THROUGH MEAN VLOS 50

4.4 SELECTION OF THE SUBSET FOR GNSS COMPARISON 51
4.5 DERIVATION OF C-INDEX AND VSLOPE 52
4.6 COMPARISON BETWEEN EGMS AND GNSS 53
4.7 COMPARISON BETWEEN EGMS AND HISTORICAL INSAR DATASETS 53
5. RESULTS 55
5.1 DISTRIBUTION OF LANDSLIDES CONTAINING MPS BY STATE OF ACTIVITY FROM THE PAI INVENTORY 55
5.2 DISTRIBUTION OF LANDSLIDES CONTAINING MP BY TYPOLOGY 60
5.3 DISTRIBUTION OF THE MEAN VLOS IN THE PAI DATA 63
5.4 ANALYSIS OF LANDSLIDE DISTRIBUTION BY ABSOLUTE MEAN VLOS CLASSES 67
5.5 COMPARISON BETWEEN MEAN VELOCITY OF EGMS AND GNSS 86
5.6 COMPARISON BETWEEN EGMS AND OTHER INSAR DATASETS 109
5.7 TIME-SERIES COMPARISON BETWEEN EGMS AND GNSS 118
6. SUMMARY OF RESULTS AND CONCLUSIONS 123
REFERENCES 127

LIST OF FIGURES

Figure 1. The coverage of Piemonte by EGMS ascending orbits 22
Figure 2.The coverage of Piemonte by the EGMS descending orbits 22
Figure 3. Map of ERS Ascending InSAR dataset coverage — Piemonte (Italy) 26
Figure 4. Map of ERS Descending InSAR dataset coverage — Piemonte (Italy) 27
Figure 5. Map of RADARSAT Ascending InSAR dataset coverage — Piemonte (Italy) 28
Figure 6. Map of RADARSAT Descending InSAR dataset coverage — Piemonte (Italy) 29
Figure.7 Map of landslides from the PAI Landslide Inventory _ Piemonte 33
Figure 8. Spatial Distribution of In Situ Monitoring Instruments in Piemonte 34
Figure 9.Study Area Map of the Piemonte Region with the Four Selected Sub-Areas 45
Figure 10. Methodological workflow of the study 48
Figure 11. Distribution of Landslides with MP by Orbit and State of Activity across ALPI 56
Figure 12. Distribution of Landslides with MP by Orbit and State of Activity across Langhe and Monferrato 57
Figure 13. Distribution of Landslides with MP by Orbit and State of Activity across Collina di Torino 59
Figure 14. Distribution of Landslides with PS by Orbit and State of Activity across appennino .59
Figure 15. Histograms of mean VLOS values (2019–2023) for measurement points located within PAI landslides across the Piemonte region 64
Figure 16. Frequency distribution of mean VLOS values (2019–2023) for measurement points within PAI landslides in the Turin Hills sub-area 65
Figure 17. Frequency distribution of mean VLOS values (2019–2023) for measurement points within PAI landslides in the Turin Hills 66
Figure 18. Frequency distribution of mean VLOS values (2019–2023) for measurement points within PAI landslides in the Apennines 66
Figure 19. Frequency distribution of mean VLOS values (2019–2023) for measurement points within PAI landslides in the Apennines 67
Figure 20. Three active very high hazard landslides in Valprato Soana with absolute mean VLOS greater than 16 mm/yr Detected by ascending orbit 088 70

Figure 21. Active very high hazard landslide in Sampeyre with absolute mean VLOS greater than 16 mm/yr Detected by ascending orbit 088 71

Figure 22. Active very high hazard landslides in Cesana Torinese with absolute mean VLOS greater than 16 mm/yr Detected by Descending orbit 066 74

Figure 23. Dormant high hazard landslides in Cesana Torinese with absolute mean VLOS greater than 16 mm/yr Detected by Descending orbit 066 75

Figure 24. Active very high hazard landslides in Sampeyre with absolute mean VLOS greater than 16 mm/yr Detected by Descending orbit 066 76

Figure 25. Absolute Mean VLOS distribution of Landslides covered by Descending orbit 066 in Appennino 78

Figure 26. Absolute Mean VLOS distribution of Landslides covered by Ascending orbit 088 in Appennino 79

Figure 27. Location of stabilised landslides showing absolute mean ascending VLOS greater than 3 mm/year 84

Figure 28. Location of stabilised landslides showing absolute mean descending VLOS greater than 3 mm/year 85

Figure 29. Comparison between Mean Ascending VLOS and GNSS Mean Velocity 88

Figure 30. Comparison between Mean Descending VLOS and GNSS Mean Velocity 89

Figure 31. Comparison between Mean Ascending VSLOPE and GNSS Mean Velocity 90

Figure 32. Comparison between Mean Descending VSLOPE and GNSS Mean Velocity 91

Figure 33. Comparison of GNSS Mean Velocity and EGMS Mean VLOS and VSLOPE at Selected Stations in Valprato Soana 94

Figure 34. Ascending-orbit EGMS slope-parallel displacement time series at G6VPSA3 95

Figure 35. Descending-orbit EGMS slope-parallel displacement time series at G6VPSA3 95

Figure 36.C-index map of the Ascending orbit at Valprato Soana landslide area 96

Figure 37. C-index map of the Descending orbit at Valprato Soana landslide area 97

Figure 38. Digital elevation model of the Valprato Soana landslides area 98

Figure 39. Representative EGMS Ortho displacement time series at Valprato Soana (source: Copernicus European Ground Motion Service, EGMS Explorer) 99

Figure 40. Spatial Distribution of GNSS Stations, EGMS Measurement Points, and Landslide Typologies in the Valprato Soana Case Study 100

Figure 41. Comparison of GNSS Mean Velocity and EGMS Mean VLOS and VSLOPE at Selected Stations in Sampeyre 101

Figure 42. Spatial Distribution of GNSS Stations, EGMS Measurement Points, and Landslide Typologies in the Sampeyre Case Study 102

Figure 43. Comparison of GNSS Mean Velocity and EGMS Mean VLOS and VSLOPE at Selected Stations in Paroldo 103

Figure 44. Spatial Distribution of GNSS Stations, EGMS Measurement Points, and Landslide Typologies in the Paroldo Case Study 104

Figure 45. Comparison of GNSS Mean Velocity and EGMS Mean VLOS and VSLOPE at Selected Stations in Castelmagno 105

Figure 46. Spatial Distribution of GNSS Stations, EGMS Measurement Points, and Landslide Typologies in the Castelmagno Case Study 106

Figure 47. Comparison of GNSS Mean Velocity and EGMS Mean VLOS and VSLOPE at Selected Stations in Prunetto 107

Figure 48. Spatial Distribution of GNSS Stations, EGMS Measurement Points, and Landslide Typologies in the Prunetto Case Study 108

Figure 49. The legend of the graphs 109

Figure 50. Mean VLOS of Ascending InSAR datasets for landslide 001-02042-04 111

Figure 51. Mean VLOS of Descending InSAR datasets for landslide 001-02042-04 111

Figure 52. Mean VLOS of Ascending InSAR datasets for landslide 004-60273-00 113

Figure 53. Mean VLOS of Descending InSAR datasets for landslide 001-02042-04 113

Figure 54. Mean VLOS of Ascending InSAR datasets for landslide 004-20283-01 115

Figure 55. Mean VLOS of Descending InSAR datasets for landslide 004-20283-01 115

Figure 56. Mean VLOS of Ascending InSAR datasets for landslide 004-00061-04 117

Figure 57. Mean VLOS of Descending InSAR datasets for landslide 004-00061-04 117

Figure 58. Time-series comparison between GNSS and ascending EGMS displacement at benchmark G6VPSA1, Valprato Soan 120

Figure 59. Time-series comparison between GNSS and ascending EGMS displacement at benchmark G6VPSA2, Valprato Soan 120

Figure 60. Time-series comparison between GNSS and descending EGMS displacement at benchmark G6VPSA2, Valprato Soan 121

Figure 61. Time-series comparison between GNSS and ascending EGMS displacement at benchmark G6VPSA3, Valprato Soan 121

Figure 62. Time-series comparison between GNSS and descending EGMS displacement at benchmark G6VPSA3, Valprato Soan 122

Figure 63. Time-series comparison between GNSS and ascending EGMS displacement at benchmark G6VPSA5, Valprato Soan 122

LIST OF TABLES

Table 1. Overview of the SAR datasets used in this thesis 25

Table 2.Landslide typologies for IFFI inventory 35

Table 3. Landslide state of activity for PAI inventory 35

Table 4. Distribution of landslides monitored by in situ instruments according to monitoring system 36

Table 5. Distribution of monitored landslides by state of activity (PAI Inventory) 36

Table 6. Distribution of landslides covered by different orbits in the Alps by order of state of activity 56

Table 7. Distribution of landslides covered by different orbits in the Langhe and Monferrato by order of state of activity 58

Table 8. Distribution of landslides covered by different orbits in the Turin Hills by order of state of activity 59

Table 9. Distribution of landslides covered by different orbits in the Apennines by order of state of activity 60

Table 10. Distribution of landslides containing EGMS measurement points by typology in the Alps sub-area 61

Table 11. Distribution of landslides containing EGMS measurement points by typology in the Langhe and Monferrato 61

Table 12. Distribution of landslides containing EGMS measurement points by typology in the Turin Hills 62

Table 13. Distribution of landslides containing EGMS measurement points by typology in the Apennines 63

Table 14. Absolute Mean VLOS distribution of landslides in Alpi covered by ascending orbit 088 68

Table 15. the main attributes reported by PAI of the four landslides with absolute mean VLOS greater than 16 mm/yr in the Alps sector covered by ascending orbit 088 69

Table 16. Absolute Mean VLOS distribution of landslides in Alpi covered by Descending orbit 066 73

Table 17. the main attributes reported by PAI of the four landslides with absolute mean VLOS greater than 16 mm/yr in the Alps sector covered by descending orbit 066 73

Table 18. Absolute Mean VLOS distribution of landslides in Appennino covered by Descending orbit 066 77

Table 19. Absolute Mean VLOS distribution of landslides in Appennino covered by Ascending orbit 088 78

Table 20. Absolute Mean VLOS distribution of landslides in Langhe E Monferrato covered by Descending orbit 066 80

Table 21. Absolute Mean VLOS distribution of landslides in Langhe E Monferrato covered by Ascending orbit 088 80

Table 22. Absolute Mean VLOS distribution of landslides in Collina di Torino covered by Descending orbit 066 81

Table 23. Absolute Mean VLOS distribution of landslides in Collina di Torino covered by Ascending orbit 088 82

Table 24. Stabilised landslides detected by the ascending orbit with absolute mean VLOS greater than 3 mm/year by sub-area 82

Table 25. Stabilised landslides detected by the descending orbit with absolute mean VLOS greater than 3 mm/year by sub-area 83

Table 26. Distribution of the 62 selected landslides by visibility class in the descending orbit 87

Table 27. Distribution of the 62 selected landslides by visibility class in the ascending orbit 87

Table 28. Descending-orbit cases with very low VSLOPE values relative to GNSS mean velocity 91

Table 29. Descending-orbit cases with very high VSLOPE values relative to GNSS mean velocity 92

Table 30. Ascending-orbit cases with very high VSLOPE values relative to GNSS mean velocity 92

Table 31. Ascending-orbit cases with very low VSLOPE values relative to GNSS mean velocity 92

Table 32. number of MPs and Mean VLOS of InSAR datasets for landslide 001-02042-04 110

Table 33. number of MPs and Mean VLOS of InSAR datasets for landslide 004-60273-00 112

Table 34. number of MPs and Mean VLOS of InSAR datasets for landslide 004-20283-01 114

Table 35. number of MPs and Mean VLOS of InSAR datasets for landslide 004-00061-04 116

LIST OF SYMBOLS

S	= Slope of terrain
A	= Aspect of terrain
θ	= Azimuth of satellite
α	= Incidence angle of satellite
RI	= Range Index

1.INTRODUCTION

1.1 BACKGROUND

Landslides are one of the most common natural hazards in mountainous and hilly regions, where they can impact communities, transportation systems, and critical infrastructure, often causing major economic damage and, in some cases, loss of life [Solari et al., 2020]. Their occurrence and development are influenced by a mix of geological, geomorphological, hydrological, and climatic conditions, making their monitoring essential for hazard evaluation and effective risk management.

Landslide investigations have traditionally been based on field surveys, geomorphological mapping, and in situ monitoring techniques. Ground-based instruments such as GNSS, inclinometers, extensometers, and piezometers can provide precise and direct data on displacement and slope dynamics, but their coverage is generally limited to specific points or selected locations [Bordoni et al., 2023]. As a result, remote sensing has become an increasingly valuable tool in landslide studies over the past few decades, particularly for analysing large areas, updating landslide inventories, and identifying active zones that may need further field validation [Solari et al., 2020].

Among remote sensing techniques, Interferometric Synthetic Aperture Radar (InSAR) is one of the most commonly used techniques for detecting and measuring ground deformation. Multi-temporal InSAR methods allow researchers to estimate average deformation rates and reconstruct displacement time series for a large number of measurement points, making them highly useful for landslide mapping, characterization, and monitoring [Solari et al., 2020; Pedretti et al., 2023]. Nevertheless, the technique has several important limitations, as it measures displacement only along the satellite's line of sight, and its effectiveness depends on factors such as slope geometry, land cover, coherence conditions, and the rate of movement [Notti et al., 2014; Bonì et al., 2020].

In this context, the European Ground Motion Service (EGMS), based on InSAR technology, provides a valuable resource for evaluating the activity of slow-moving landslides. Through the continuous monitoring of large areas with satellite observations, particularly Sentinel-1 radar data, EGMS makes it possible to detect even very small ground displacements with high precision. This capability is especially important for the

development of early warning systems and the improvement of risk management strategies [Monserrat et al., 2024].

1.2 OBJECTIVES

The aim of this thesis is to assess how effectively InSAR datasets can detect ground movement at regional scale, with a specific focus on the European Ground Motion Service (EGMS) in the Piemonte Region.

The study is intended to understand how useful EGMS can be for landslide monitoring when analysed in relation to other available datasets. In this way, the thesis aims to highlight both the potential and the limitations of EGMS, and to better define its role within regional-scale landslide investigations.

1.3 THESIS DESCRIPTION

This thesis investigates the use of the European Ground Motion Service (EGMS) for landslide monitoring in the Piemonte Region, with the aim of understanding the usefulness of this product in compared with in situ monitoring data and historical InSAR datasets. The base idea is that regional-scale landslide analysis needs observations that are both spatially extensive and consistent, and that EGMS may offer an important contribution in this sense.

The study begins with the regional landslide framework, using the available inventories as the reference basis for the analysis. From there, the EGMS data are examined to see where ground motion is detected within mapped landslides and how the distribution of measurement points changes across different areas and conditions. This makes it possible to evaluate how well the service captures deformation within the regional landslide setting. Also to seek any possible changes in the state of activity that the reginal inventories report in compare with the movement that EGMS MPs velocities shown.

To put the EGMS results into a broader context, they are also compared with historical multi-temporal InSAR datasets from previous satellite missions. This allows the recent deformation patterns observed by EGMS to be considered together with older satellite observations, making it possible to evaluate similarities, differences, and possible changes through time.

The thesis also includes a comparison with in situ monitoring data, especially GNSS measurements where available. This step is important because it provides an independent reference for assessing how consistent the satellite-derived motion is with ground-based observations.

Overall, the thesis provides maps and analyses that summarize where EGMS effectively captures ground movemnt, how confidently the measurements can be interpreted at a regional scale, and how EGMS can be integrated with inventories, other InSAR sources, and GNSS to improve landslide state-of-activity evaluation and regional risk-management applications.

1.4 DATA SOURCE DESCRIPTION

1.4.1.1 European Ground Motion Service

The primary source of data on ground surface deformation for this study is the European Ground Motion Service (EGMS). EGMS provides consistent and spatially continuous measurements of ground motion across Europe, making it ideal for analyzing slow surface deformations at a regional scale.

The analysis uses EGMS Calibrated datasets from 2019 to 2023, incorporating both ascending and descending satellite data to minimize geometric effects and improve spatial coverage of ground motion patterns. These datasets cover the entire Piemonte region, ensuring reliable and homogeneous data for the study. [Figure.1], [Figure.2]

EGMS is part of the Copernicus Programme, which integrates satellite and ground-based data to support scientific research, environmental monitoring, and risk management. The data is generated using Sentinel-1 SAR and Advanced Differential InSAR (A-DInSAR) techniques, providing displacement velocities and time series measurements along the satellite's line of sight. The calibrated data is referenced to a common European frame for better consistency and comparison across regions.

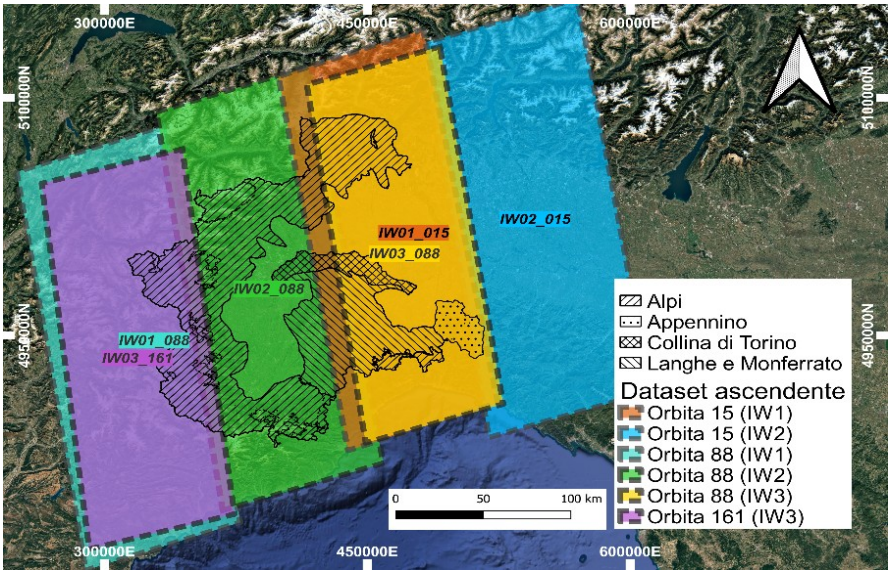

Figure 1. The coverage of Piemonte by EGMS ascending orbits

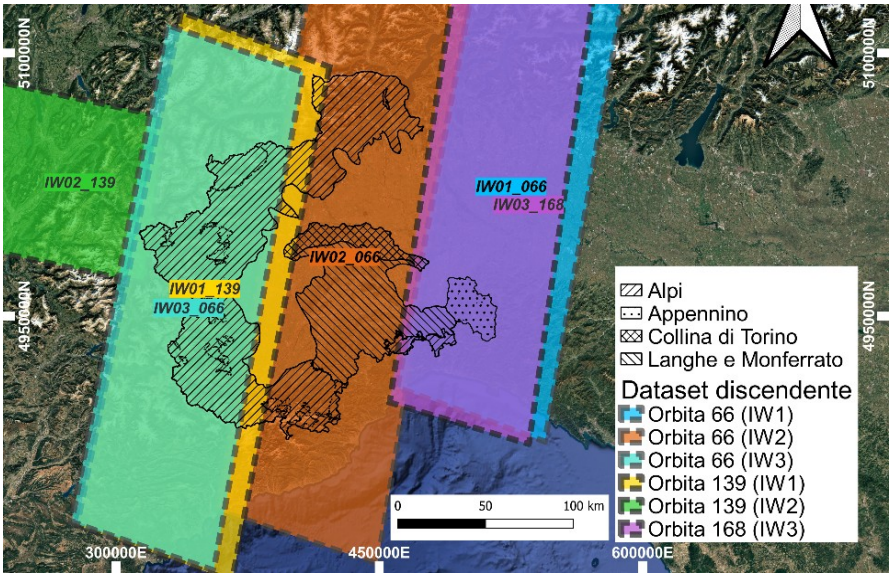

Figure 2.The coverage of Piemonte by the EGMS descending orbits

1.4.1.2 European Remote Sensing

As a complement to the EGMS datasets and existing landslide inventories, historical radar observations from the European Remote Sensing (ERS) missions are also considered. The ERS programme, operated by the European Space Agency, was designed to acquire Synthetic Aperture Radar (SAR) data for Earth surface and environmental monitoring.

ERS SAR data have been widely used to derive interferometric displacement measurements, providing valuable information for reconstructing long-term ground deformation trends. Although these observations refer to earlier periods, they remain particularly useful for interpreting the historical evolution of landslides over extended time spans.

In this study, both ascending and descending ERS datasets are used to analyse ground deformation from different viewing geometries, supporting a more complete interpretation of historical displacement patterns over the study area. [Figure.3]. [Figure.4].

The ERS,dataset used in this study were provided within the framework of an agreement between the Department of Earth and Environmental Sciences, University of Pavia, and ARPA Piemonte.

1.4.1.3 Radarsat

RADARSAT data, developed by the Canadian Space Agency, are included as an additional complementary source of interferometric information. RADARSAT missions were designed to provide reliable SAR observations under all-weather conditions and flexible acquisition geometries, making them suitable for surface deformation and geohazard studies, especially in areas with complex topography.

Their main contribution lies in extending the temporal coverage of deformation analyses and integrating multiple observation geometries. In this study, both ascending and descending RADARSAT datasets are considered to support the interpretation of ground motion patterns from complementary viewing directions. [Figure.5]. [Figure.6].

The RADARSAT dataset used in this study were provided within the framework of an agreement between the Department of Earth and Environmental Sciences, University of Pavia, and ARPA Piemonte.

1.4.1.4 ENVISAT

The ENVISAT mission, operated by the European Space Agency between 2002 and 2012, represents another important source of historical SAR data. ENVISAT carried the Advanced Synthetic Aperture Radar (ASAR) instrument, which supported a wide range of interferometric applications related to land surface deformation.

Despite the end of the mission, ENVISAT ASAR datasets remain a key reference for regional-scale ground deformation studies, including landslide investigations. In this research, both ascending and descending ENVISAT datasets are used to improve the interpretation of deformation patterns through time.

The ENVISAT dataset used in this study were provided within the framework of an agreement between the Department of Earth and Environmental Sciences, University of Pavia, and ARPA Piemonte.

1.4.1.5 SENTINEL-1

The Sentinel-1 mission, part of the Copernicus Earth observation programme, is the primary operational source of SAR data for ground motion monitoring in Europe. Operating in C-band, Sentinel-1 follows a systematic acquisition strategy that ensures consistent spatial coverage and regular revisit times.

Sentinel-1 data are particularly suitable for detecting slow and persistent ground deformation processes over large areas and provide the foundation for several operational services, including the European Ground Motion Service (EGMS).

Sentinel-1 data were made available through an agreement between the Department of Earth and Environmental Sciences, University of Pavia, and Regione Piemonte, within the projects AdVitam (J85C17000120007) and RiskFor (J69F18001670007), covering the period 2019–2020.

1.4.1.6 COSMO-SkyMed

The COSMO-SkyMed constellation, operated by the Italian Space Agency (ASI), provides high-resolution X-band SAR data specifically designed for detailed Earth observation applications. These datasets are particularly well suited for analysing localized ground deformation phenomena affecting urban areas and infrastructure.

Although COSMO-SkyMed coverage is generally limited to selected areas of interest, its high spatial resolution makes it a valuable complementary data source when integrated with wider-coverage radar missions.

The COSMO-SkyMed dataset used in this study were provided within the framework of an agreement between the Department of Earth and Environmental Sciences, University of Pavia, and ARPA Piemonte.

Table 1. Overview of the SAR datasets used in this thesis

Dataset	Observation Period (used in the thesis)	SAR band	Revisit (day)
ERS-1/2	1992–2000	C-band	35
ENVISAT	2002–2010	C-band	35
RADARSAT	2003–2009	C-band	24
COSMO-SkyMed	2011–2014	X-band	16
Sentinel-1	2014–2020	C-band	12 (6 with twin)
EGMS (from Sentinel-1)	2019–2023	C-band	12 (6 with twin)

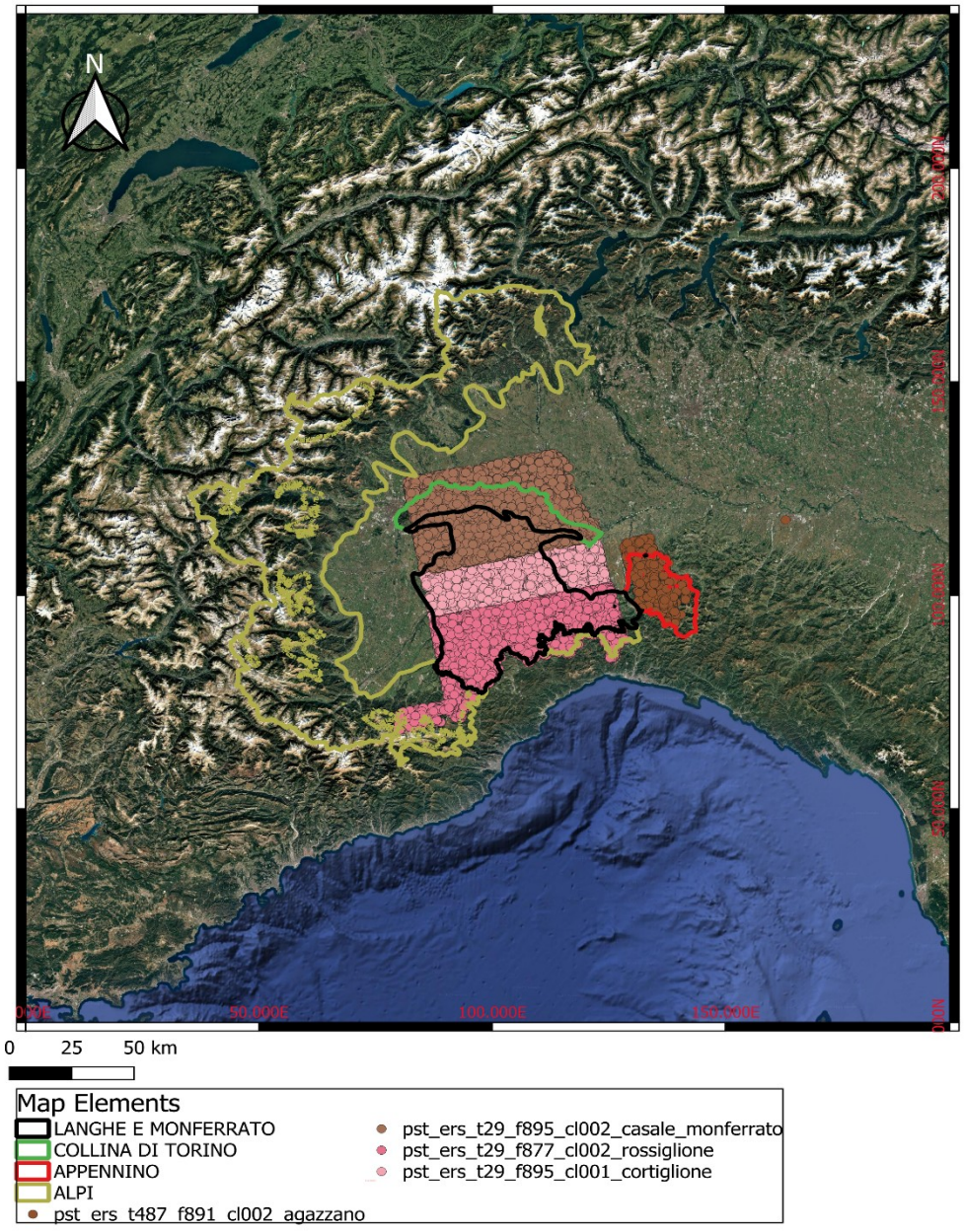

Figure 3. Map of ERS Ascending InSAR dataset coverage — Piemonte (Italy)

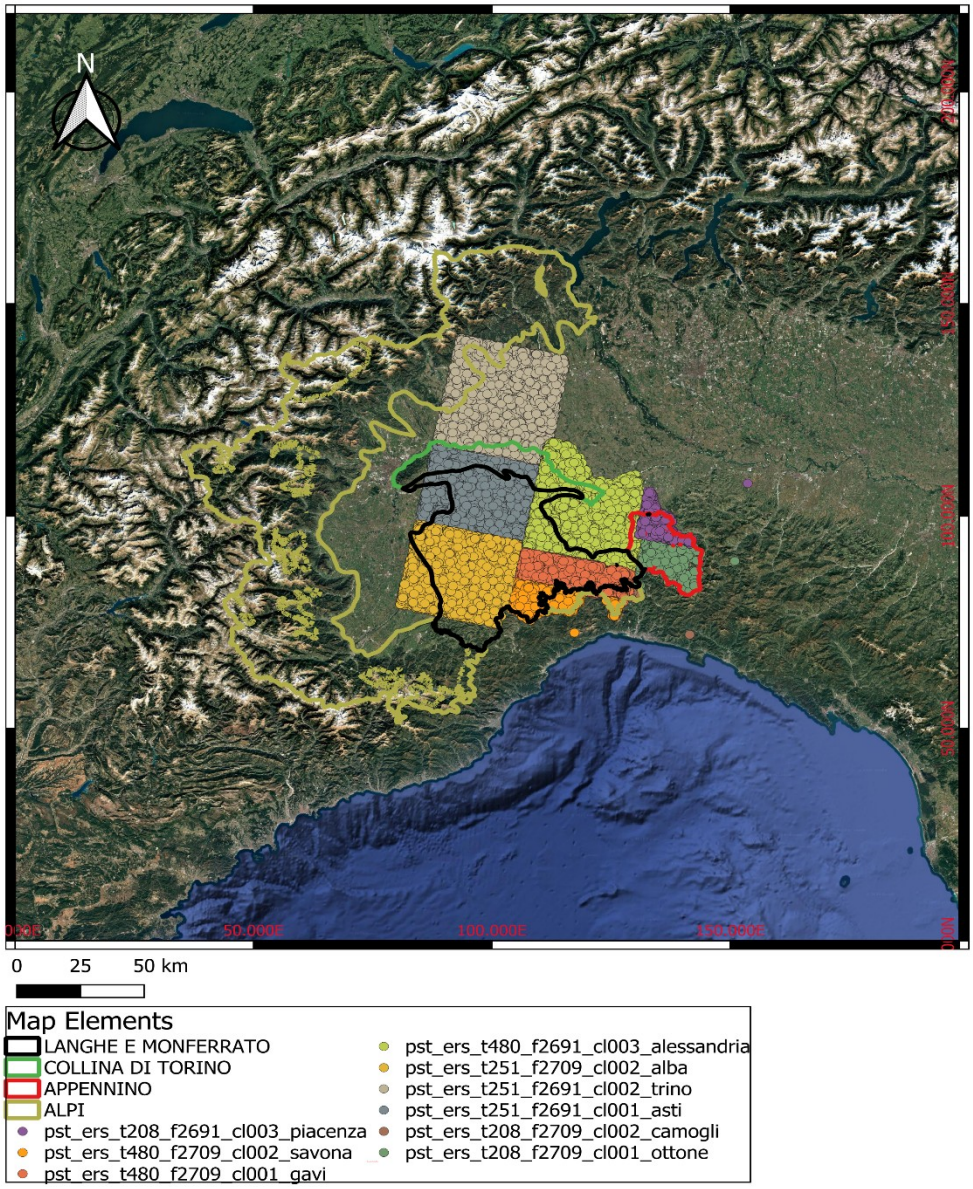

Figure 4. Map of ERS Descending InSAR dataset coverage — Piemonte (Italy)

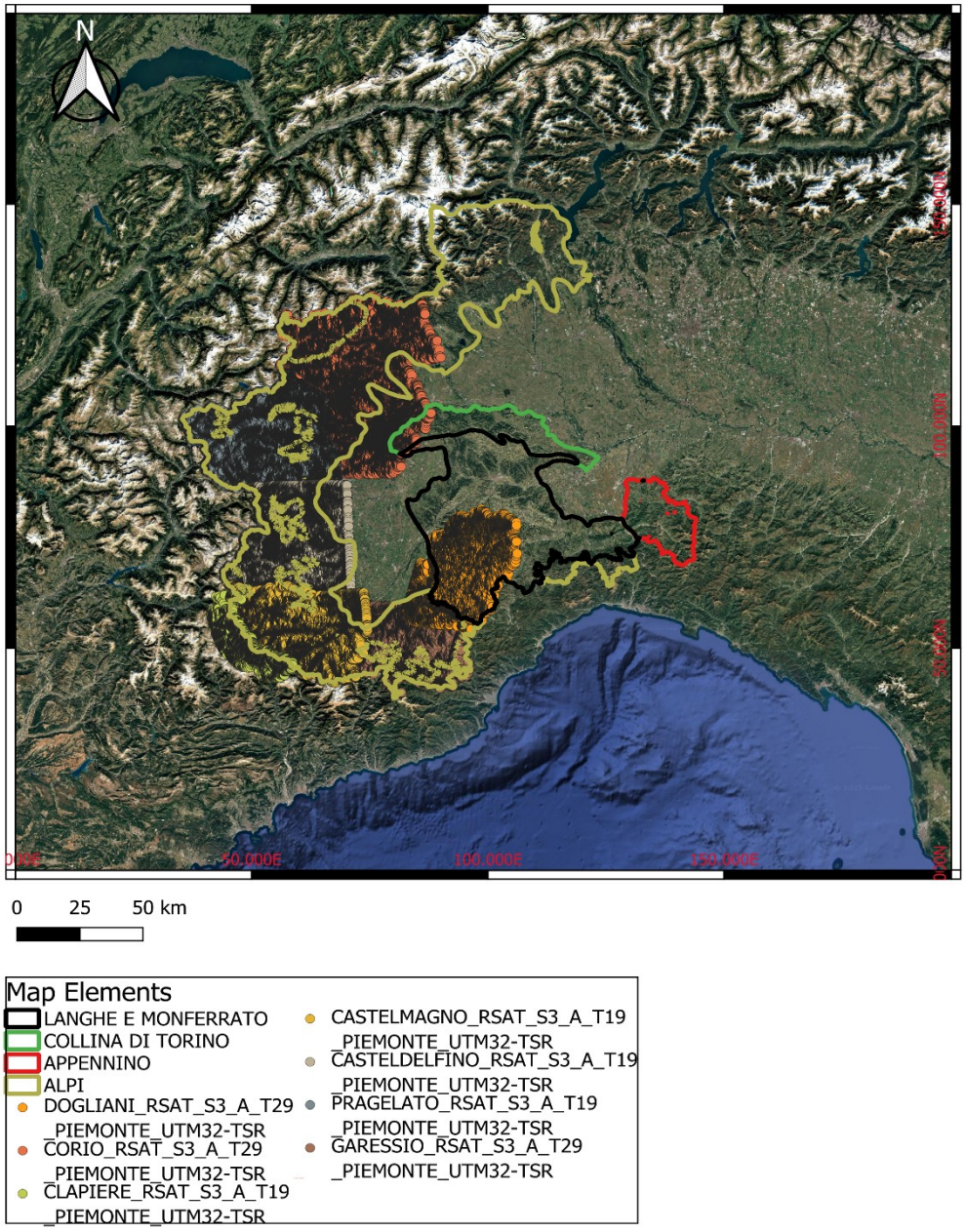

Figure 5. Map of RADARSAT Ascending InSAR dataset coverage — Piemonte (Italy)

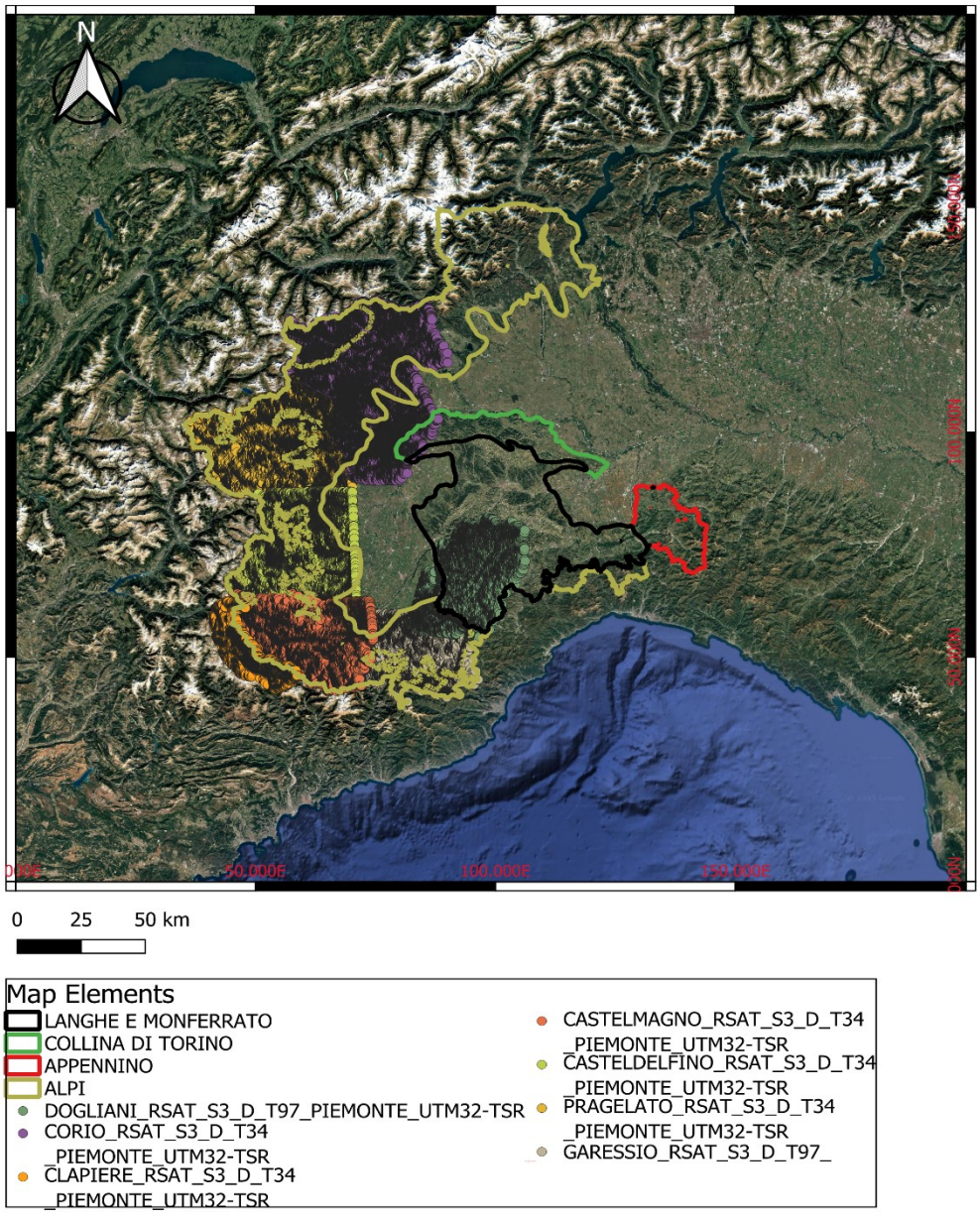

Figure 6. Map of RADARSAT Descending InSAR dataset coverage — Piemonte (Italy)

1.4.1.7 Landslide inventories

In addition to the analysis of interferometric synthetic aperture radar (InSAR) data, it is essential to consider the role of landslide inventories compiled by geological and research institutions. These inventories provide an organized overview of areas affected by slope instabilities and represent the outcome of extensive field surveys, historical analyses and previous investigations.

The primary purpose of such inventories is to establish a consistent reference framework that identifies and delineates known landslide phenomena across the territory. Within the context of this study, these inventories are used to support the interpretation of satellite-derived deformation data and to define the areas of interest for further analysis. The landslide inventories considered in this work include:

SIFraP –Landslide Information System of the Piemonte Region

SIFraP, the Sistema Informativo delle Frane in Piemonte, is the regional landslide inventory created and maintained by Regione Piemonte. It offers a detailed and systematic overview of landslide events across the region and serves as one of the key reference datasets for landslide research at the regional scale.

The inventory brings together information from multiple sources, including field surveys, aerial photograph analysis, remote sensing data, and historical records. It contains spatially referenced details on the location, type, extent, and activity of landslides, which makes it a valuable resource for both scientific studies and land management. Since the database is updated on a regular basis, it can incorporate new observations and revisions resulting from ongoing research and monitoring activities [Regione Piemonte, 2024]; [Bonì et al., 2018].

In this study, the landslide inventory data provided by SIFraP are used for the Piemonte region as a reference framework for the interpretation of satellite-derived ground deformation measurements. The inventory allows the comparison between mapped landslide phenomena and interferometric displacement patterns, supporting the evaluation of landslides by different typologies behaviour [Table.1].

PAI – Hydrogeological Setting Plan

The PAI – Piano di Assetto Idrogeologico is a planning instrument developed within the framework of hydrogeological risk prevention and territorial management in Italy. The PAI

is coordinated at basin scale by the competent basin authorities and implemented at regional level in collaboration with regional administrations, including Regione Piemonte.

The main objective of the PAI is to identify areas exposed to hydrogeological hazards, such as landslides and floods, and to define rules and constraints for land use and development in order to reduce risk to people, infrastructure and economic activities. The plan integrates geomorphological, geological and hydrological information to delineate hazard-prone areas and to support decision-making processes related to territorial planning [Autorità di Bacino del Fiume Po, 2023; ISPRA, 2025].

Within the Piemonte region, the PAI represents a key reference framework for the management of landslide hazard, as it includes mapped landslide-prone areas and hazard classifications derived from existing inventories and technical studies. The PAI is closely linked to national and regional landslide inventories, such as IFFI and SIFraP, and is commonly used to support civil protection activities, emergency planning and risk mitigation strategies [Bonì et al., 2018; ISPRA, 2025].

In this study, PAI information is treated as supporting background data to help interpret landslide distribution and hazard conditions throughout the Piemonte region. The plan offers an additional point of reference for examining the spatial relationship between the activity state of mapped landslides and observed ground deformation patterns, contributing to a broader contextual understanding of landslide activity [Figure.7], [Table.2].

1.4.1.8 In-situ instruments

In situ monitoring systems provide direct measurements of landslide movement, making them a crucial complement to satellite-based observations. Within the Piemonte regional monitoring framework, surface monitoring relies on topographic benchmarks surveyed with total stations or GPS antennas, while subsurface conditions are typically tracked using instruments such as inclinometers and piezometers. ARPA Piemonte also emphasizes that integrating multiple types of instruments at the same site improves the overall effectiveness of landslide monitoring, although these systems are generally better suited to slow-moving landslides than to rapid early-warning applications [Figure.8].

The PAI inventory analysis indicates that 96 landslides are equipped with in situ monitoring instruments. GNSS/GPS benchmarks are the dominant system, being present on 79 landslides, while 11 landslides are monitored exclusively by inclinometers and 6 landslides by both techniques. This distribution confirms that GNSS/GPS represents the most widespread and most relevant in situ dataset for the purposes of this research [Table.3].

With regard to the state of activity, the monitored subset includes 64 active landslides and 32 dormant landslides, whereas stabilised landslides are absent. This indicates that monitoring efforts are mainly directed towards landslides that still show evidence of movement or remain potentially reactivable [Table.4].

The in-situ instrument datasets used in this study were provided within the framework of an agreement between the Department of Earth and Environmental Sciences, University of Pavia, and ARPA Piemonte.

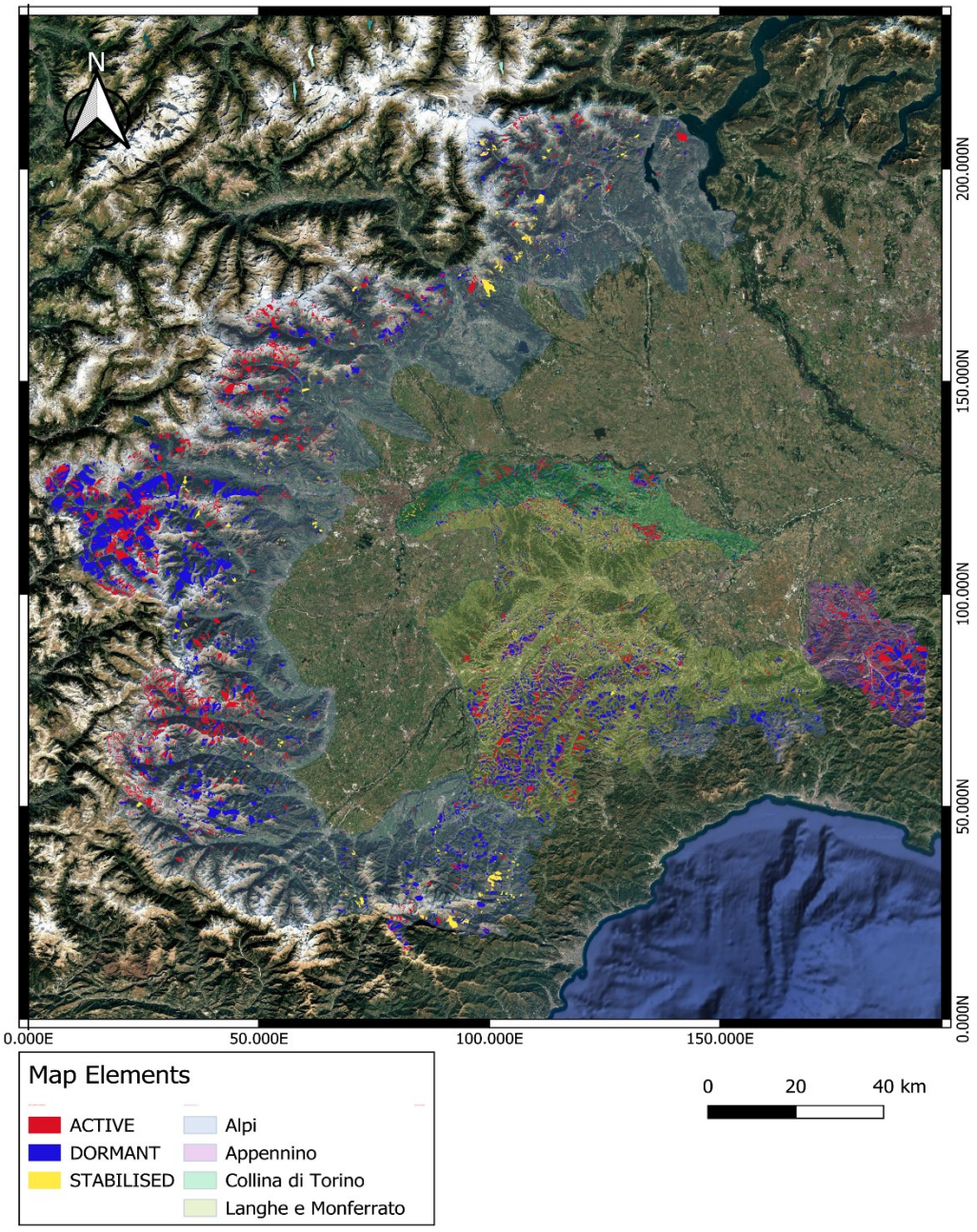

Figure.7 Map of landslides from the PAI Landslide Inventory _ Piemonte

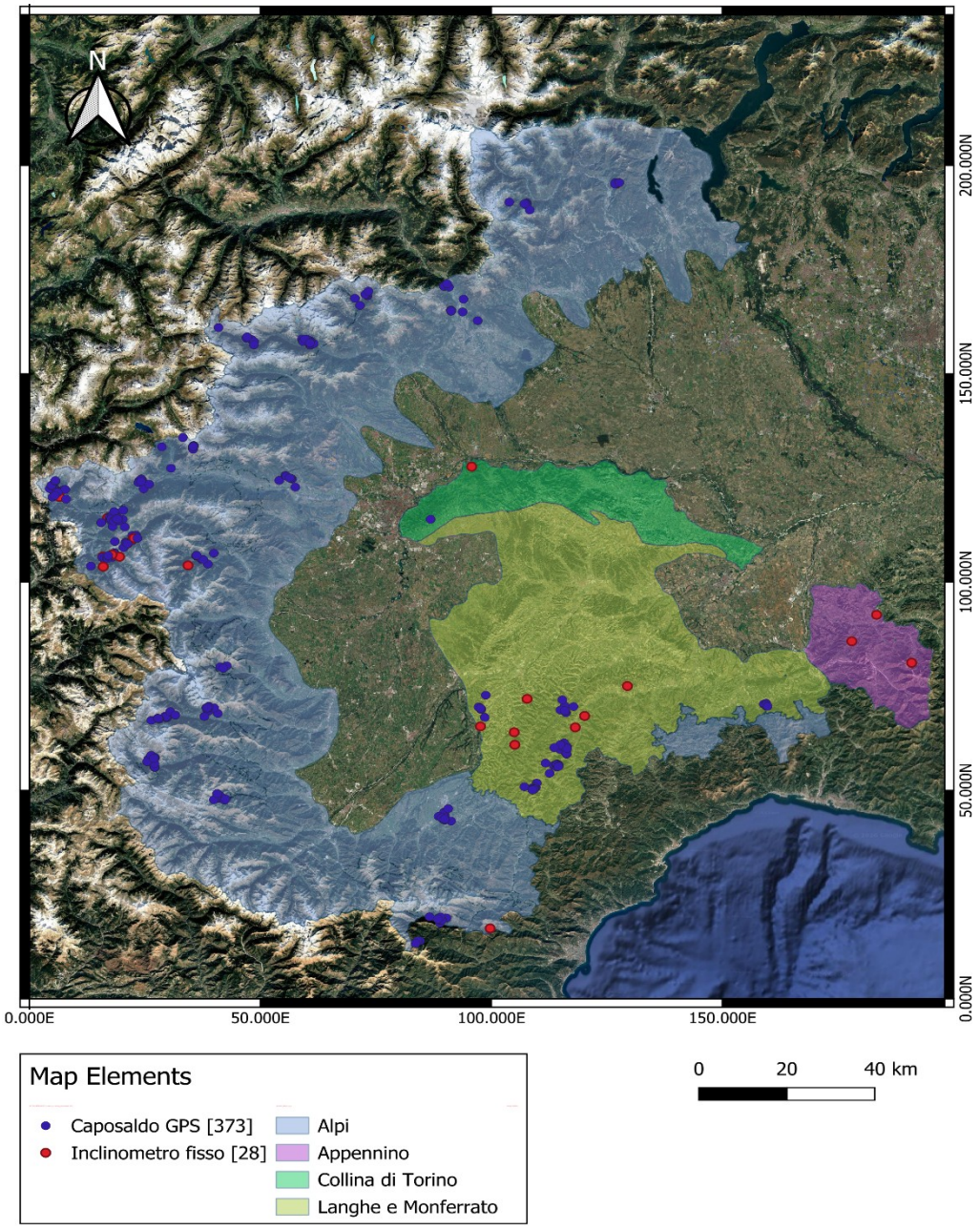

Figure 8. Spatial Distribution of In Situ Monitoring Instruments in Piemonte

Table 2.Landslide typologies for IFFI inventory

Type of landslide	Number of landslides	%
Areas affected by diffuse falls/topples	3596	12,8%
Areas affected by diffuse shallow landslides	5230	18,6%
Areas affected by diffuse sinkholes	5	0,0%
Slow flow	3022	10,7%
Rapid flow	1459	5,2%
Complex landslide	2298	8,2%
Falls/Topples	1184	4,2%
DGPV / DSGSD	468	1,7%
Not determined (N.D.)	1117	4,0%
Rotational/Translational slide	9016	32,0%
CARG sector	741	2,6%
Sinkhole	32	0,1%
Spread / Lateral spread	1	0,004%
Totals	**28169**	**100,0%**

Table 3. Landslide state of activity for PAI inventory

State of activity	Alpine		Appenine		Turin		Langhe and Monferrato		Totals	
		%		%		%		%		%
Active	7418	52,6%	770	49,7%	2667	61,5%	6880	44,0%	17735	49,8%
Dormant	5755	40,8%	778	50,2%	1531	35,3%	8447	54,0%	16511	46,3%
Stabilised	943	6,7%	1	0,1%	137	3,2%	315	2,0%	1396	3,9%
Totals	**14116**	**100,0%**	**1549**	**100,0%**	**4335**	**100,0%**	**15642**	**100,0%**	**35642**	**100,0%**

Table 4. Distribution of landslides monitored by in situ instruments according to monitoring system

Type of monitoring system	number of Landslides monitored by in-situ instruments
GNSS/GPS	79
INCLONOMETER	11
BOTH	6
Totals	**96**

Table 5. Distribution of monitored landslides by state of activity (PAI Inventory)

State of activity	number of monitored landslides
Active	64
Dormant	32
Stabilised	0
Totals	**96**

2.LITERATURE REVIEW

This literature review examines the studies most closely aligned with the objectives of this thesis, particularly the use of the European Ground Motion Service (EGMS) for landslide monitoring and its comparison with in situ observations and historical multi-temporal InSAR datasets.

The review focuses on four main themes, including the characteristics and validation of EGMS products, the use of InSAR for landslide investigations, the value of multi-temporal satellite datasets for regional-scale interpretation, and the role of independent ground-based monitoring in supporting the interpretation of satellite-derived deformation.

2.1 THE EGMS PRODUCTS AND THEIR CURRENT USE

A helpful starting point is the review by Crosetto et al. [2025], which stands as the first studies using EGMS products and identifies the main ways the service has been used. The authors describe how the EGMS archive is structured, explain the differences between the Basic, Calibrated, and Ortho products, and highlight the main trends that emerged in early EGMS-based research. Their review indicates that EGMS is becoming a key resource for large-scale ground motion analysis because it provides standardised, openly accessible deformation data across Europe. At the same time, they stress that the value of the service depends on several factors, including the quality of the measurement points, the product selected, and the interpretation and filtering methods used. By examining examples of individual point time series, the authors also show that point quality is not uniform across the archive, and that lower temporal coherence is often associated with noisier and more scattered time-series patterns.

A more targeted assessment of the products themselves is provided by Vradi et al. [2023], who investigated the validation of EGMS measurement point density and spatial coverage. Their study considered twelve validation sites across Europe, covering both urban and rural settings and including all four EGMS processing entities. The authors analysed how point density varies among land-cover classes and assessed several quality parameters linked to EGMS time series, such as temporal coherence, RMSE, and amplitude dispersion. They

also addressed a preprocessing challenge that is common in EGMS full-resolution products, namely the presence of overlapping bursts from different Sentinel-1 tracks, and introduced a custom algorithm to identify unique non-overlapping burst polygons. Their findings show that the practical value of EGMS depends not only on whether measurement points are present, but also on how spatially consistent they are and on the reliability of their associated quality indicators.

A more local-scale example is provided by Cuervas-Mons et al. [2024], who evaluated the potential and limitations of EGMS for landslide studies in Asturias, Spain. Their research combined EGMS-derived motion data with a geomorphological map, a local inventory of landslide-related infrastructure damage, and rainfall time series. In this case, the authors did not examine EGMS as an abstract product, but as a practical source of information for interpreting slope instability in areas where no direct in situ monitoring was available. Their results showed that EGMS can help identify deformation patterns and support landslide analysis, but they also highlighted that interpretation becomes less robust in areas with limited measurement point coverage or where the detected deformation cannot be confirmed by external evidence.

2.2 InSAR DATASET FOR LANDSLIDE INVESTIGATIONS

A broader picture of the role of InSAR in landslide research is offered by Solari et al. [2020], who reviewed more than 250 papers on satellite interferometry for landslide detection in Italy. Their analysis grouped the existing studies according to their main applications, including back-analysis, characterization, mapping, inventory updating, and monitoring. The review found that most studies used InSAR mainly for landslide characterization and mapping, while relatively fewer focused on continuous monitoring. Another important result is that a large proportion of the reviewed studies validated their interferometric findings using field data or other remote sensing sources. This is particularly relevant to the present thesis because it confirms that, in landslide research, satellite-derived deformation is rarely interpreted in isolation and is usually assessed together with independent sources of information.

This methodological framework was further developed by Bonì et al. [2020] through the ALFA methodology, which was designed to evaluate the feasibility of Sentinel-1 data for large-scale landslide monitoring. The authors applied the method to the Alpine sector of Piemonte, covering an area of about 5300 km² affected by thousands of mapped landslides. Their workflow was divided into two stages. In the pre-processing stage, they assessed visibility and land-cover suitability to predict where Sentinel-1 measurement points were likely to occur. In the post-processing stage, they analysed the actual distribution of measurement points within mapped landslides and introduced a homogeneity index to account for how those points are distributed across the landslide body. This study is

particularly relevant because it goes beyond simply asking whether Sentinel-1 data are available, and instead evaluates whether those data are truly suitable for landslide interpretation at a regional scale.

In this context, Del Soldato et al. (2021) stress the importance of evaluating data feasibility and reliability before interpreting InSAR results at regional scale. Their work introduces practical criteria such as visibility conditions, measurement point density, and uncertainty indicators, which allow the identification of areas where InSAR observations can be considered reliable and where caution is required.

Taken together, these contributions show that while A-DInSAR represents a powerful tool for landslide monitoring, its application to landslide activity assessment must be supported by a preliminary evaluation of data quality and by an awareness of the intrinsic limitations of the technique.

2.3 MULTI-TEMPORAL INSAR FOR REGIONAL-SCALE INTERPRETATION

The importance of combining datasets acquired during different time periods is clearly demonstrated by Bonì et al. [2018], who developed the LAMBDA methodology to update landslide state-of-activity maps in Piemonte using ERS-1/2, Radarsat, and COSMO-SkyMed data. Their work projected LOS velocity into VSLOPE, defined representative landslide velocities, and implemented a multi-temporal activity matrix to update the activity state of mapped landslides. They also introduced a confidence degree assessment based on measurement point distribution and movement variability. The main contribution of this study is that it shows how historical and more recent A-DInSAR datasets can be combined to reconstruct landslide behaviour over different observation periods. Although the present thesis does not specifically focus on state-of-activity mapping, this paper is important because it demonstrates the value of a comparative, multi-temporal approach in the Piemonte region.

A similar multi-temporal perspective is presented in the work of Confuorto et al. [2023], who used Sentinel-1 P-SBAS data to update the state of activity of the Italian national landslide inventory. In their study, older inventory information and previous Envisat data were compared with more recent Sentinel-1 results. The authors used VSLOPE as the main kinematic variable and introduced a reliability matrix based on measurement point density and the variability of representative landslide velocity. This paper is particularly useful because it shows how recent Sentinel-1 datasets can be incorporated into a national-scale interpretation framework, while also emphasising the importance of assessing data reliability when updating landslide information.

Pedretti et al. [2023] contributed another important aspect to this type of analysis by focusing on displacement time series rather than relying only on average velocity values. Through the ONtheMOVE methodology, they classified Sentinel-1 time series as linear, non-linear, or uncorrelated, and identified significant deformation events by estimating their beginning, end, duration, and cumulative displacement. The method was tested in the Alpine and Apennine sectors of Piemonte and validated against in situ measurements, rainfall, snow conditions, and previously documented events. This study is particularly relevant because it shows that regional-scale InSAR datasets can be used not only to locate moving areas, but also to interpret how deformation evolves over time.

2.4 INTEGRATION WITH IN SITU MONITORING AND INDEPENDENT DATASETS

The importance of integrating satellite observations with ground-based monitoring is clearly illustrated by Nikolakopoulos et al. [2023], who combined UAV surveys, GNSS measurements, and archived PSI data from EGMS to analyse a landslide in Western Greece. In their study, repeated UAV campaigns and GNSS surveys were used to monitor recent deformation in detail, while archived EGMS PSI measurements were used to extend the observation period further back in time. Their results showed that archived PSI data are useful for identifying broader and earlier deformation patterns, whereas GNSS and UAV observations are more effective for local-scale validation and detailed monitoring. This paper is relevant to the present thesis because it demonstrates that satellite and in situ measurements do not provide the same type of information, but rather complement one another when integrated within a single analysis.

2.5 TIME-SERIES ANALYSIS AND COMPARISON WITH GROUND-BASED MONITORING

In addition to average velocity values, several studies have highlighted the importance of analysing deformation time series in order to better understand the temporal behaviour of slope movements. Pedretti et al. [2023] developed the ONtheMOVE methodology to classify Sentinel-1 displacement time series and to identify significant non-linear events by estimating their beginning, end, duration, and cumulative displacement. Their work showed that time-series analysis can provide information that is not visible from average velocities alone, especially when deformation behaviour changes through time.

A more direct comparison with ground-based monitoring is presented by Meisina et al. [2018], who analysed large Alpine landslides in Piemonte using A-DInSAR and compared satellite-derived time series with GPS observations. In the Brenvetto case, the paper reports that both the spatial distribution of movement and the temporal evolution recorded by satellite data were in good agreement with GPS measurements. The study therefore showed

that, where a sufficient number of measurement points is available, satellite time series can effectively support the interpretation of landslide behaviour through time.

3.STUDY AREA: PIEMONTE

3.1 GENERAL DESCRIPTION

The Piemonte region is located in north-western Italy and extends over an area of approximately 25,000 km². Considering previous regional-scale studies on landslide processes and ground deformation in north-western Italy, the region is characterized by a complex morphostructural setting that results in pronounced topographic and environmental variability.

For the purposes of this study, the territory of Piemonte is subdivided into four main sub-areas: the Alpine sector (Alpi), the Apennine sector (Appennino), the Collina di Torino, and the Langhe e Monferrato hills. This subdivision follows the main physiographic domains of the region and is consistent with the spatial frameworks adopted in previous investigations carried out in Piemonte and surrounding areas [Bonì et al., 2018; Solari et al., 2020].

The Alpine sector occupies the northern and western portions of Piemonte and is characterized by high relief energy, with elevations locally exceeding 4,000 m a.s.l. The Apennine sector, located in the southern part of the region, presents lower elevations but steep and deeply incised hillslopes. The Collina di Torino forms a hilly relief separating the Alpine domain from the Po Plain, while the Langhe e Monferrato area is characterized by wide hilly landscapes with gentler slopes and widespread slope instabilities.

Overall, this subdivision reflects not only morphological differences, but also distinct geological, geomorphological and landslide characteristics. In line with the regional frameworks proposed in the literature, this heterogeneity makes Piemonte a suitable area for investigating slow-moving landslides across different environmental settings [Bonì et al., 2018; Solari et al., 2020].

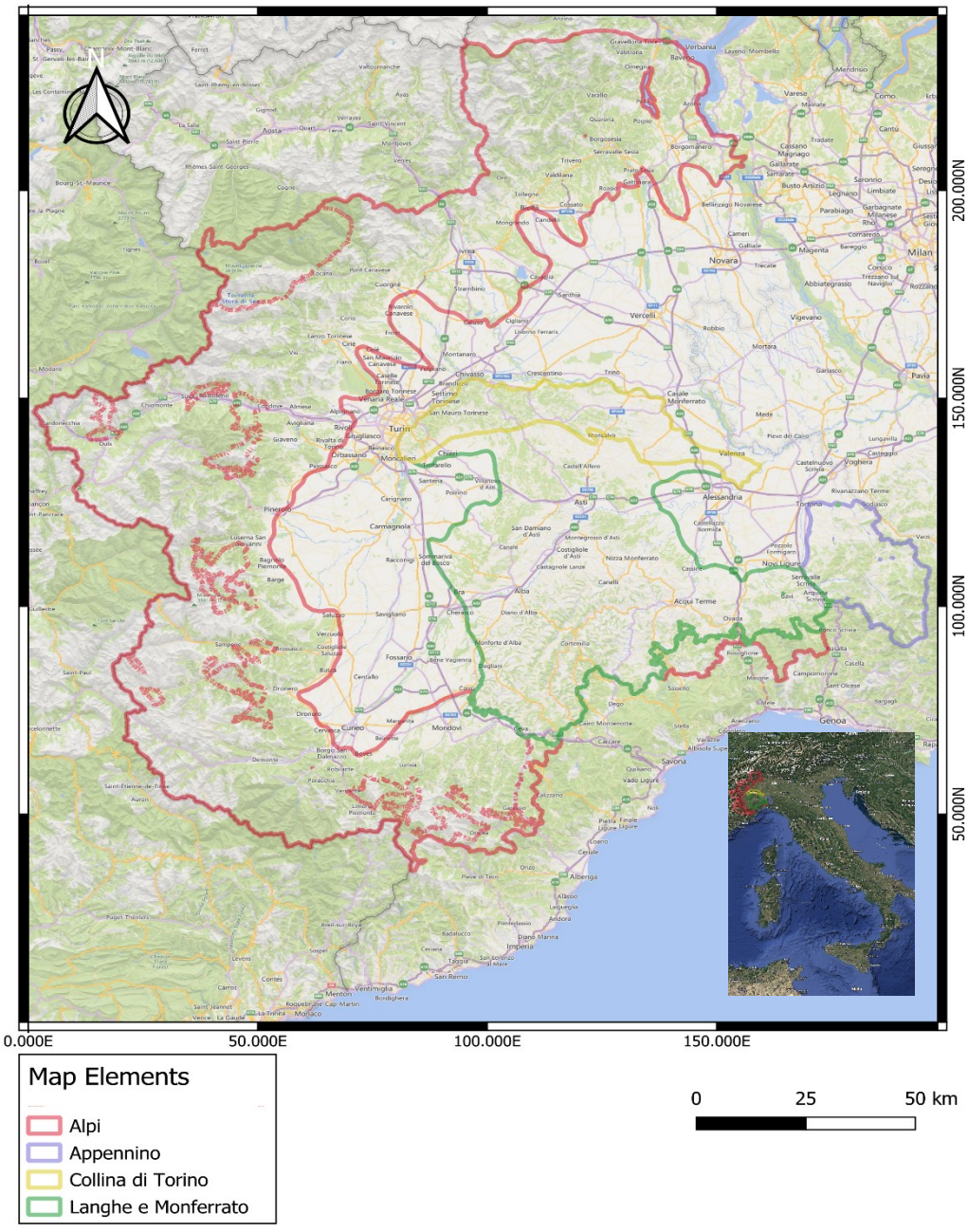

Figure 9.Study Area Map of the Piemonte Region with the Four Selected Sub-Areas

3.2 GEOLOGICAL DESCRIPTION

Considering the regional-scale geomorphological frameworks described in previous studies, the Piemonte region is characterized by a highly variable landscape shaped by the interaction between tectonic activity, long-term erosion processes, and fluvial dynamics [Solari et al., 2020].

The geomorphology of the region is strongly controlled by elevation gradients, which range from high-relief mountainous areas to lowland plains. The Alpine sector is dominated by steep slopes, narrow valleys and pronounced relief energy, resulting from glacial and fluvial processes that have shaped the landscape over time. In contrast, the Apennine sector is characterized by elongated ridges and deeply incised hillslopes, where erosional processes play a key role in defining the present-day morphology [Bonì et al., 2018], [Figure 1.8].

The hilly domains, including the Collina di Torino and the Langhe e Monferrato areas, show smoother relief compared to the mountainous sectors, but still present significant slope gradients and widespread surface processes. These areas are characterized by rolling hills, asymmetric valleys and slope systems that reflect the combined influence of lithological contrasts and fluvial incision.

The lowland areas associated with the Po Plain are characterized by very gentle slopes and extensive flat surfaces shaped by fluvial deposition and channel migration. These geomorphological conditions create a clear contrast with the surrounding hilly and mountainous environments, contributing to the strong spatial variability observed across the Piemonte region [Solari et al., 2020].

Overall, the geomorphological setting of Piemonte reflects the coexistence of multiple landform systems within a relatively limited area, resulting in a complex and heterogeneous landscape consistent with the regional descriptions provided in the existing literature [Bonì et al., 2018; Solari et al., 2020].

3.3 HAZARD DESCRIPTION

The Piemonte region, characterized by a combination of mountainous, hilly and lowland environments, as well as a complex geological and geomorphological framework, is affected by a wide range of natural hazards. The interaction between geomorphological conditions, land use and climatic factors plays a key role in controlling the occurrence and intensity of hazardous phenomena such as landslides, floods, soil erosion and extreme meteorological events [Solari et al., 2020].

Among these hazards, landslides represent one of the most widespread and relevant processes across the region. Regional-scale studies highlight that different landslide typologies are distributed throughout Piemonte, with slow-moving landslides being particularly common in both hilly and mountainous sectors. These phenomena are often associated with heterogeneous geological settings, where alternating lithologies and structural discontinuities favour slope instability [Bonì et al., 2018; Bonì et al., 2020].

Slow-moving landslides in Piemonte typically show a gradual evolution over time, with displacement rates that may vary over seasonal or multi-annual time scales. Several studies report that these landslides can experience phases of acceleration or reactivation, often in response to external forcing factors such as prolonged or intense rainfall events [Confuorto et al., 2023]. Rainfall infiltration contributes to an increase in pore water pressure and a reduction in soil shear strength, thereby facilitating slope movement.

In addition to natural factors, human activities can significantly influence landslide hazard in the region. Modifications of the terrain related to agriculture, deforestation, road construction and urban development may alter drainage conditions and stress distribution within slopes, potentially increasing the susceptibility to reactivation of existing landslides [Solari et al., 2020].

Overall, the combination of diverse geomorphological settings, complex geological conditions and variable climatic forcing makes Piemonte particularly prone to landslide-related hazards. This context highlights the importance of a regional-scale understanding of landslide processes as a basis for hazard assessment and land management strategies [Bonì et al., 2018; Confuorto et al., 2023].

4.METHODOLOGY

This chapter describes the methodological workflow adopted to assess the European Ground Motion Service (EGMS) for landslide monitoring in the Piemonte Region through the integration of landslide inventories and comparison with in situ GNSS measurements and historical multi-temporal InSAR datasets. The workflow was organised into four main stages, which are summarised in the workflow diagram [Figure 9].

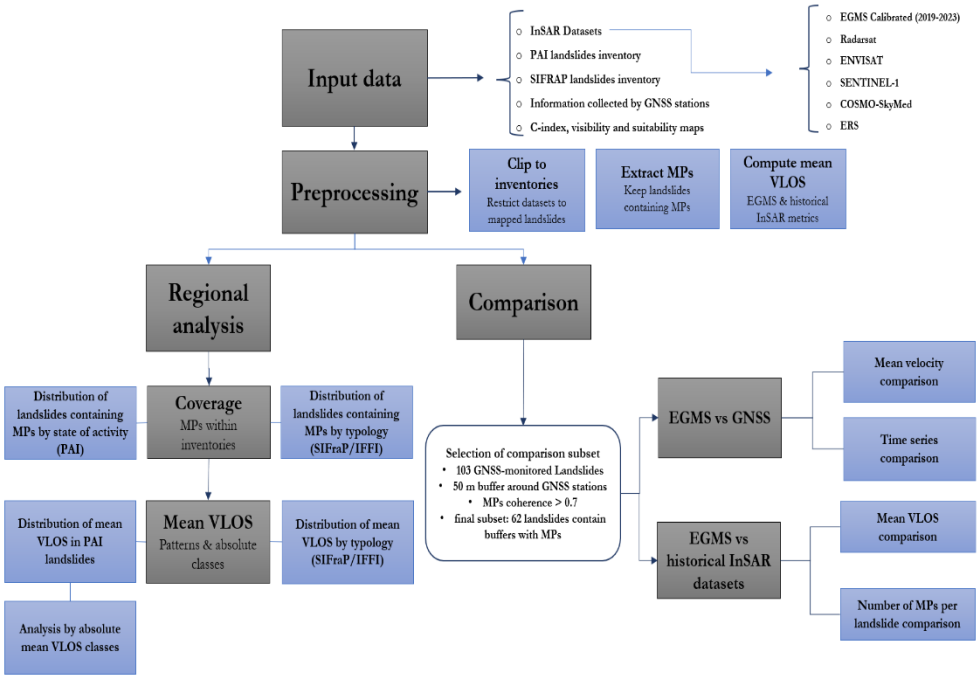

Figure 10. Methodological workflow of the study

4.1 PREPROCESSING

The preprocessing phase was necessary to make all datasets comparable in the same spatial and analytical environment. Since the different datasets came from different sources and had different formats, the first task was to harmonise them in a QGIS environment. This included checking the coordinate reference system and clipping the layers to the Piemonte study area.

Preprocessing of the EGMS datasets began with clipping the ascending and descending point layers to the Piemonte study area, so that only the measurement points located within the area of interest were retained. Ascending and descending datasets were kept distinct because they do not observe the ground from the same direction, and therefore they may capture different components of landslide motion. The preprocessing also included preparing the attribute tables so that the key parameters needed later in the workflow, such as velocity values, orbit information, and point counts, could be extracted and summarised at landslide scale.

Once the datasets had been prepared, they were further clipped to the available landslide inventories in order to analyse only the points located within mapped landslide polygons. The EGMS datasets were intersected with both the PAI and SIFRaP inventories. The PAI inventory was used for the analysis of landslide state of activity, whereas the SIFRaP inventory was used for the analysis of landslide typology.

The historical InSAR datasets, on the other hand, were clipped only to the SIFRaP inventory, as they were used only for the typological and comparative analyses. Finally, the spatial intersection between the measurement points and the landslide polygons was used to quantify the percentage of landslides containing at least one measurement point according to state of activity and typology, and to produce the coverage graphs used in the Results chapter.

For the landslides containing measurement points (MPs), the mean velocity along the satellite line of sight (mean VLOS) was computed. The mean VLOS of the MPs inside a polygon shows the state of the movement of that landslide that will be compared then with the state of activity of the landslides to find any cases that showing differences, stablilised or suspended landslides maybe showing a reactivation phase.

The mean velocity recorded at each GNSS reference point was also calculated for the 2019–2023 period in order to support the subsequent comparison between GNSS and EGMS data.

4.2 EGMS Coverage within the Landslide Inventories

The first analytical step consisted of integrating the EGMS measurement points with the mapped landslides of the Piemonte Region. This operation was carried out by spatially intersecting the EGMS point layers with the polygons of the PAI and SIFRaP inventories. The purpose of this step was to identify which landslides contain at least one EGMS measurement point and therefore can be considered covered by the service.

This operation was necessary because the presence of EGMS measurement points inside a landslide is the basic condition for any further interpretation. Before analysing the deformation signal, it was first necessary to evaluate the spatial coverage of the service within the regional landslide framework. The PAI inventory was used to analyse the distribution of landslides containing measurement points according to state of activity, while the SIFRaP inventory was used to analyse their distribution according to typology.

For each landslide polygon, the number of EGMS measurement points was calculated separately for each orbit. This made it possible to quantify the coverage provided by the different acquisition geometries and to identify the orbits that contributed most strongly to the regional analysis. On the basis of this step, the detailed inventory-based interpretation was focused mainly on the two dominant EGMS geometries, ascending orbit 088 and descending orbit 066, as these provided the widest and most representative coverage in the study area.

4.3 Regional Kinematic Characterization through Mean VLOS

After identifying the landslides containing EGMS measurement points, the next step consisted of characterising the detected deformation at landslide scale. This was done by calculating the mean line-of-sight velocity (mean VLOS) of the EGMS points located inside each landslide polygon. The use of a mean value was preferred because the objective of the study was not to describe isolated point behaviour, but to obtain a synthetic kinematic indicator representative of each mapped landslide.

The mean VLOS values were first analysed at regional scale in order to describe the overall behaviour of the EGMS-detected landslide subset. The same analysis was then repeated within the main sub-areas of Piemonte, so that differences in the distribution of the LOS signal could be examined in relation to the regional physiographic setting. This step produced the histograms and frequency distributions presented in the Results chapter.

A further elaboration consisted of grouping the landslides according to absolute mean VLOS thresholds. This classification was introduced to distinguish the large number of landslides characterised by low LOS motion from the smaller subset showing stronger motion signals. In methodological terms, this operation allowed the analysis to move from a general regional description of velocity distribution to a more targeted identification of landslides affected by more significant deformation. This is why, in the Results chapter, the absolute mean VLOS values were later discussed in terms of threshold classes rather than only as continuous variables.

4.4 SELECTION OF THE SUBSET FOR GNSS COMPARISON

Once the regional inventory-based analysis had been completed, the workflow moved to the validation branch. This phase was aimed at identifying the subset of landslides suitable for a direct comparison between EGMS and in-situ monitoring data. Since GNSS stations provide precise ground-based measurements of surface displacement, they were selected as the reference system for the validation stage.

The selection started from the landslides monitored by GNSS instruments. Around each GNSS station, a 50 m buffer was generated in order to extract the EGMS measurement points located in the immediate surroundings of the monitoring point. This choice was important because the comparison had to be carried out at a local scale around the instrument rather than at the scale of the entire landslide polygon.

In addition, a temporal coherence threshold greater than 0.7 was applied in order to retain EGMS measurement points with more reliable and interpretable time series. This choice is supported by previous studies showing that lower temporal coherence is generally associated with noisier and more dispersed displacement series, which can complicate motion interpretation, especially in localized applications such as landslide analysis (Crosetto et al., 2025). Temporal coherence is also recognised as one of the main quality parameters of EGMS products (Vradi et al., 2023).

More generally, previous InSAR studies have excluded points with coherence below 0.65 and, in some cases, applied stricter thresholds such as >0.75 to reduce noise in landslide investigations (Meisina et al., 2006; Notti et al., 2014). Therefore, the threshold of >0.7 was adopted in this study as a balance between data quality and the need to preserve a sufficient number of points for comparison with GNSS measurements.

By applying these spatial and quality criteria, the original population of GNSS-monitored landslides was reduced to the final subset used in the validation stage. The final comparison subset consisted of 123 GNSS buffers distributed within 62 landslides. This subset was then used for the comparison between EGMS mean velocities and GNSS mean velocities,

as well as for the subsequent selection of representative case studies. The reduction from the initial inventory to this smaller subset is methodologically important because it shows that only part of the regional dataset satisfies the conditions required for a meaningful direct comparison between satellite and ground measurements.

4.5 DERIVATION OF C-INDEX AND VSLOPE

To account for the influence of terrain geometry on InSAR measurements, the C-index and VSLOPE were calculated. The C-index measures the visibility of each landslide based on its slope and the satellite acquisition geometry. The VSLOPE is the conversion of the Line-of-Sight velocity to the actual slope velocity, which provides a more accurate measure of deformation in mountainous regions where slope angles can be steep.

the "C-index" introduced by Notti et al., [2014] can be calculated by the following equation (1.1):

$$C = (nlos * \cos(S) * \sin(A - 1.571)) + \left(elos * (-1 * \cos(S) * \cos(A - 1.571)) + (hlos * \sin(S))\right)$$
$$hlos = \cos(a)$$
$$nlos = \cos(1.571 - a) * \cos(3.142 - \theta)$$
$$elos = \cos(1.571 - a) * \cos(4.712 - \theta)$$

where S and A describe the local terrain geometry, corresponding to slope angle and aspect, while a and θ describe the satellite acquisition geometry, corresponding to the LOS incidence and azimuth angles. The coefficients nlos, elos, and hlos are the north, east, and vertical components of the radar LOS unit vector. Their combination defines the C-index, which represents the proportion of actual downslope displacement that can be detected by InSAR along the satellite Line of Sight.

The velocity along the slope (Vslope) can be calculated with the following equation (1.2):

$$Vslope = Vlos/C$$

This step was necessary because InSAR measures displacement along the satellite Line of Sight, but in steep terrain, the true displacement can differ significantly. The C-index and VSLOPE were used to correct for these geometric effects and improve the accuracy of the deformation measurements.

4.6 COMPARISON BETWEEN EGMS AND GNSS

For each of the selected GNSS buffers, the mean VLOS and mean VSLOPE of the EGMS measurement points were calculated separately for ascending and descending geometries. These values were then compared with the mean velocity measured by the corresponding GNSS station. The GNSS reference value was considered in terms of horizontal ground displacement, expressed as the mean velocity derived from the X and Y components over the common observation period.

The comparison was performed through scatter plots and 1:1 reference lines, which made it possible to evaluate the agreement between the satellite-derived and ground-based measurements. The comparison between mean VLOS and GNSS mean velocity was used to assess how well the LOS measurements captured the presence and relative magnitude of ground deformation. The comparison between mean VSLOPE and GNSS mean velocity was used to evaluate whether the slope projection provided a more realistic representation of landslide motion.

This step was not interpreted only in terms of numerical agreement. Special attention was also given to the number of EGMS measurement points available inside each buffer, because a mean value derived from a single point is less representative than one derived from several observations. For this reason, the comparison was interpreted together with the local point density and the geometric setting of each monitored sector. This approach allowed the most discrepant cases to be identified not simply as outliers, but as situations requiring a more detailed analysis of the local geomorphological and observational conditions.

Considering these points some outlier cases have been analysed more specificly by creating the map to see in which typology they are located and how they show trend with respect to other GNSS reference points may be in their proximity and what is the reason of the remarkably difference that they are showing between EGMS and GNSS.

For further evaluation, the displacement time series derived from the EGMS measurement points within the buffers were compared with the GNSS displacement values at the available observation dates. The aim was to assess the overall trend of deformation and to verify whether possible acceleration phases recorded by GNSS were also captured by EGMS, or whether they may have been missed because of the high movement velocity.

4.7 COMPARISON BETWEEN EGMS AND HISTORICAL INSAR DATASETS

The last step of the analysis was the comparison between EGMS and the historical InSAR datasets. This was carried out for the selected landslides where EGMS and at least one older InSAR dataset were both available within the same landslide polygon. In this way,

the analysis moved beyond the comparison with GNSS and was extended to a broader multi-temporal perspective based on previous satellite observations.

For each dataset and for each acquisition geometry, two parameters were calculated at landslide scale, the number of measurement points and the mean VLOS. The number of points was used to evaluate how well each dataset covered the landslide, while the mean VLOS was used to compare the average deformation detected by the different missions. The same landslide polygons were used for all datasets in order to keep the comparison spatially consistent.

At the same time, the historical InSAR datasets and EGMS cannot be considered directly equivalent. Their comparison must be interpreted carefully, because the datasets differ not only in observation period, but also in radar wavelength, revisit time, and other acquisition characteristics. These differences can affect both the detectability of landslide movement and the way the deformation signal is represented.

For this reason, the comparison was not treated as a direct validation, but rather as a way to place the EGMS results within a longer temporal framework. Where similar deformation patterns were observed, they were interpreted as evidence of persistent movement through time. Where differences emerged, they were considered in relation both to possible changes in landslide behaviour and to the technical differences between the SAR missions.

5. RESULTS

5.1 DISTRIBUTION OF LANDSLIDES CONTAINING MPS BY STATE OF ACTIVITY FROM THE PAI INVENTORY

The first phase of the analysis consisted of integrating the regional PAI (Piano Stralcio per l'Assetto Idrogeologico) landslide inventory with the calibrated EGMS dataset for the period 2019–2023. This procedure made it possible to identify the landslides containing at least one EGMS measurement point (MP) and to analyse their distribution according to the state of activity reported in the PAI inventory within each sub-area.

In the Alps sub-area, active landslides represent the most frequent class in the inventory (52.55%), followed by dormant landslides (40.77%), while stabilised landslides account for a smaller proportion (6.68%). EGMS coverage is mainly concentrated in DES-066 and ASC-088, which account for 35.4% and 34.5% of the covered landslides, respectively, with an additional contribution from DES-139 (22.4%). The same general pattern is observed for the different activity classes, with active and dormant landslides mainly represented in the same geometries. Overall, the Alps show a strong concentration of EGMS coverage in a limited number of dominant orbits, while maintaining a distribution by state of activity that is broadly consistent with the inventory [Figure.11], [Table.6].

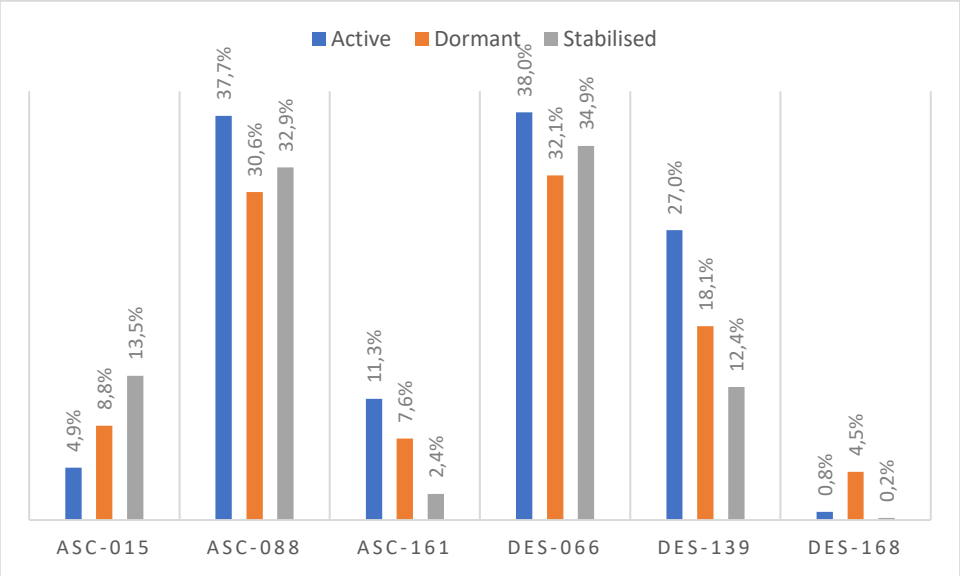

Figure 11. Distribution of Landslides with MP by Orbit and State of Activity across ALPI

Table 6. Distribution of landslides covered by different orbits in the Alps by order of state of activity

State of Activity	Totals	ASC-015		ASC-088		ASC-161		DES-066		DES-139		DES-168	
			%		%		%		%		%		%
Active	7418	362	4,9%	2797	37,7%	838	11,3%	2820	38,0%	2006	27,0%	57	0,8%
Dormant	5755	507	8,8%	1760	30,6%	438	7,6%	1850	32,1%	1040	18,1%	259	4,5%
Stabilised	943	127	13,5%	310	32,9%	23	2,4%	329	34,9%	117	12,4%	2	0,2%
Totals	**14116**	**996**	**7,1%**	**4867**	**34,5%**	**1299**	**9,2%**	**4999**	**35,4%**	**3163**	**22,4%**	**318**	**2,3%**

Although Langhe e Monferrato includes a large number of inventoried landslides, the number of landslides with EGMS measurement points is considerably lower than in the Alpine sector. This suggests that landslide occurrence and InSAR detectability do not necessarily coincide. The difference is likely related to the dominant geomorphological and landslide conditions of the Langhe area, where shallow landslides and rainfall-triggered translational rock-block slides are common and may contain rapid movement during reactivation phases, limiting interferometric detection. By contrast, the Alpine sector is characterized by larger and more persistent slope instabilities, which are generally more favourable for satellite-based monitoring. This interpretation agrees with Meisina et al. (2008), who found that only 8% of landslides in the Langhe area had PS information, compared with 20% in the Alpine sector, and noted that the detectable PS mainly reflected slower post-failure deformation. [Figure.12], [Table.7].

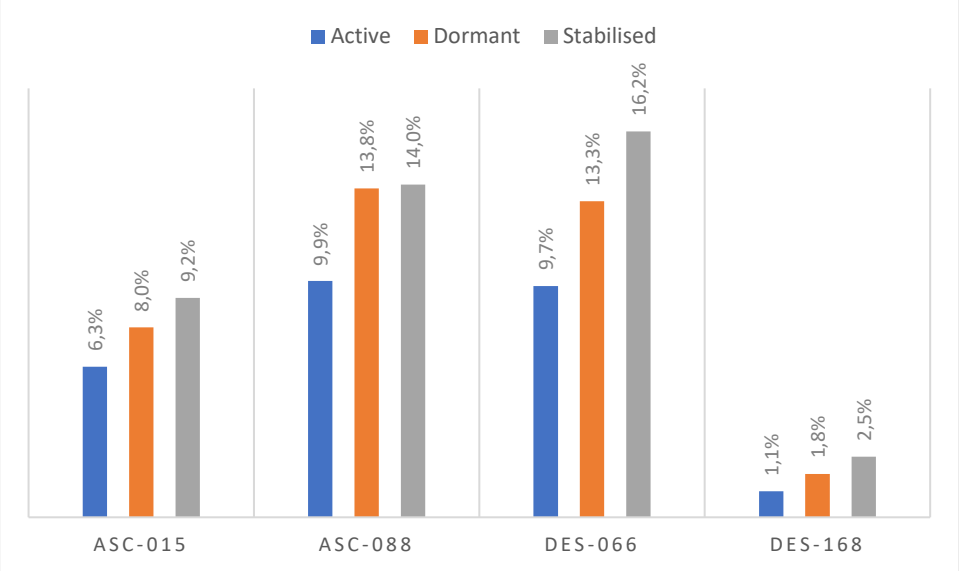

Figure 12. Distribution of Landslides with MP by Orbit and State of Activity across Langhe and Monferrato

Table 7. Distribution of landslides covered by different orbits in the Langhe and Monferrato by order of state of activity

State of Activity	Total count	%	ASC-015		ASC-088		DES-066		DES-168		Covered
				%		%		%		%	
Active	6880	44,0%	435	6,3%	682	9,9%	668	9,7%	75	1,1%	1860
Dormant	8447	54,0%	673	8,0%	1166	13,8%	1120	13,3%	154	1,8%	3113
Stabilised	315	2,0%	29	9,2%	44	14,0%	51	16,2%	8	2,5%	132
Totals	**15642**	**100,0%**	**1137**	**7,3%**	**1892**	**12,1%**	**1839**	**11,8%**	**237**	**1,5%**	5105

In the Turin Hills sub-area, the inventory is most consisting of active landslides (61.5%), followed by dormant landslides (35.3%), while stabilised landslides represent only a small proportion (3.2%). EGMS coverage is mainly concentrated in the ASC-088 and DES-066 orbits, which cover 10.6% and 10.5% of the mapped landslides, respectively, whereas ASC-015 and DES-139 show lower values (4.5% and 2.8%). The distribution by state of activity is generally preserved for active and dormant landslides, but stabilised landslides show a different pattern, with much higher coverage in ASC-088 (49.6%), DES-066 (48.2%), and DES-139 (36.5%). Overall, these results indicate that EGMS coverage in this sub-area is mainly provided by ASC-088 and DES-066, although the representation of stabilised landslides appears more orbit-dependent [Figure.13], [Table.8].

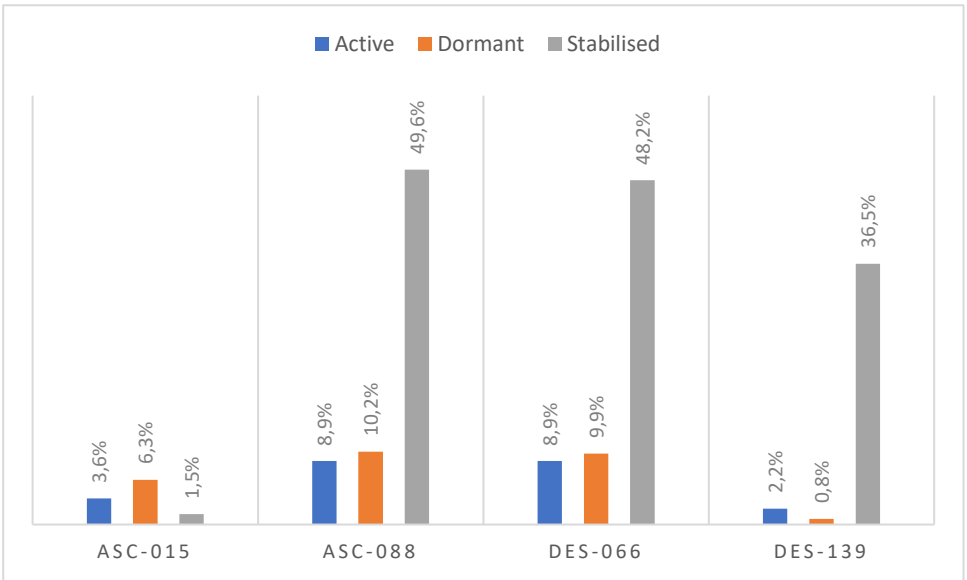

Figure 13. Distribution of Landslides with MP by Orbit and State of Activity across Collina di Torino

Table 8. Distribution of landslides covered by different orbits in the Turin Hills by order of state of activity

State of Activity	Total count	%	ASC-015		ASC-088		DES-066		DES-139		Covered
				%		%		%		%	
Active	2667	61,5%	97	3,6%	237	8,9%	237	8,9%	59	2,2%	630
Dormant	1531	35,3%	96	6,3%	156	10,2%	152	9,9%	12	0,8%	416
Stabilised	137	3,2%	2	1,5%	68	49,6%	66	48,2%	50	36,5%	186
Totals	**4335**	**100,0%**	**195**	**4,5%**	**461**	**10,6%**	**455**	**10,5%**	**121**	**2,8%**	**1232**

In the Apennines sub-area, active and dormant landslides are almost equally represented in the inventory, accounting for 49.7% and 50.2%, respectively, while stabilised landslides are practically absent. EGMS coverage is quite evenly distributed among the available orbits, with total values ranging from 16.8% in ASC-015 to 19.2% in DES-168. The distribution by state of activity is also generally preserved, since both active and dormant landslides show similar percentages across all geometries. Overall, these results indicate a homogeneous EGMS coverage in the Apennines sub-area, with no marked orbit-dependent differences [Figure.14], [Table.9].

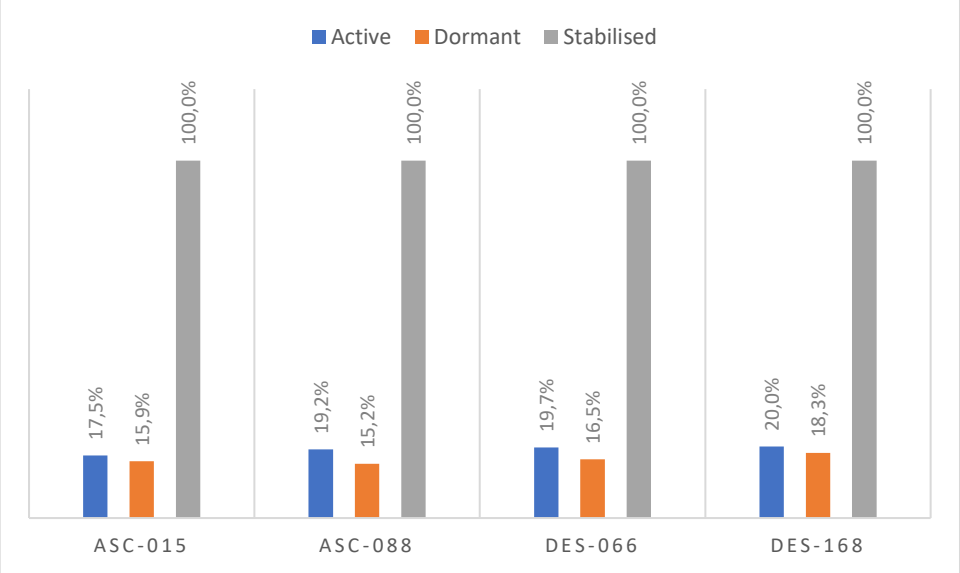

Figure 14. Distribution of Landslides with PS by Orbit and State of Activity across appennino

Table 9. Distribution of landslides covered by different orbits in the Apennines by order of state of activity

State of Activity	Total count	ASC-015		ASC-088		DES-066		DES-168	
			%		%		%		%
Active	770	135	17,5%	148	19,2%	152	19,7%	154	20,0%
Dormant	778	124	15,9%	118	15,2%	128	16,5%	142	18,3%
Stabilised	1	1	100,0%	1	100,0%	1	100,0%	1	100,0%
Totals	**1549**	**260**	**16,8%**	**267**	**17,2%**	**281**	**18,1%**	**297**	**19,2%**

Overall, the results show that EGMS coverage is not uniformly distributed across the region. In most sub-areas, the largest proportion of covered landslides is associated with a limited number of satellite orbits, mainly ASC-088 and DES-066, whereas other geometries contribute less. At the same time, the distribution of the covered landslides by state of activity is generally consistent with that of the PAI inventory, indicating that EGMS provides a representative sample of mapped landslides in several sectors of the study area.

5.2 DISTRIBUTION OF LANDSLIDES CONTAINING MP BY TYPOLOGY

In the second part of the analysis, the SIFraP inventory, which represents the regional Piemonte implementation of the Italian landslide inventory (IFFI framework), was used to examine the distribution of landslide typologies within the subset of landslides covered by EGMS. Based on the results of the previous section, the analysis was restricted to the two main covering orbits, Ascending-088 and Descending-066, as they provided the widest and most representative coverage. This allowed a more detailed evaluation of the typological distribution of landslides detected within the EGMS-covered dataset across the different sub-areas.

In the Alps sub-area, descending orbit 066 and ascending orbit 088 show very similar overall coverage of SIFraP typologies, with values of 60.3% and 59.2%, respectively. The best represented classes are deep-seated gravitational slope deformations (DSGSDs) and areas affected by diffuse falls and topples, both showing very high coverage in the two orbits, whereas rapid flows show the lowest values, below 30%. Overall, this suggests that EGMS more effectively captures typologies related to slow or progressive deformation than those associated with faster processes [Table.10].

Table 10. Distribution of landslides containing EGMS measurement points by typology in the Alps sub-area

Typology	Total count	Descending orbit		Ascending orbit	
			%		%
Areas affected by diffuse falls and topples	3545	2998	84,6%	3005	84,8%
Areas affected by diffuse shallow landslides	827	338	40,9%	316	38,2%
Areas affected by diffuse sinkholes	5	5	100,0%	5	100,0%
slow flows	527	241	45,7%	208	39,5%
Rapid flows	770	222	28,8%	216	28,1%
Complex landslides	1330	786	59,1%	771	58,0%
Falls/Topples	1139	649	57,0%	623	54,7%
DSGSDs	466	415	89,1%	407	87,3%
Not determined	377	101	26,8%	98	26,0%
Rotational/translational slides	1579	620	39,3%	601	38,1%
CARG sectors	5	2	40,0%	2	40,0%
Sinkholes	1	1	100,0%	1	100,0%
Totals	**10571**	**6378**	**60,3%**	**6253**	**59,2%**

In the Langhe and Monferrato sub-area, the two selected EGMS orbits show lower overall coverage than in the Alps, with 13.0% for descending orbit 066 and 16.1% for ascending orbit 088. Among the main typologies, the highest coverage is observed for CARG sectors, which exceed 54% in both geometries, while areas affected by diffuse shallow landslides and rotational/translational slides represent the most numerous classes but show more limited coverage, generally below 18% and around 9–10%, respectively. Lower values are found for slow flows and especially rapid flows, which remain below 8% and 5.1%. Overall, these results indicate that EGMS coverage in the Langhe and Monferrato sub-area is more limited than in the Alps and appears less effective for typologies related to flow processes, while some specific classes, such as CARG sectors, are more strongly represented [Table 11].

Table 11. Distribution of landslides containing EGMS measurement points by typology in the Langhe and Monferrato

Typology	Total count	Descending orbit		Ascending orbit	
			%		%
Areas affected by diffuse falls and topples	43	9	20,9%	13	30,2%

Areas affected by diffuse shallow landslides	4075	525	12,9%	728	17,9%
slow flows	965	42	4,4%	74	7,7%
Rapid flows	175	2	1,1%	9	5,1%
Complex landslides	234	49	20,9%	63	26,9%
Falls/Topples	24	3	12,5%	7	29,2%
DSGSDs	1	1	100,0%	1	100,0%
Not determined	73	8	11,0%	15	20,5%
Rotational/translational slides	5139	451	8,8%	520	10,1%
CARG sectors	736	398	54,1%	414	56,3%
Sinkholes	16	4	25,0%	5	31,3%
Totals	**11481**	**1492**	**13,0%**	**1849**	**16,1%**

In the Turin Hills sub-area, the two selected EGMS orbits show very similar overall coverage, with 11.4% for the descending orbit and 11.8% for the ascending orbit. The highest coverage is observed for complex landslides (17.7% in both orbits), followed by slow flows (13.4% and 15.0%). Rapid flows, DSGSDs, and not determined typologies show similar intermediate values, around 10%. In contrast, rotational/translational slides are only weakly represented, and some typologies, such as falls/topples and lateral spread, are not covered. Overall, the results show a similar coverage pattern in the two orbits, with no major differences between them [Table 12].

Table 12. Distribution of landslides containing EGMS measurement points by typology in the Turin Hills

Typology	Total count	Descending orbit		Ascending orbit	
Areas affected by diffuse falls and topples	1	0	0,0%	0	0,0%
Areas affected by diffuse shallow landslides	109	11	10,1%	10	9,2%
slow flows	493	66	13,4%	74	15,0%
Rapid flows	493	52	10,5%	51	10,3%
Complex landslides	554	98	17,7%	98	17,7%
Falls/Topples	17	0	0,0%	0	0,0%
DSGSDs	665	68	10,2%	69	10,4%
Not determined	2061	207	10,0%	219	10,6%
Rotational/translational slides	16	1	6,3%	1	6,3%

Lateral spread	1	0	0,0%	0	0,0%
Totals	**4410**	**503**	**11,4%**	**522**	**11,8%**

In the Apennines sub-area, the two selected EGMS orbits show similar overall coverage, with 19.7% for the descending orbit and 18.1% for the ascending orbit. The highest coverage is observed for complex landslides, with values above 35% in both geometries. Slow flows are also relatively well represented, with values around 17–19%, while areas affected by diffuse shallow landslides and rotational/translational slides show lower percentages. Some typologies, such as DSGSDs and not determined classes, are not covered in either orbit, although they are represented by very few cases. Overall, the results show a similar pattern in the two orbits, with slightly better coverage in the descending geometry [Table 13].

Table 13. Distribution of landslides containing EGMS measurement points by typology in the Apennines

Typology	Total count	Descending orbit		Ascending orbit	
			%		%
Areas affected by diffuse falls and topples	8	2	25,0%	2	25,0%
Areas affected by diffuse shallow landslides	231	40	17,3%	37	16,0%
slow flows	1040	198	19,0%	181	17,4%
Rapid flows	23	6	26,1%	6	26,1%
Complex landslides	194	72	37,1%	68	35,1%
Falls/Topples	4	1	25,0%	1	25,0%
DSGSDs	2	0	0,0%	0	0,0%
Not determined	3	0	0,0%	0	0,0%
Rotational/translational slides	278	32	11,5%	28	10,1%
Totals	**1783**	**351**	**19,7%**	**323**	**18,1%**

5.3 DISTRIBUTION OF THE MEAN VLOS IN THE PAI DATA

The mean VLOS of the measurement points (MPs) located within the landslides of the PAI inventory was calculated for the 2019–2023 period. The frequency distribution of these mean VLOS values was then analysed in order to evaluate the general pattern of LOS motion within the mapped landslides.

The mean VLOS values calculated for the PAI landslides containing EGMS measurement points across the Piemonte region are strongly concentrated around 0 mm/yr in both ASC-088 and DES-066, with most values falling within approximately ±2 mm/yr. This indicates that the EGMS-detected subset of landslides is generally characterised by low mean LOS motion during the 2019–2023 period. The mean values are close to zero in both orbits, although DES-066 shows a slightly more negative tendency (-0.97 mm/yr) than ASC-088 (-0.25 mm/yr). The median values, which remain close to zero in both cases, confirm that the central part of the distribution is dominated by stable or very slow-moving conditions. At the same time, the standard deviation is higher than in the individual sub-areas (2.59 for ASC-088 and 2.87 for DES-066), and the more extreme minimum values indicate a wider spread of velocities. This suggests that, although low-motion conditions dominate at the regional scale, the Piemonte dataset also includes a limited number of landslides with stronger motion signals, making it more variable than the individual sub-area distributions. [Figure 15].

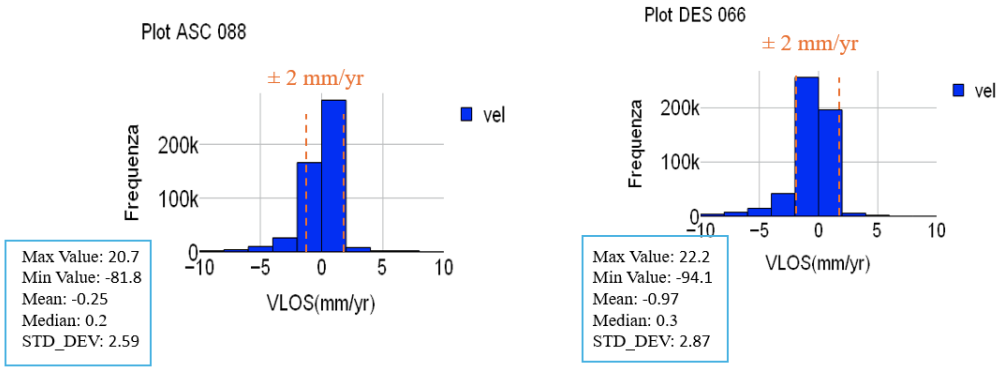

Figure 15. Histograms of mean VLOS values (2019–2023) for measurement points located within PAI landslides across the Piemonte region

The frequency distribution of mean VLOS values in the Turin Hills sub-area is narrow and centred close to 0 mm/yr in both ASC-088 and DES-066, with most values falling within approximately ±2 mm/yr. This suggests that the majority of the mapped PAI landslides in this sub-area are characterised by very low mean LOS motion during the 2019–2023 period. Compared with the regional dataset, the lower standard deviation indicates a more homogeneous behaviour, while the slightly more negative distribution observed in DES-066 suggests a limited orbit-dependent difference in the recorded signal. Overall, the results indicate that the Turin Hills sub-area is characterised by a generally low-motion and relatively uniform VLOS pattern, with only a small number of points showing stronger motion [Figure 16].

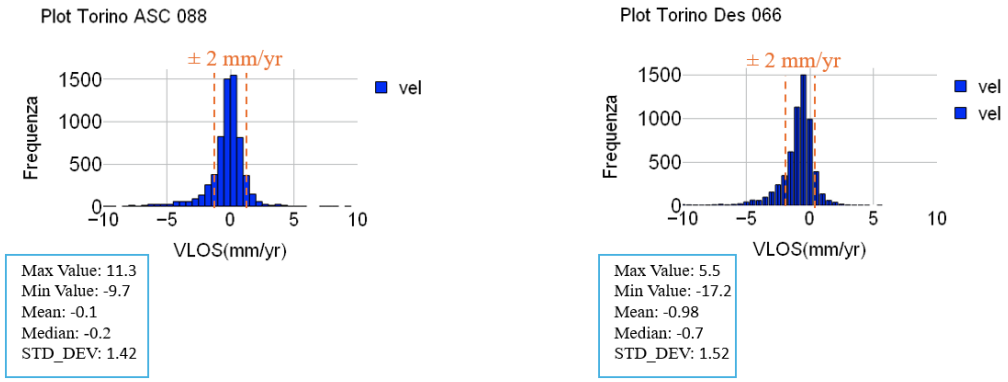

Figure 16. Frequency distribution of mean VLOS values (2019–2023) for measurement points within PAI landslides in the Turin Hills sub-area

In the Langhe and Monferrato sub-area, the histograms show a very compact distribution of mean VLOS values in both ASC-088 and DES-066, with a clear peak around 0 mm/yr and most values falling within approximately ±2 mm/yr. This indicates that most of the PAI landslides in this sector are characterised by very low mean LOS motion during the 2019–2023 period. The low standard deviation values further suggest a rather homogeneous behaviour of the mapped landslides. Although the two distributions are generally consistent, DES-066 shows a slightly more negative tendency than ASC-088, as reflected by its lower mean and median values. Overall, these results suggest that the Langhe and Monferrato sub-area is characterised by a low-motion and weakly dispersed VLOS pattern, with limited evidence of strongly active landslides during the analysed period. [Figure 17].

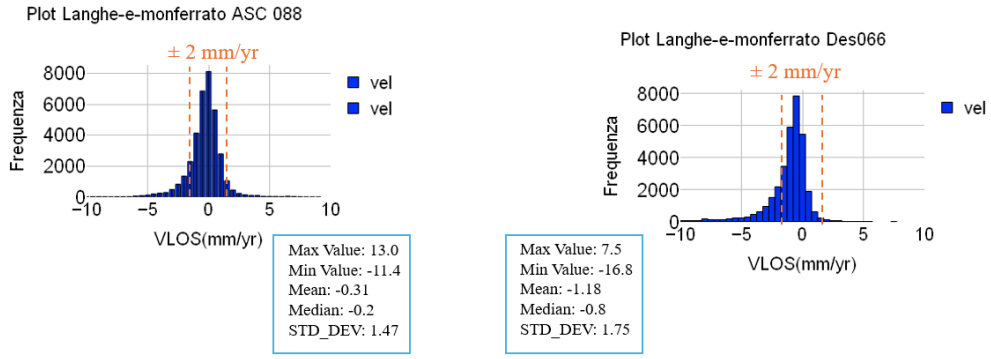

Figure 17. Frequency distribution of mean VLOS values (2019–2023) for measurement points within PAI landslides in the Turin Hills

In the Apennines sub-area, mean VLOS values remain centred close to 0 mm/yr in both ASC-088 and DES-066, with most values falling within approximately ±2 mm/yr. This is consistent with the low mean values observed in both orbits (-0.34 mm/yr for ASC-088 and -1.10 mm/yr for DES-066), indicating that the subset of PAI landslides containing EGMS measurement points is characterised by low average LOS motion during the 2019–2023 period. The median values are also close to zero (-0.2 mm/yr and -0.6 mm/yr), confirming that the central tendency of the distribution is concentrated around stable or very slow-moving conditions. The two histograms show a similar overall shape, although the slightly higher standard deviation in DES-066 (2.12 compared with 1.81 in ASC-088) indicates a somewhat wider spread of values and therefore slightly greater variability in the descending geometry. Overall, these results suggest a generally low-motion VLOS pattern in the EGMS-detected landslide subset of the Apennines sub-area. [Figure 18].

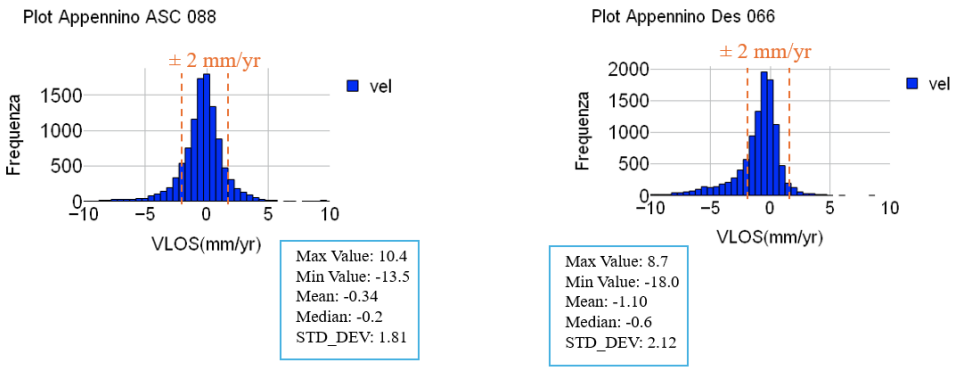

Figure 18. Frequency distribution of mean VLOS values (2019–2023) for measurement points within PAI landslides in the Apennines

In the Alps sub-area, the mean VLOS values of the PAI landslides containing EGMS measurement points are still mainly concentrated around 0 mm/yr, with most values falling within approximately ±2 mm/yr in both ASC-088 and DES-066. However, compared with the other sub-areas, the Alps show a wider distribution, as indicated by the higher standard deviation values (2.69 for ASC-088 and 2.96 for DES-066). This suggests a greater variability of motion within the EGMS-detected landslide subset. The mean and median values remain close to zero in both orbits, although DES-066 is slightly more negative (mean = -0.96 mm/yr; median = -0.3 mm/yr) than ASC-088 (mean = -0.24 mm/yr; median = 0.2 mm/yr). The wider tails and more extreme minimum values, reaching -94.1 mm/yr in DES-066 and -81.1 mm/yr in ASC-088, indicate the presence of a limited number of landslides with stronger motion signals. Overall, these results suggest that, although the Alps are still dominated by low mean LOS velocities, they represent the most variable sub-area, with a greater presence of more active cases within the EGMS-detected landslide subset. [Figure 19].

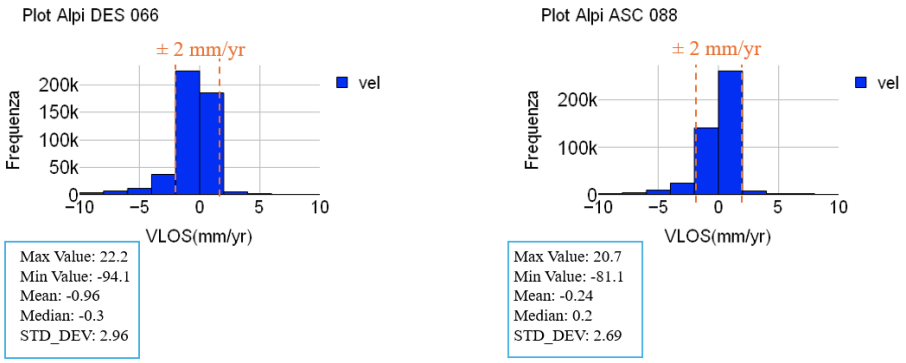

Figure 19. Frequency distribution of mean VLOS values (2019–2023) for measurement points within PAI landslides in the Apennines

5.4 ANALYSIS OF LANDSLIDE DISTRIBUTION BY ABSOLUTE MEAN VLOS CLASSES

This analysis was performed on the landslides containing at least one EGMS measurement point (MP) from ascending orbit 088 and descending orbit 066 in the four study sub-areas. The distribution of absolute mean VLOS values was then analysed to assess how the detected landslides are distributed among different velocity ranges and activity classes.

In the Alps covered by ascending orbit 088, a total of 4,867 landslides containing at least one EGMS measurement point were analysed. Among them, active landslides represent the largest proportion (2,797; 57.5%), followed by dormant landslides (1,760; 36.2%) and stabilised landslides (310; 6.4%) [Table 14].

The highest absolute mean VLOS threshold identified only a very limited number of cases. In the Alps covered by ascending orbit 088, only four landslides with at least one EGMS measurement point show a mean VLOS magnitude greater than 16 mm/yr. Three of these landslides are located in the municipality of Valprato Soana and are all classified in the inventory as active landslides with very high hazard. More specifically, they correspond to an active deep-seated gravitational slope deformation, an active fall, and an active complex landslide [Figure 19]. The fourth case is located in Sampeyre and is classified as an active translational slide with very high hazard [Table 15], [Figure 20].

Table 14. Absolute Mean VLOS distribution of landslides in Alpi covered by ascending orbit 088

Absolute Mean VLOS	Stabilised		Active		Dormant	
Range	N. Landslide	Percentage	N. Landslide	Percentage	N. Landslide	Percentage
Greater than 2mm/year	22	7.1%	209	7.5%	151	8.6%
Greater than 3mm/year	8	2.6%	116	4.1%	78	4.4%
Greater than 4mm/year	3	1.0%	71	2.5%	42	2.4%
Greater than 5mm/year	3	1.0%	47	1.7%	26	1.5%
Greater than 16mm/year	0	0.0%	4	0.1%	0	0.0%
Totals	**310**	**100.0%**	**2797**	**100.0%**	**1760**	**100.0%**

Table 15. the main attributes reported by PAI of the four landslides with absolute mean VLOS greater than 16 mm/yr in the Alps sector covered by ascending orbit 088

Landslide ID	State of activity	Hazard	Typology	Location	Number of MP	Mean VLOS (mm/year)
22813	Active	very high hazard	DSGSD	Valprato Soana	906	-19,807174
22875	Active	very high hazard	Falls	Valprato Soana	9	-33,222222
22887	Active	very high hazard	complex landslide	Valprato Soana	289	-54,711073
33485	Active	very high hazard	translational slide	Sampeyre	69	-17,617391

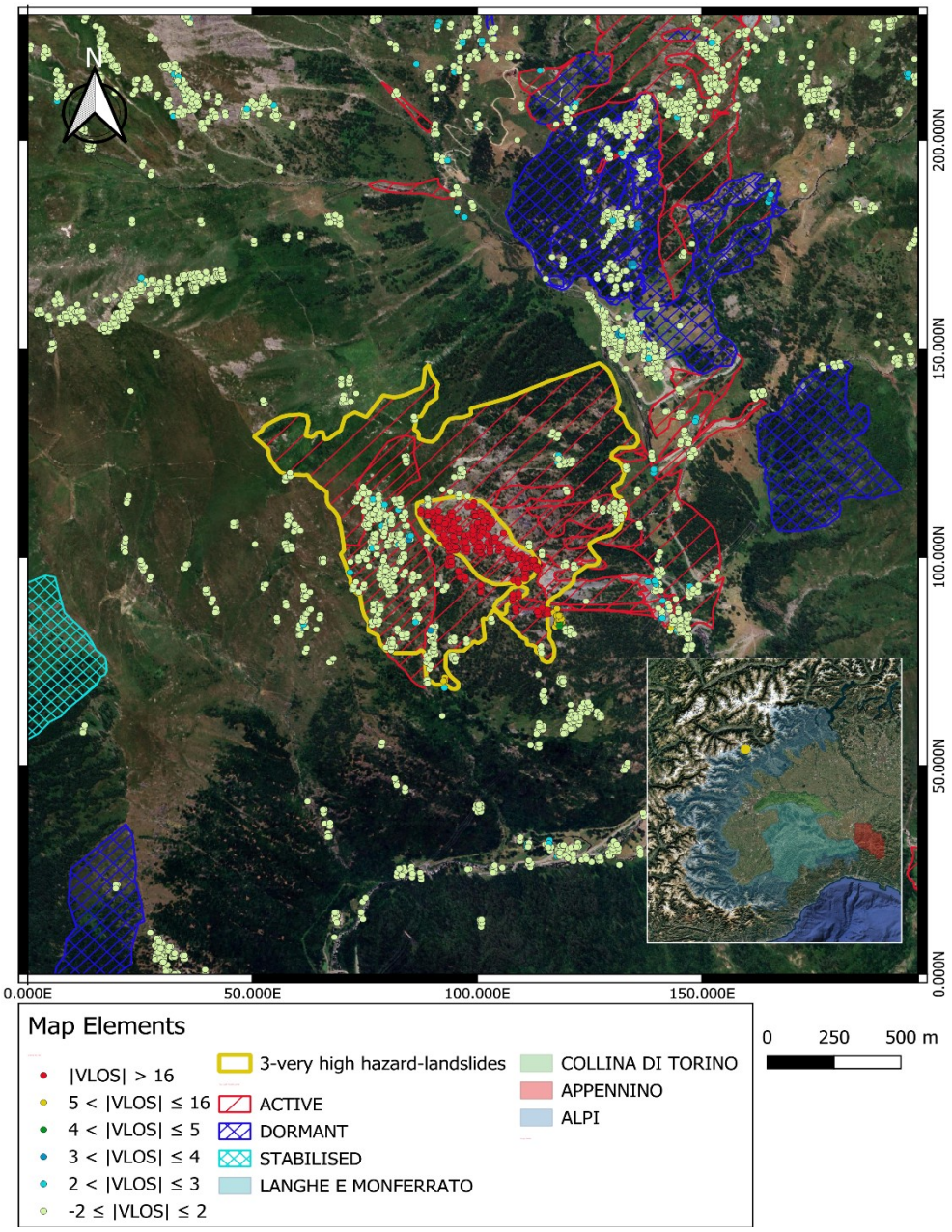

Figure 20. Three active very high hazard landslides in Valprato Soana with absolute mean VLOS greater than 16 mm/yr Detected by ascending orbit 088

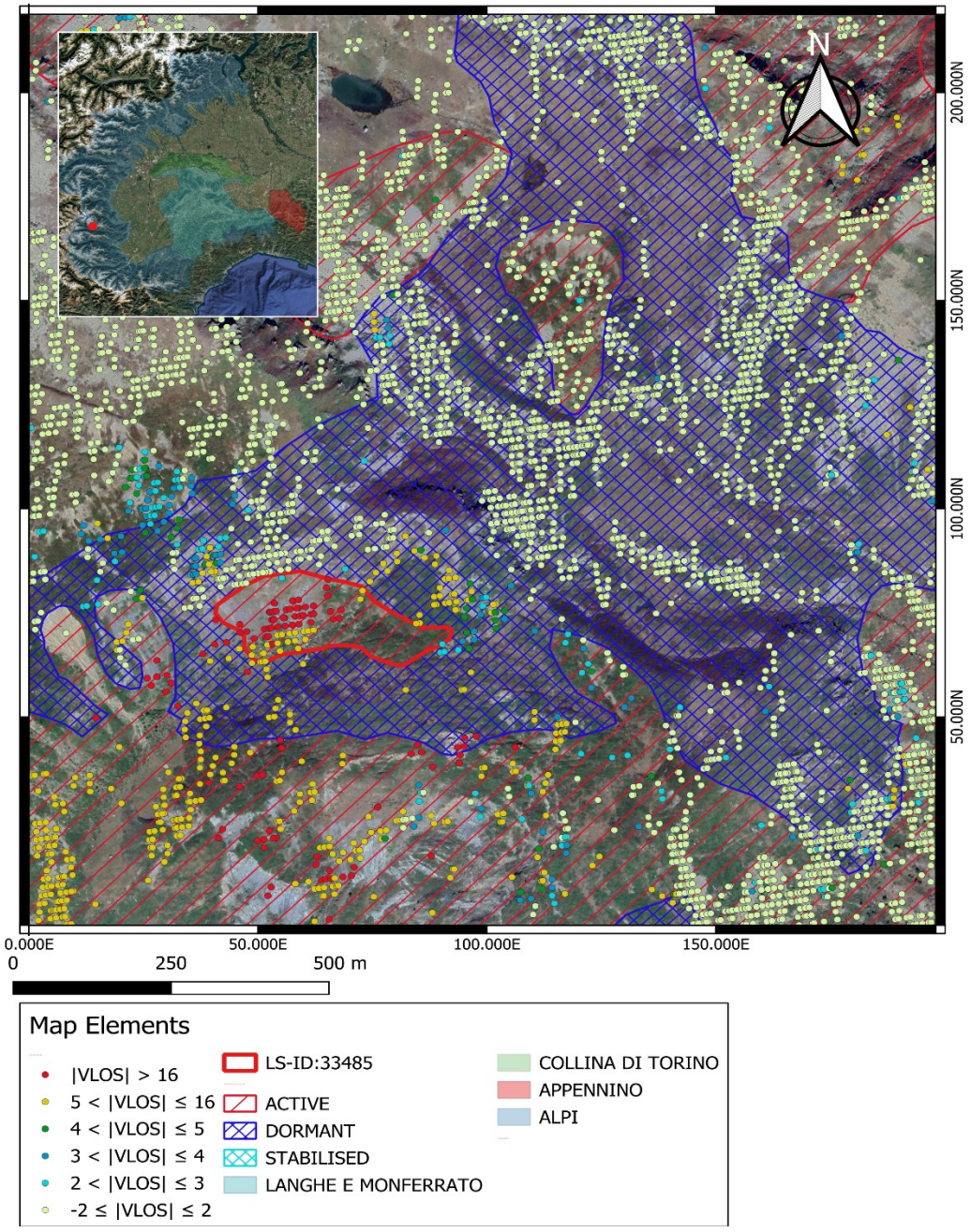

Figure 21. Active very high hazard landslide in Sampeyre with absolute mean VLOS greater than 16 mm/yr Detected by ascending orbit 088

For the landslides in the Alpi covered by descending orbit 066, a total of 4,999 landslides containing EGMS measurement points were analysed. Among them, active landslides are the most represented class (2,820; 56%), followed by dormant landslides (1,850; 37%) and stabilised landslides (329; 7%).

The distribution of absolute mean VLOS values shows that the proportion of landslides exceeding the selected thresholds decreases progressively as velocity increases, indicating that most landslides are still concentrated in the lower motion ranges. At the 2 mm/yr threshold, the highest proportion is observed in the dormant class, with about 11.5% of landslides exceeding this value, followed by the active class (8.5%) and the stabilised class (6.1%). This suggests that detectable motion is not limited to landslides classified as active, but is also present in a relevant part of the dormant class.

At higher thresholds, the same general pattern remains, although the percentages decrease in all classes. Above 3 mm/yr, about 6.5% of dormant landslides and 5.2% of active landslides exceed the threshold, while the stabilised class remains lower (2.4%). Above 4 mm/yr, the percentages further decrease to about 4.2% for dormant, 3.3% for active, and 1.8% for stabilised landslides. Above 5 mm/yr, only a limited proportion remains [Table 16]

Only a very limited number of landslides exceed the highest threshold of 16 mm/yr in the Alps covered by descending orbit 066. These cases include both active and dormant landslides, indicating that very high mean motion is not restricted to the active class alone. The mapped cases are distributed among Salbertrand, Sauze d'Oulx, Cesana Torinese, Valprato Soana, Bellino, and Sampeyre, with Cesana Torinese showing the highest local concentration, where four landslides exceed this threshold [Table 17]

Among them, the most robust case is the active complex landslide in Cesana Torinese (LS-ID 20364), which contains 288 measurement points and shows a mean VLOS of about -20.01 mm/yr. Another significant case is the active fall in Sampeyre (LS-ID 33303), with 73 measurement points and a mean VLOS of about -17.95 mm/yr. Some other polygons exceed the threshold with only a limited number of points, so their mean values should be interpreted more cautiously [Figure 22], [Figure 23].

Table 16. Absolute Mean VLOS distribution of landslides in Alpi covered by Descending orbit 066

Absolute Mean VLOS	Stabilised		Active		Dormant	
Range	N. Landslide	Percentage	N. Landslide	Percentage	N. Landslide	Percentage
Greater than 2mm/year	20	6,08%	241	73,25%	212	64,44%
Greater than 3mm/year	8	2,43%	147	44,68%	120	36,47%
Greater than 4mm/year	6	1,82%	94	28,57%	77	23,40%
Greater than 5mm/year	4	1,22%	67	20,36%	50	15,20%
Greater than 16mm/year	0	0,00%	5	1,52%	4	1,22%
Totals	**329**	**100,00%**	**2820**	**100,00%**	**1850**	**100,00%**

Table 17. the main attributes reported by PAI of the four landslides with absolute mean VLOS greater than 16 mm/yr in the Alps sector covered by descending orbit 066

Landslide ID	State of activity	Hazard	Typology	Location	Number of MP	Mean VLOS (mm/year)
9410	Active	very high hazard	complex landslide	Salbertrand	17	-19,658824
16453	Dormant	high hazard	complex landslide	Sauze d'Oulx	5	-17,26
20282	Active	very high hazard	Falls	Cesana Torinese	15	-23,04
20364	Active	very high hazard	complex landslide	Cesana Torinese	288	-20,009375
20447	Dormant	high hazard	complex landslide	Cesana Torinese	6	-17,383333
20456	Dormant	high hazard	translational slide	Cesana Torinese	6	-20,35
22875	Active	very high hazard	Falls	Valprato Soana	3	17,866667
28243	Dormant	high hazard	complex landslide	Bellino	11	-18,618182
33303	Active	very high hazard	Falls	Sampeyre	73	-17,950685

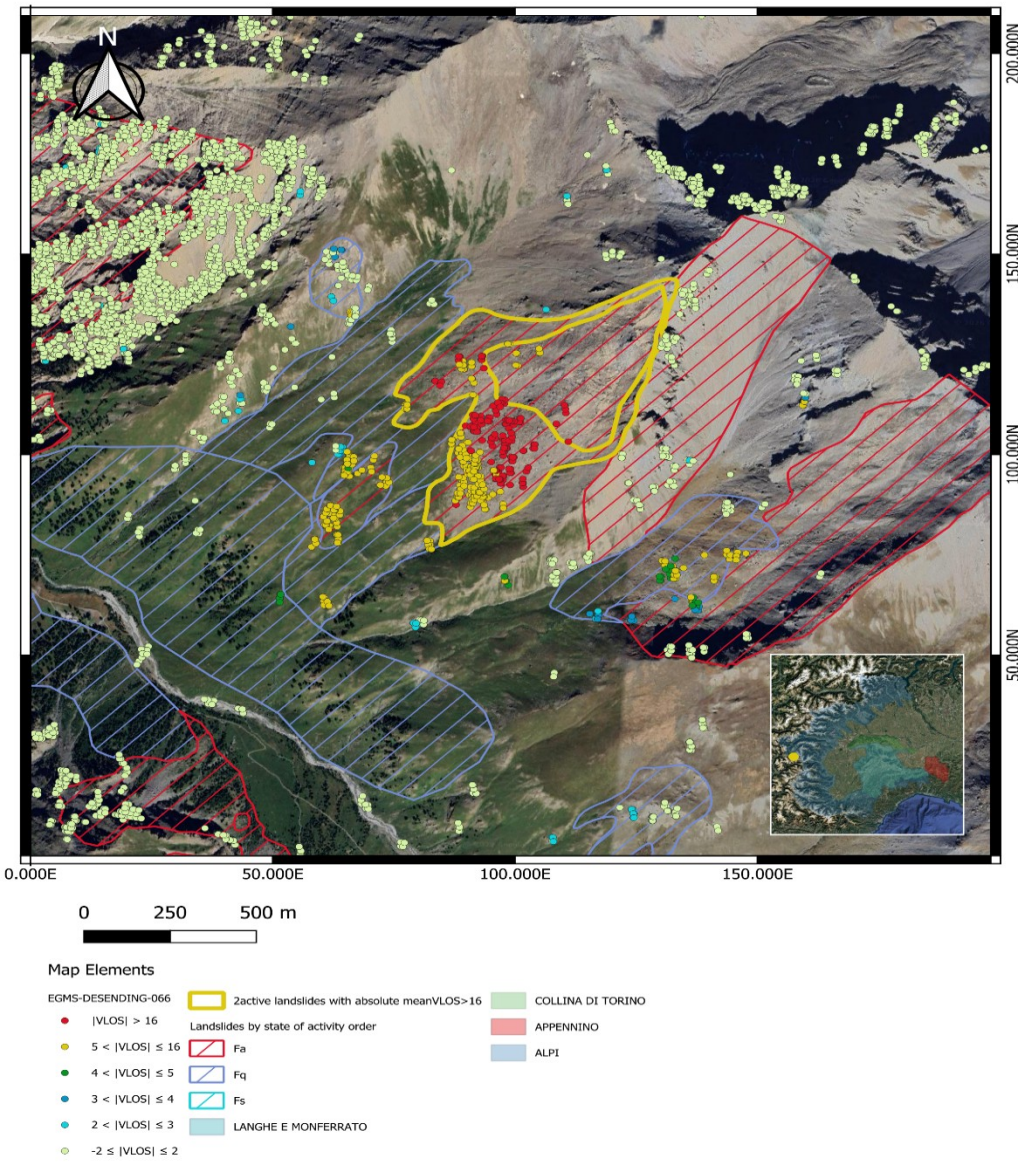

Figure 22. Active very high hazard landslides in Cesana Torinese with absolute mean VLOS greater than 16 mm/yr Detected by Descending orbit 066

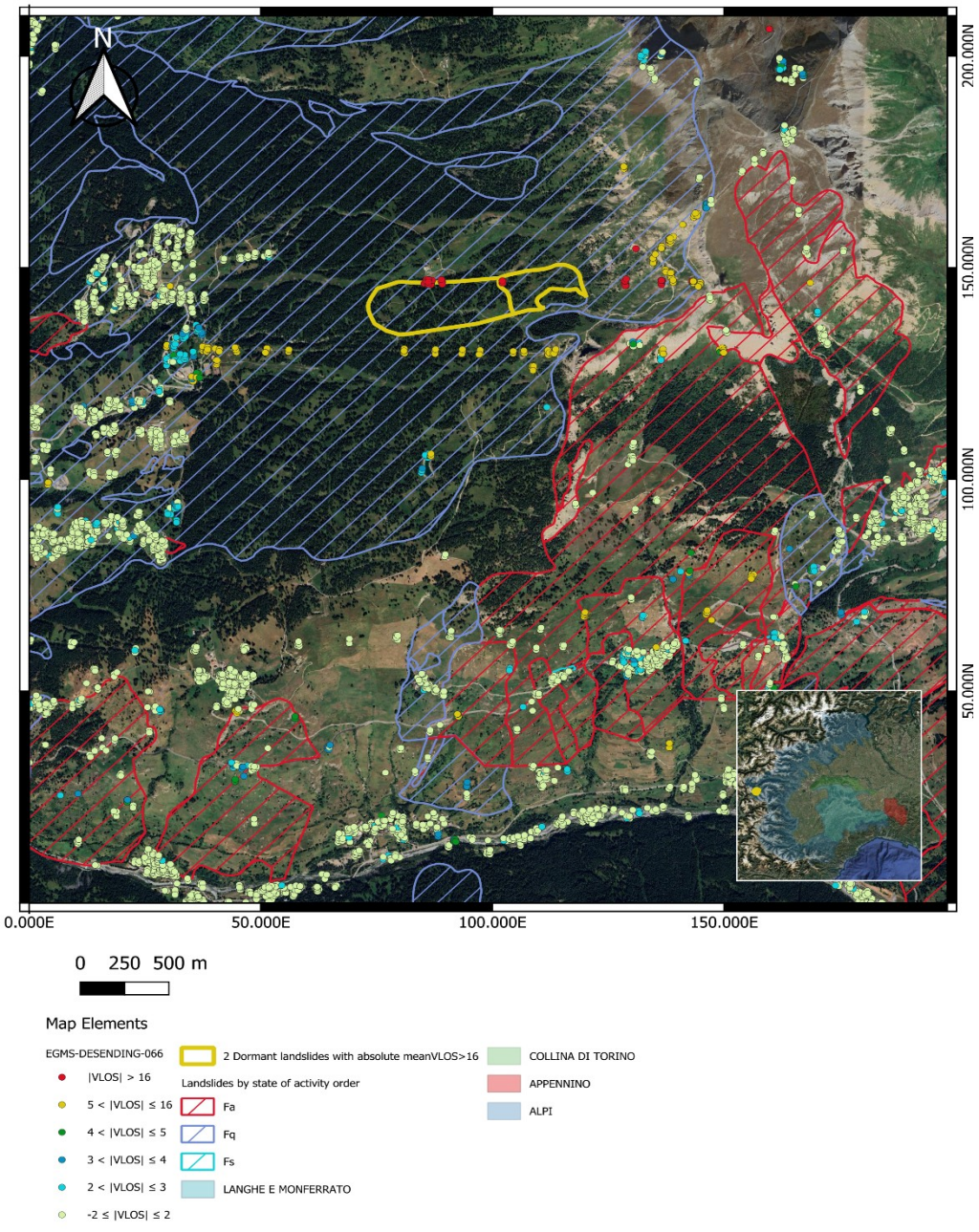

Figure 23. Dormant high hazard landslides in Cesana Torinese with absolute mean VLOS greater than 16 mm/yr Detected by Descending orbit 066

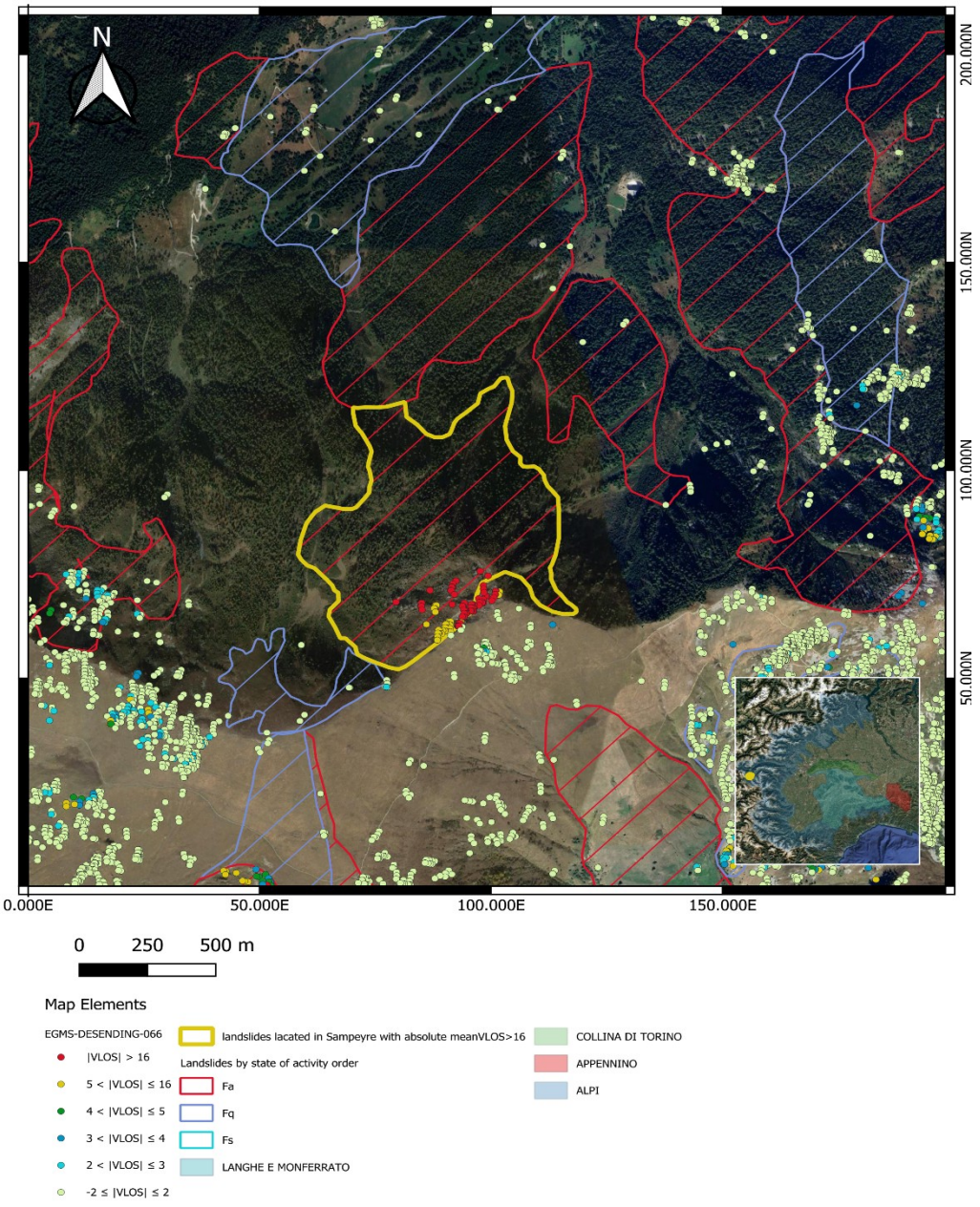

Figure 24. Active very high hazard landslides in Sampeyre with absolute mean VLOS greater than 16 mm/yr Detected by Descending orbit 066

In the Appennino sub-area covered by descending orbit 066, the distribution of landslides across the selected absolute mean VLOS thresholds reflects the expected kinematic behaviour of the different activity classes.

both the active and dormant classes show measurable proportions above the selected thresholds. At the 2 mm/yr threshold, 21.7% of active landslides and 22.7% of dormant landslides exceed this value, indicating that detectable motion is present in a relevant fraction of both classes. Since dormant landslides are generally expected to be less active than the active class, the slightly higher percentage observed in the dormant group suggests that some landslides classified as dormant still retain measurable kinematic activity. This same pattern remains visible at the higher thresholds, with the dormant class maintaining slightly higher percentages than the active class above 3 mm/yr (16.4% vs 15.1%), 4 mm/yr (11.7% vs 7.9%), and 5 mm/yr (9.4% vs 5.3%) [Table 18].

Table 18. Absolute Mean VLOS distribution of landslides in Appennino covered by Descending orbit 066

Absolute Mean VLOS	**Stabilised**		**Active**		**Dormant**	
Range	N. Landslide	Percentage	N. Landslide	Percentage	N. Landslide	Percentage
Greater than 2mm/year	0	0.0%	33	21.7%	29	22.7%
Greater than 3mm/year	0	0.0%	23	15.1%	21	16.4%
Greater than 4mm/year	0	0.0%	12	7.9%	15	11.7%
Greater than 5mm/year	0	0.0%	8	5.3%	12	9.4%
Greater than 16mm/year	0	0.0%	0	0.0%	0	0.0%
Totals	**1**	**100.00%**	**152**	**100.00%**	**128**	**100.00%**

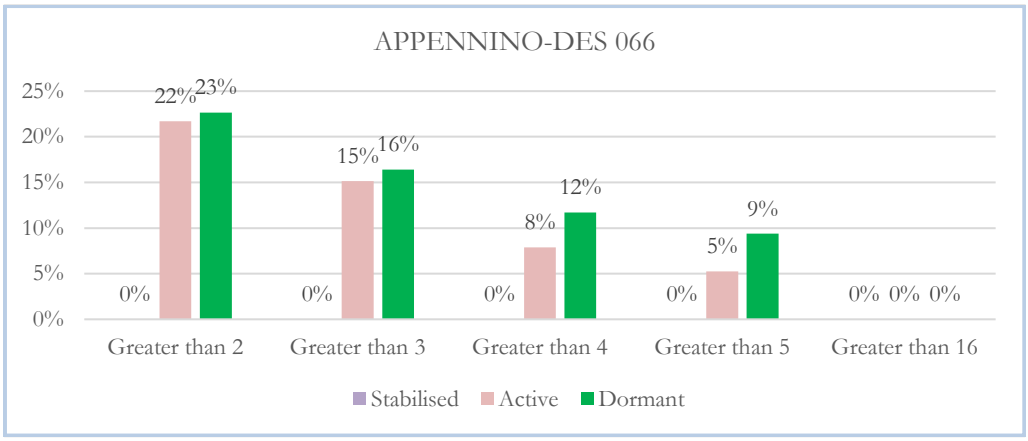

Figure 25. Absolute Mean VLOS distribution of Landslides covered by Descending orbit 066 in Appennino

In the Appennino sub-area covered by ascending orbit 088 also only one stabilised landslide was detected, and its mean VLOS remains below 2 mm/yr. Active landslides are represented across all thresholds up to 5 mm/yr, while dormant landslides also exceed the lower and intermediate thresholds. No landslides exceed the 16 mm/yr threshold. Overall, the results indicate mainly low-to-moderate mean motion conditions, with detectable deformation concentrated in the active class and, to a lesser extent, in part of the dormant class [Table 19].

Table 19. Absolute Mean VLOS distribution of landslides in Appennino covered by Ascending orbit 088

Absolute Mean VLOS	Stabilised		Active		Dormant	
Range	N. Landslide	Percentage	N. Landslide	Percentage	N. Landslide	Percentage
Greater than 2mm/year	0	0.00%	22	14.86%	15	12.71%
Greater than 3mm/year	0	0.00%	13	8.78%	7	5.93%
Greater than 4mm/year	0	0.00%	8	5.41%	2	1.69%
Greater than 5mm/year	0	0.00%	4	2.70%	2	1.69%

Greater than 16mm/year	0	0.00%	0	0.00%	0	0.00%
Totals	**1**	**100.00%**	**148**	**100.00%**	**118**	**100.00%**

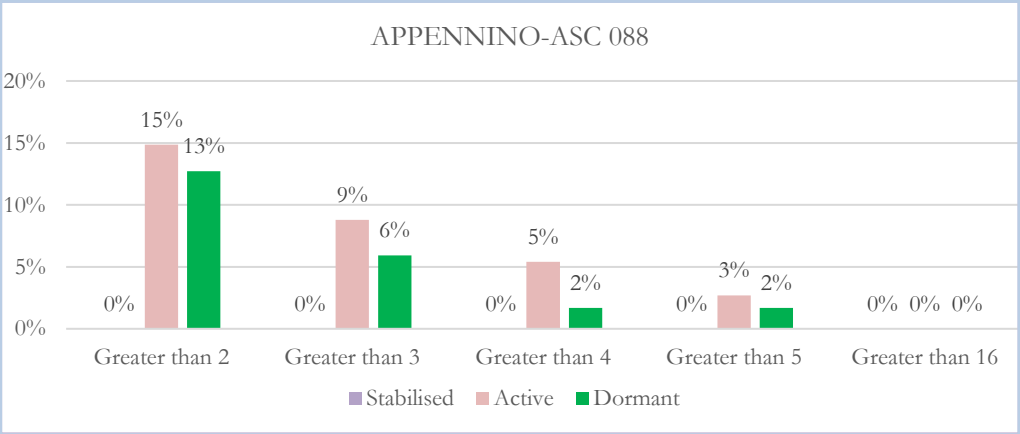

Figure 26. Absolute Mean VLOS distribution of Landslides covered by Ascending orbit 088 in Appennino

The distribution of absolute mean VLOS values in the Langhe e Monferrato sub-area covered by descending orbit 066 shows a more complex kinematic pattern than expected from the inventory activity states. In this case, not only active and dormant landslides, but also a relevant proportion of stabilised landslides exceed the selected thresholds. In particular, 15.69% of stabilised landslides have an absolute mean VLOS greater than 2 mm/yr, and some cases remain represented up to the 5 mm/yr threshold. This is an interesting result, because stabilised landslides are generally expected to be concentrated in the lowest velocity range.

The active class behaves consistently with its expected state, as a relevant proportion of active landslides exceeds all thresholds from 2 to 5 mm/yr, although the percentages progressively decrease with increasing velocity. This confirms that EGMS is able to detect measurable slow-movement in a significant fraction of landslides classified as active. The dormant class also remains represented across the same thresholds, suggesting that part of this class still shows detectable movement.

No landslides in any activity state exceed the 16 mm/yr threshold, indicating that in the Langhe e Monferrato sub-area the detected motion is generally limited to low-to-moderate mean velocity values. Overall, the results suggest that descending orbit 066 captures measurable deformation in all three activity classes, but the most noteworthy outcome is the presence of stabilised landslides above the selected thresholds, since these cases may deserve further investigation [Table 20].

Table 20. Absolute Mean VLOS distribution of landslides in Langhe E Monferrato covered by Descending orbit 066

Absolute Mean VLOS	Stabilised		Active		Dormant	
Range	N. Landslide	Percentage	N. Landslide	Percentage	N. Landslide	Percentage
Greater than 2mm/year	8	15.69%	118	17.66%	181	16.16%
Greater than 3mm/year	5	9.80%	64	9.58%	88	7.86%
Greater than 4mm/year	3	5.88%	36	5.39%	46	4.11%
Greater than 5mm/year	2	3.92%	23	3.44%	25	2.23%
Greater than 16mm/year	0	0.00%	0	0.00%	0	0.00%
Totals	**51**	**100.00%**	**668**	**100.00%**	**1120**	**100.00%**

The distribution of absolute mean VLOS values in the Langhe e Monferrato sub-area covered by ascending orbit 088 shows that measurable motion is present in all three activity classes, although it progressively decreases as the velocity threshold increases. The active class behaves consistently with expectations, since it maintains the highest representation across all thresholds from 2 to 5 mm/yr, confirming that EGMS captures detectable motion in a relevant proportion of landslides classified as active.

The most noteworthy result concerns the stabilised class. Although stabilised landslides are generally expected to remain within the lowest velocity range, 11.36% exceed the 2 mm/yr threshold and isolated cases remain present up to 5 mm/yr. This suggests that some polygons classified as stabilised may still be affected by residual deformation, local reactivation, or ground-motion conditions not fully consistent with their current inventory classification [Table 21].

The dormant class is also represented across the selected thresholds, indicating that part of this class still shows detectable motion. This pattern may reflect residual activity or limited local reactivation, which is compatible with the transitional nature of dormant landslides. No landslides in any activity class exceed the 16 mm/yr threshold, indicating that in this sub-area the detected motion is mainly limited to low-to-moderate mean velocity values.

Table 21. Absolute Mean VLOS distribution of landslides in Langhe E Monferrato covered by Ascending orbit 088

Absolute Mean VLOS	Stabilised	Active	Dormant

Range	N. Landslide	Percentage	N. Landslide	Percentage	N. Landslide	Percentage
Greater than 2mm/year	5	11.36%	107	15.69%	120	10.29%
Greater than 3mm/year	1	2.27%	68	9.97%	48	4.12%
Greater than 4mm/year	1	2.27%	32	4.69%	31	2.66%
Greater than 5mm/year	1	2.27%	21	3.08%	16	1.37%
Greater than 16mm/year	0	0.00%	0	0.00%	0	0.00%
Totals	**44**	**100.00%**	**682**	**100.00%**	**1166**	**100.00%**

In the Collina di Torino sub-area covered by descending orbit 066, the stabilised class is mostly confined to the lowest motion range, with only 4.55% of landslides exceeding 2 mm/yr and no cases above 5 mm/yr. Active landslides show measurable motion across all thresholds, decreasing from 16.88% above 2 mm/yr to 2.53% above 5 mm/yr, which is consistent with their expected activity state. Dormant landslides are also represented at all thresholds, from 18.42% above 2 mm/yr to 4.61% above 5 mm/yr, suggesting that part of this class still shows detectable deformation, possibly related to residual activity or local reactivation. No landslides in any class exceed 16 mm/yr, indicating that the detected motion is limited to low-to-moderate mean velocity values [Table 22].

Table 22. Absolute Mean VLOS distribution of landslides in Collina di Torino covered by Descending orbit 066

Absolute Mean VLOS	**Stabilised**		**Active**		**Dormant**	
Range	N. Landslide	Percentage	N. Landslide	Percentage	N. Landslide	Percentage
Greater than 2mm/year	3	4.55%	40	16.88%	28	18.42%
Greater than 3mm/year	1	1.52%	21	8.86%	14	9.21%
Greater than 4mm/year	1	1.52%	12	5.06%	8	5.26%
Greater than 5mm/year	0	0.00%	6	2.53%	7	4.61%
Greater than 16mm/year	0	0.00%	0	0.00%	0	0.00%
Totals	**66**	**100.00%**	**237**	**100.00%**	**152**	**100.00%**

In the Collina di Torino sub-area covered by ascending orbit 088, the stabilised class is almost entirely confined to the lowest motion range, with only 1.47% of landslides exceeding 2 mm/yr and no cases above the higher thresholds. Active landslides remain represented from 2 to 5 mm/yr, decreasing from 8.02% to 1.27%, which is consistent with measurable but generally low-to-moderate motion. Dormant landslides are also detected across all thresholds up to 5 mm/yr, from 12.18% above 2 mm/yr to 3.21% above 5 mm/yr, suggesting that part of this class still shows detectable deformation, possibly related to residual activity or local reactivation. No landslides in any class exceed 16 mm/yr [Table 23].

Table 23. Absolute Mean VLOS distribution of landslides in Collina di Torino covered by Ascending orbit 088

Absolute Mean VLOS	**Stabilised**		**Active**		**Dormant**	
Range	N. Landslide	Percentage	N. Landslide	Percentage	N. Landslide	Percentage
Greater than 2mm/year	1	1.47%	19	8.02%	19	12.18%
Greater than 3mm/year	0	0.00%	6	2.53%	13	8.33%
Greater than 4mm/year	0	0.00%	5	2.11%	8	5.13%
Greater than 5mm/year	0	0.00%	3	1.27%	5	3.21%
Greater than 16mm/year	0	0.00%	0	0.00%	0	0.00%
Totals	**68**	**100.00%**	**237**	**100.00%**	**156**	**100.00%**

What is most interesting from this part of the analysis is that some landslides classified as stabilised in the PAI inventory show absolute mean VLOS values greater than 3 mm/year. This suggests that these cases may require further investigation, as their current state of activity may need to be updated.

Table 24. Stabilised landslides detected by the ascending orbit with absolute mean VLOS greater than 3 mm/year by sub-area

Sub Area	**comune**	**Number MPs**	**Mean VLOS Ascending**
Alpi	Alagna Valsesia	8	-12,6625
Alpi	Angrogna	76	-3,235526
Alpi	Coassolo Torinese	3	6,2
Alpi	Strona	1	-5,8

Alpi	Limone Piemonte	2	3,1
Langhe e Monferrato	Costigliole d'Asti	2	-5,25

Table 25. Stabilised landslides detected by the descending orbit with absolute mean VLOS greater than 3 mm/year by sub-area

Sub Area	Comune	Number MPs	Mean VLOS Descending (mm/y)
Alpi	San Secondo di Pinerolo	4	-7,00
Alpi	Alagna Valsesia	1	4,10
Alpi	Alagna Valsesia	96	-6,88
Alpi	Bobbio Pellice	23	-6,63
Alpi	Carema	2	-7,40
Alpi	Settimo Vittone	73	-3,20
Alpi	Bobbio Pellice	45	-4,95
Alpi	Limone Piemonte	206	-3,44
Langhe e Monferrato	Ricaldone	8	-5,06
Langhe e Monferrato	San Damiano d'Asti	8	-5,36
Langhe e Monferrato	Costigliole d'Asti	8	-3,85
Langhe e Monferrato	Carrosio	1	-4,10
Langhe e Monferrato	Castellinaldo d'Alba	5	-3,68
Collina di Torino	Castiglione Torinese	6	-4,12

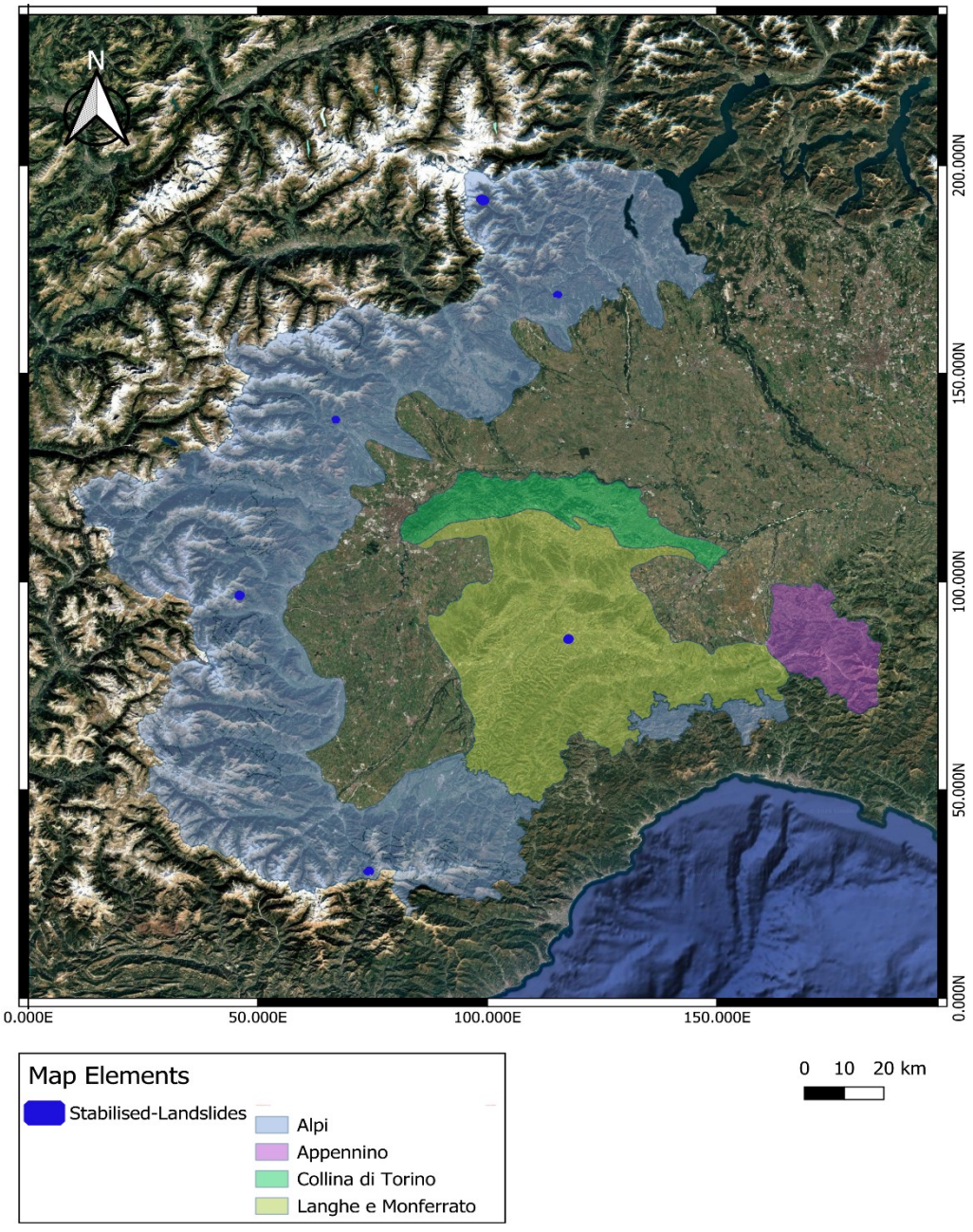

Figure 27. Location of stabilised landslides showing absolute mean ascending VLOS greater than 3 mm/year

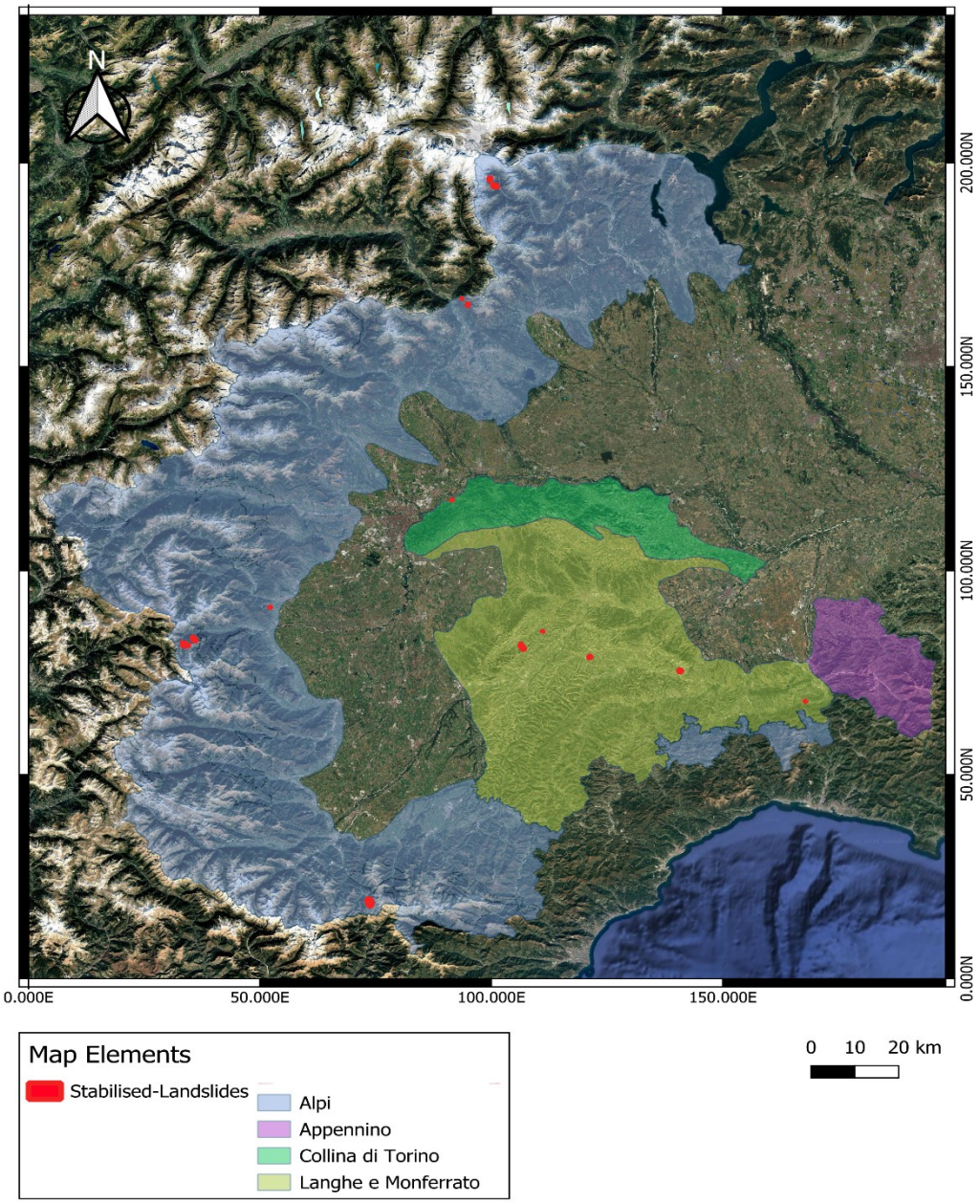

Figure 28. Location of stabilised landslides showing absolute mean descending VLOS greater than 3 mm/year

5.5 Comparison between mean velocity of EGMS and GNSS

Selection of Landslides Suitable for EGMS–GNSS Validation

The regional inventory includes a total of 495 in-situ monitoring points, of which 401 are classified as active. These instruments are distributed over 139 SIFRAP landslides within the study area. Out of these 139 landslides, 123 contain at least one in-situ monitoring instrument, confirming that the majority of monitored landslides are equipped with ground-based observations. Among the different instrument types, GNSS (Caposaldo GPS) is the most frequently installed system, monitoring 103 landslides. In comparison, 28 landslides are monitored by inclinometer measurements.

These results show that GNSS monitoring represents the dominant in-situ dataset available for comparison purposes. Since GNSS provides continuous and precise displacement measurements, it was selected as the primary reference for the EGMS validation phase. The distribution of monitoring instruments also highlights that only a subset of the total mapped landslides can be used for direct satellite–ground comparison. Therefore, the validation stage is necessarily limited to those landslides where reliable in-situ data are available.

Starting from the 103 landslides monitored by GNSS, a further selection was carried out in order to define the subset that can be used for a direct comparison with EGMS. A buffer of 50 meter was applied around each GNSS instrument location and the presence of EGMS measurement points (MPs) by the coherence greater than 0.7 inside this buffer was checked. After this step, only landslides showing EGMS MPs with that specific coherence filter close to the GNSS stations were considered suitable for validation.

By applying these criteria, 123 GNSS stations remaned with the specific filter and the dataset was reduced from 103 to 62 landslides, which represent the final subset monitored by both GNSS instruments and EGMS measurement points and therefore suitable for the comparison and validation step.

The visibility conditions of the final subset were also evaluated separately for the two orbital geometries. In the descending orbit, the selected landslides generally show very favourable conditions, with 46 out of 62 cases (74.2%) having visibility greater than 50%, while 13 landslides (21.0%) fall in the 30–50% class. Only 3 landslides (4.8%) show no visibility and none belong to the 0–30% class [Table 26].

In the ascending orbit, the visibility is slightly lower but still overall satisfactory, with 32 landslides (51.6%) showing visibility above 50% and 27 landslides (43.5%) falling in the 30–50% range. Only 2 landslides (3.2%) are included in the 0–30% class and just 1 case (1.6%) has no visibility. Overall, these results indicate that the final subset is characterized by predominantly moderate to high visibility in both geometries, with particularly favourable coverage in the descending orbit, further supporting its suitability for the EGMS–GNSS comparison [Table 27].

Table 26. Distribution of the 62 selected landslides by visibility class in the descending orbit

Visibility class	Number of landslides	%
0%	3	4,8%
0-30%	0	0,0%
30-50%	13	21,0%
>50%	46	74,2%
Totals	**62**	

Table 27. Distribution of the 62 selected landslides by visibility class in the ascending orbit

Visibility class	Number of landslides	%
0%	1	1,6%
0-30%	2	3,2%
30-50%	27	43,5%
>50%	32	51,6%
Totals	**62**	

EGMS–GNSS Velocity Comparison

For each of the 123 selected buffers distributed within the 62 selected landslides, the mean VLOS and mean VSLOPE of the EGMS measurement points located inside the 50 m buffer were calculated and compared with the mean velocity recorded by the corresponding GNSS station.

The comparison between the mean VLOS of ascending and descending EGMS MPs and the mean GNSS velocity shows that most observations lie below the 1:1 reference line, indicating a general underestimation of velocity by the EGMS LOS measurements relative to GNSS. This behaviour is expected, since VLOS expresses only the component of displacement projected along the satellite line of sight, whereas GNSS provides a more direct measurement of ground movement.

As a result, LOS velocities capture only a portion of the actual landslide motion, particularly where the displacement vector is not well aligned with the satellite viewing geometry. This discrepancy becomes more evident at higher GNSS velocities, where both ascending and descending VLOS values remain comparatively low and do not increase proportionally. Overall, the comparison indicates that EGMS VLOS is effective in identifying the presence of deformation, but does not fully reproduce the total displacement measured by the in-situ monitoring system [Figure 29], [Figure 30].

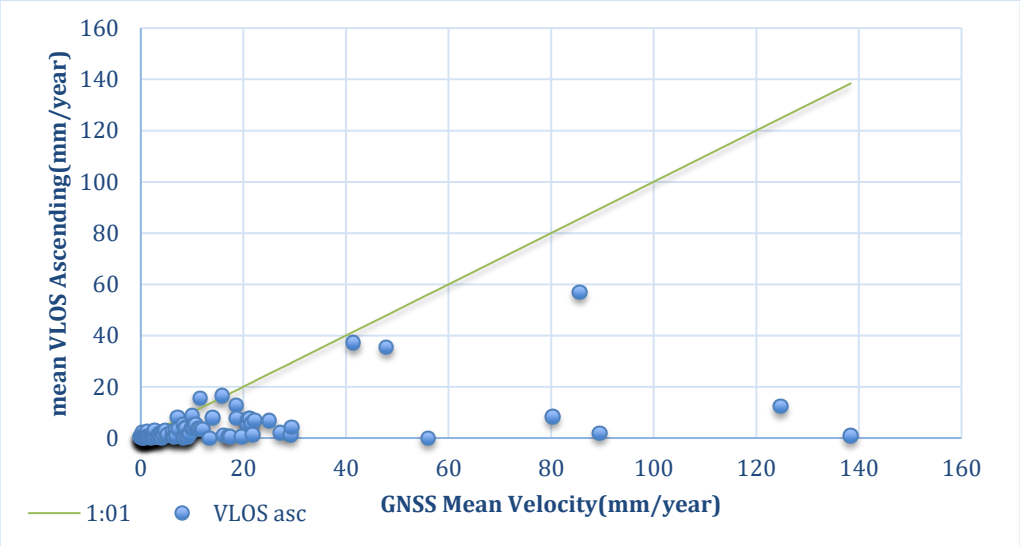

Figure 29. Comparison between Mean Ascending VLOS and GNSS Mean Velocity

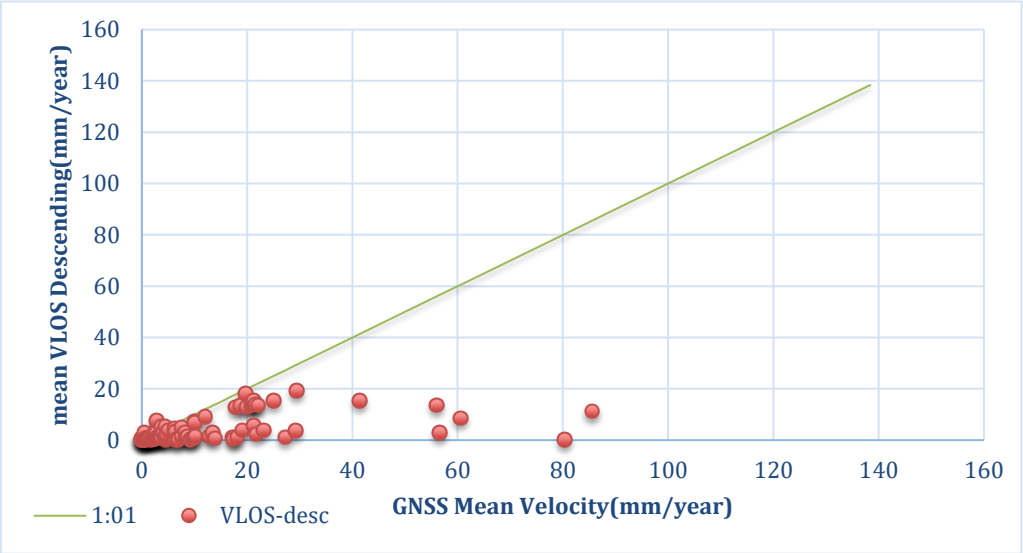

Figure 30. Comparison between Mean Descending VLOS and GNSS Mean Velocity

In the ascending VSLOPE plot, the data points are more dispersed and several values are higher than those observed in the VLOS comparison. Some observations move closer to the 1:1 reference line, suggesting that the slope projection improves the agreement with GNSS in part of the dataset. This indicates that transforming the LOS velocity into VSLOPE allows the EGMS measurements to better represent the actual slope-parallel component of landslide movement.

However, the agreement is still not consistent for all cases. While many points remain below the 1:1 line, indicating continued underestimation, some points lie above it, showing that in a few cases the projected velocities may exceed the corresponding GNSS values. This greater spread reflects the higher sensitivity of VSLOPE to local slope geometry and to the assumptions involved in the projection from LOS to slope direction in computing the C-index [Figure 31].

Part of the variability observed in the comparison can also be attributed to the number of EGMS MPs available within the selected buffers. In some cases, the mean EGMS velocity was calculated from a single measurement point only. As a result, the obtained value may

not be fully representative of the landslide sector surrounding the GNSS station and can be more strongly influenced by local conditions or by the behaviour of an individual point. A detailed inspection of these cases showed that several of the most discrepant results are associated with buffers containing only one EGMS MP.

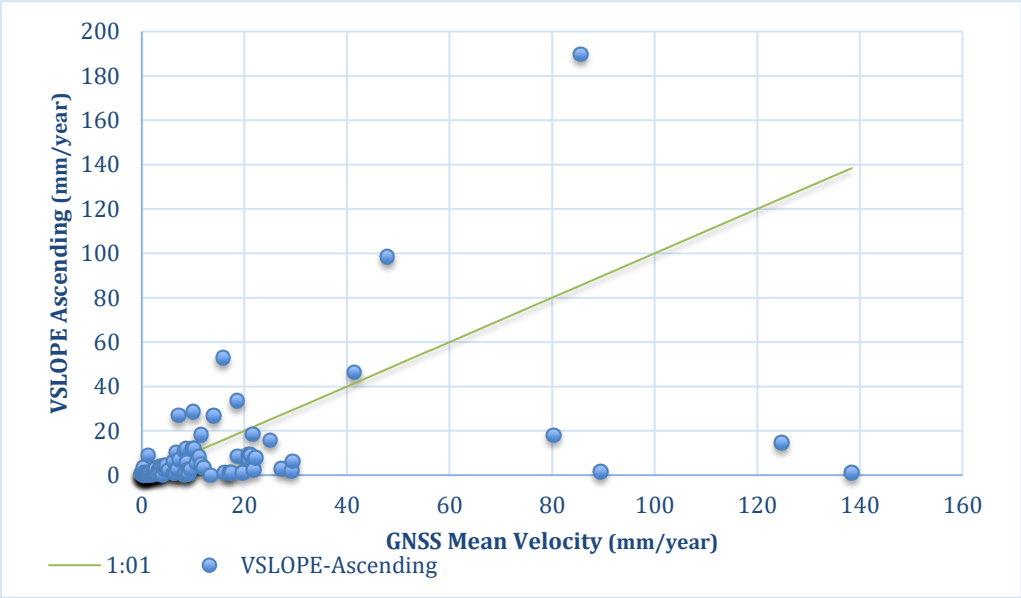

Figure 31. Comparison between Mean Ascending VSLOPE and GNSS Mean Velocity

The comparison between mean descending VSLOPE and GNSS mean velocity shows that most observations remain below the 1:1 reference line, indicating that descending slope-projected EGMS velocities are generally lower than the corresponding GNSS values. Although the VSLOPE transformation is more physically representative of landslide motion than raw VLOS, the agreement with GNSS remains limited, especially at higher velocities. Part of the observed scatter is also related to the low number of EGMS MPs within some buffers, since in several cases the mean value was derived from only one measurement point [Figure 32].

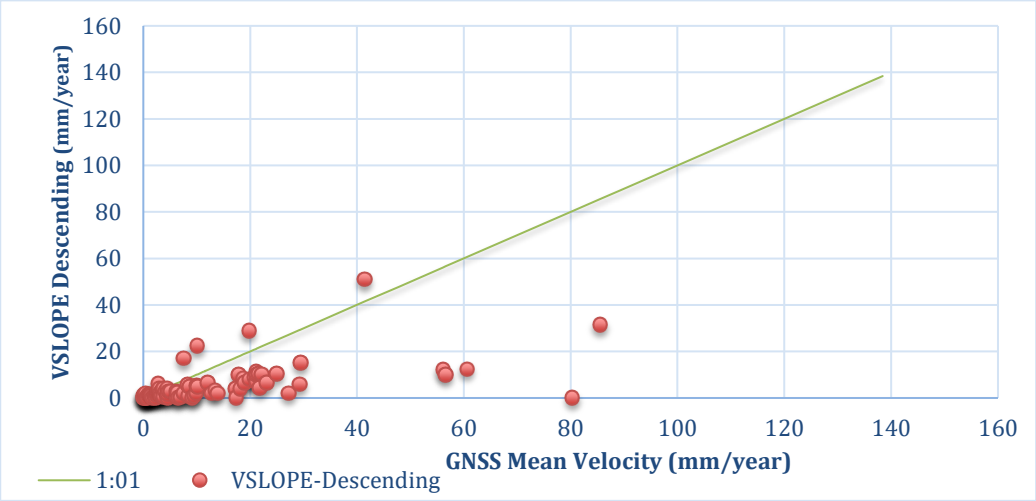

Figure 32. Comparison between Mean Descending VSLOPE and GNSS Mean Velocity

After zooming in on the VSLOPE graphs to focus on the lower-velocity range, where most of the observations are concentrated, the descending orbit shows a better agreement with the GNSS mean velocity than the ascending orbit.

In particular, the descending VSLOPE values appear less dispersed and generally closer to the 1:1 reference line, suggesting a more consistent representation of landslide motion in this velocity range.

There are some cases that showing very high or very low velocity along the slope by two orbits that I have choosed some them for further analysis. Valprato Soana is one of the locations in which for both ascending and descending orbits shows the mean VSLOPE greater than the mean velocity of in-situ monitoring. Two other locations which showing the same differences are Castelmagno and Paroldo. For these three locations I have done the further analysis [Table.28], [Table 29], [Table 30], [Table 31].

Table 28. Descending-orbit cases with very low VSLOPE values relative to GNSS mean velocity

Instrument code	Location	mean-VLOS (mm/y)	mean-VSLOPE (mm/y)	GNSS mean velocity(mm/y)	N-MPs
G6SSTC4	Sestriere	0,30	0,25	17,39	4
G6SSTC6	Sestriere	1,17	2,00	27,22	3
G4SMPA9	Sampeyre	0,20	0,00	80,32	2

Table 29. Descending-orbit cases with very high VSLOPE values relative to GNSS mean velocity

Instrument code	Location	mean-VLOS (mm/y)	mean-VSLOPE (mm/y)	GNSS mean velocity(mm/y)	N-MPs
G6PRGB3	Pragelato	6,75	22,50	10,08	2
G6SZUA9	Sauze d`Oulx	18,03	29,00	19,78	3
G6VPSA2	Valprato Soana	15,40	51,00	41,45	1

Table 30. Ascending-orbit cases with very high VSLOPE values relative to GNSS mean velocity

Instrument code	Location	Mean-VLOS (mm/y)	Mean VSLOPE (mm/y)	GNSS mean velocity(mm/y)	N-MPs
G4PARA11	Paroldo	2,60	9,00	1,24	1
G6BGIA2	Borgofranco d`Ivrea	3,10	10,33	6,76	3
G6QUIA5	Quincinetto	8,13	27,00	7,23	4
G6PRGB3	Pragelato	8,58	28,60	10,08	5
G6QUIA4	Quincinetto	15,65	18,33	11,58	6
G6VPSA1	Valprato Soana	8,00	26,67	13,96	6
G4CSMA4	Castelmagno	16,60	53,00	15,85	1
G4CSMA5	Castelmagno	12,85	33,50	18,61	2
G6VPSA5	Valprato Soana	35,50	98,50	47,87	2
G6VPSA3	Valprato Soana	57,00	189,83	85,55	6

Table 31. Ascending-orbit cases with very low VSLOPE values relative to GNSS mean velocity

Instrument code	Location	Mean-VLOS (mm/y)	Mean VSLOPE (mm/y)	GNSS mean velocity(mm/y)	N-MPs
G6BARB1	Bardonecchia	1,10	1,00	16,17	1
G6SSTC5	Sestriere	0,70	1,00	17,14	1
G6SSTC4	Sestriere	0,60	1,00	17,39	4
G6BARC1	Bardonecchia	0,50	1,00	19,63	1
G6LOCA10	Locana	1,22	2,45	21,77	40
G6SSTC6	Sestriere	2,10	3,00	27,22	2
G4SMPA13	Sampeyre	1,40	2,00	29,30	1
G6CESH3	Cesana Torinese	0,10	0,00	8,24	2
G4SMPA9	Sampeyre	8,40	18,00	80,32	1

G4SMPA4	Sampeyre	1,85	1,50	89,42	2
G4SMPA3	Sampeyre	12,30	14,50	124,78	2
G4SMPA1	Sampeyre	0,80	1,00	138,42	2

Valprato Soana contain one of the clearest cases where EGMS and GNSS show different results. The largest differences are observed for ascending VSLOPE, especially at station G6VPSA3, where VSLOPE reaches 189.83 mm/year compared with a GNSS mean velocity of 85.55 mm/year. This suggests that the slope-projection step may strongly amplify EGMS velocities in some sectors of the landslide [Figure 33].

The differences observed among the four stations at Valprato Soana can be related to both landslide typology and local geometric conditions. G6VPSA1, located in an area affected by falls/topples, which reduces the reliability of the satellite measurement. In contrast, G6VPSA2 shows a better agreement with GNSS, probably because it is located in a more geomorphologically uniform sector of the landslide. The strongest mismatch is observed at G6VPSA3, where the ascending VSLOPE appears strongly overestimated, likely due to an unfavourable relationship between slope aspect and satellite viewing geometry, which amplifies the slope-projected velocity. Finally, at G6VPSA5, the local slope orientation may limit the visibility of the descending orbit, contributing to the absence or poor representativeness of descending measurements [Figure 34].

The DEM and C-index analysis further clarify the discrepancy observed at Valprato Soana. The C-index map shows that some GNSS stations, particularly G6VPSA3 and G6VPSA5, are located in zones characterized by very low values, indicating unfavourable geometric conditions for the conversion of LOS velocity into slope-parallel velocity. Under these conditions, the VSLOPE transformation can strongly amplify the EGMS signal, leading to unrealistically high values, as observed for the ascending orbit at G6VPSA3. In addition, the DEM used for the analysis has a coarse spatial resolution relative to the size and internal complexity of the landslide, which likely smooths the local slope angle and aspect around the monitoring points. This is particularly relevant in Valprato Soana, where different landslide typologies coexist and local geomorphological conditions vary over short distances. Therefore, the mismatch between EGMS-derived VSLOPE and GNSS is more plausibly explained by the combined effect of complex kinematics, unfavourable satellite–slope geometry, and the limitations of the DEM-based slope projection, rather than by poor quality of the EGMS measurements themselves [Figure 35], [Figure 36].

Also, one very important detail is the 100 m DEM resolution is itself a strong justification. For a landslide of this size, that resolution is quite rough, so it is completely reasonable to argue that the local geometry around each GNSS point is not captured well enough for a precise VSLOPE correction [Figure 37], [Figure 38], [Figure 39].

Also, the ascending-orbit EGMS time series at G6VPSA3 shows a strong and nearly linear increase in cumulative slope-parallel displacement through time, reaching close to 1 m over the observation period. This trend is coherent and persistent, but its magnitude is clearly larger than the displacement rate indicated by GNSS. This supports the interpretation that the discrepancy is mainly introduced during the projection from LOS measurements to slope-parallel displacement, which appears to amplify the EGMS signal at this station.

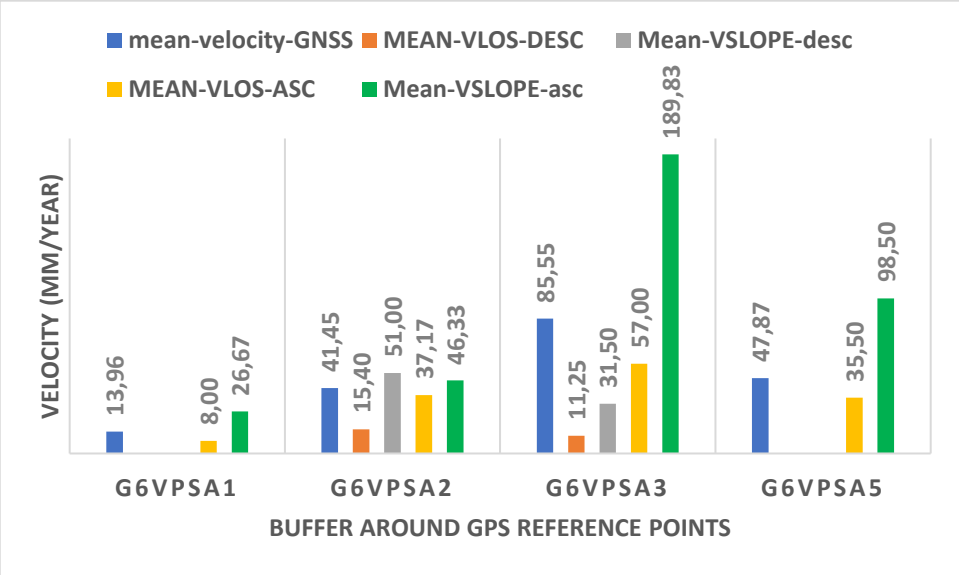

Figure 33. Comparison of GNSS Mean Velocity and EGMS Mean VLOS and VSLOPE at Selected Stations in Valprato Soana

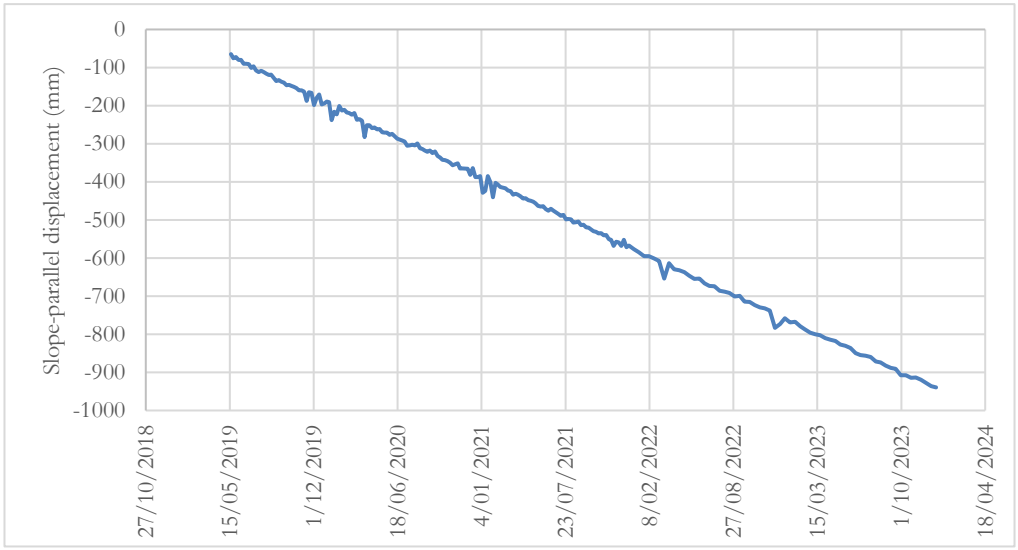

Figure 34. Ascending-orbit EGMS slope-parallel displacement time series at G6VPSA3

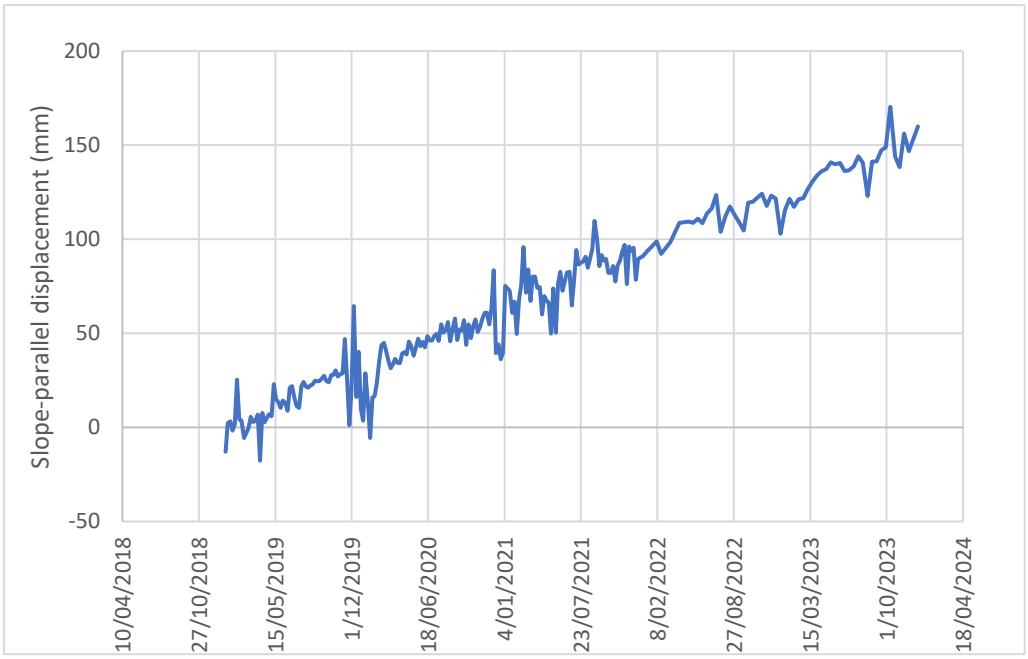

Figure 35. Descending-orbit EGMS slope-parallel displacement time series at G6VPSA3

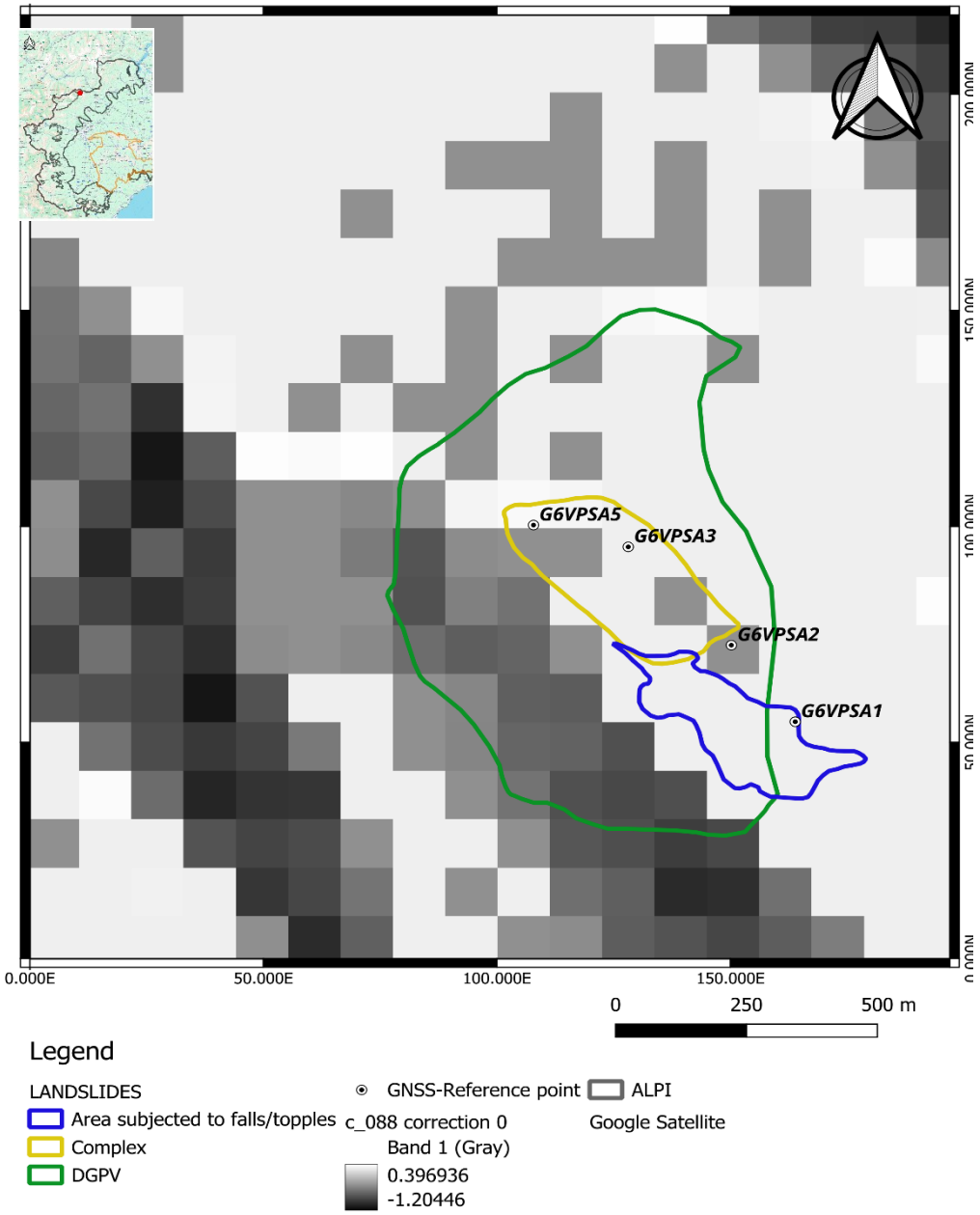

Figure 36.C-index map of the Ascending orbit at Valprato Soana landslide area

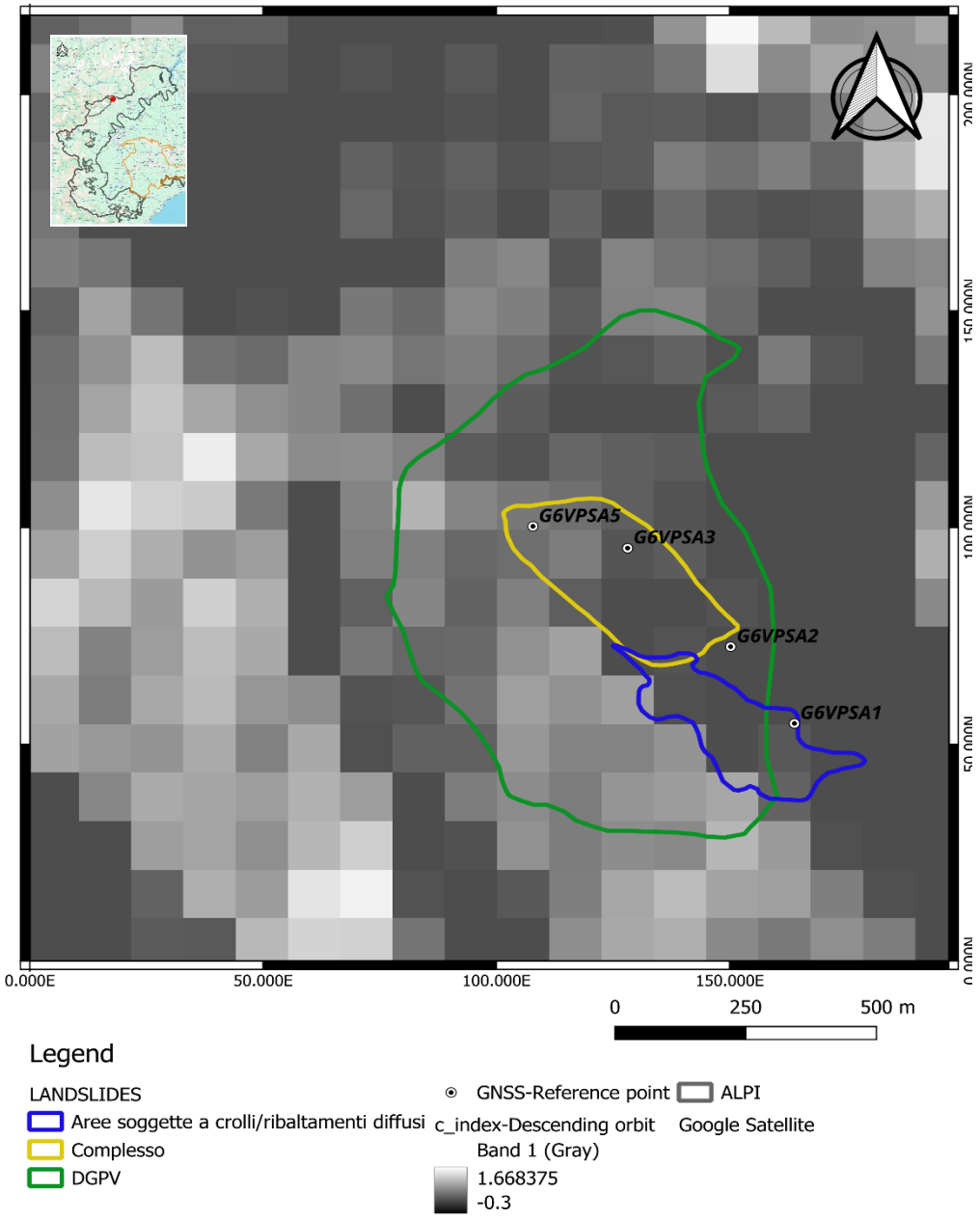

Figure 37. C-index map of the Descending orbit at Valprato Soana landslide area

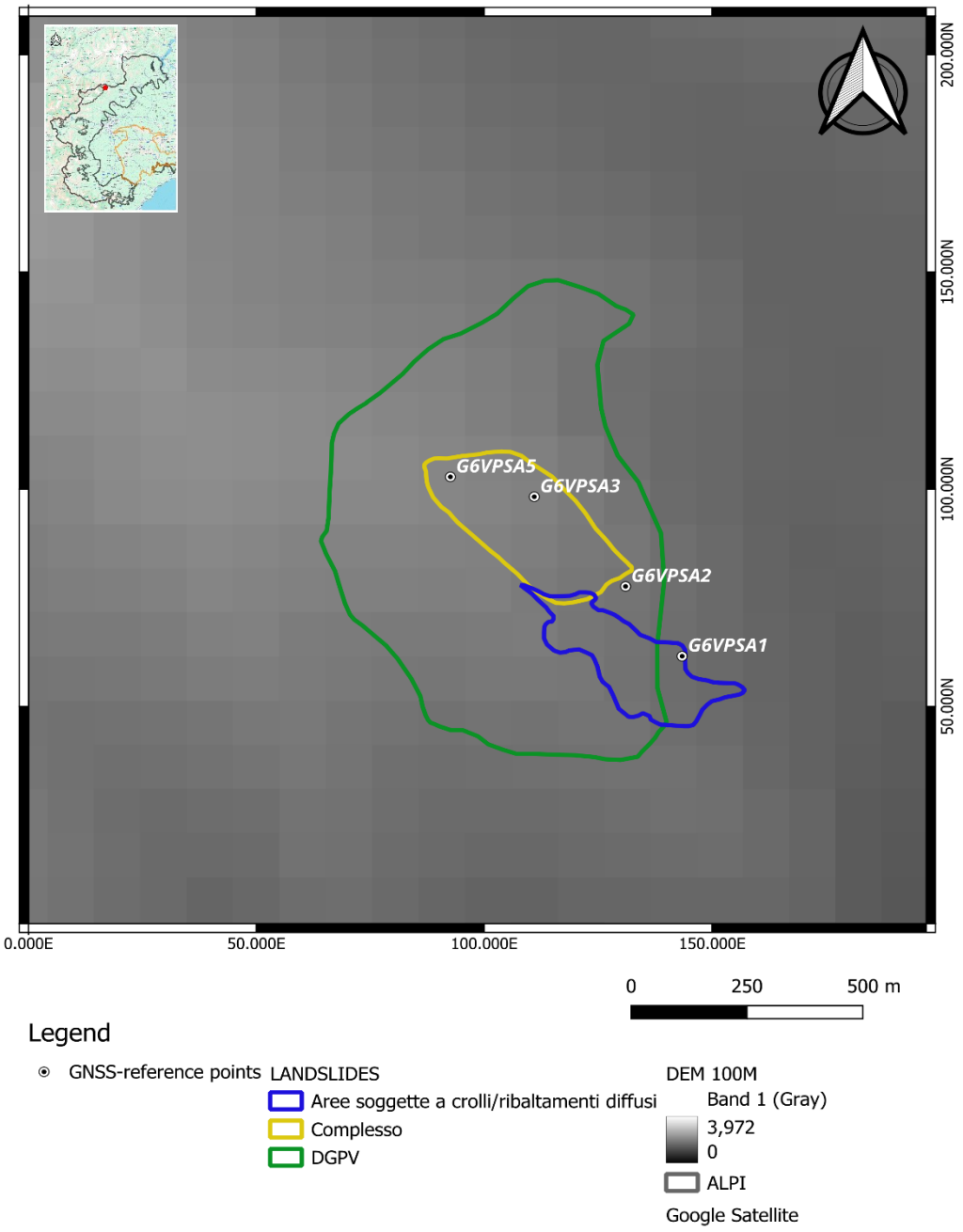

Figure 38. Digital elevation model of the Valprato Soana landslides area

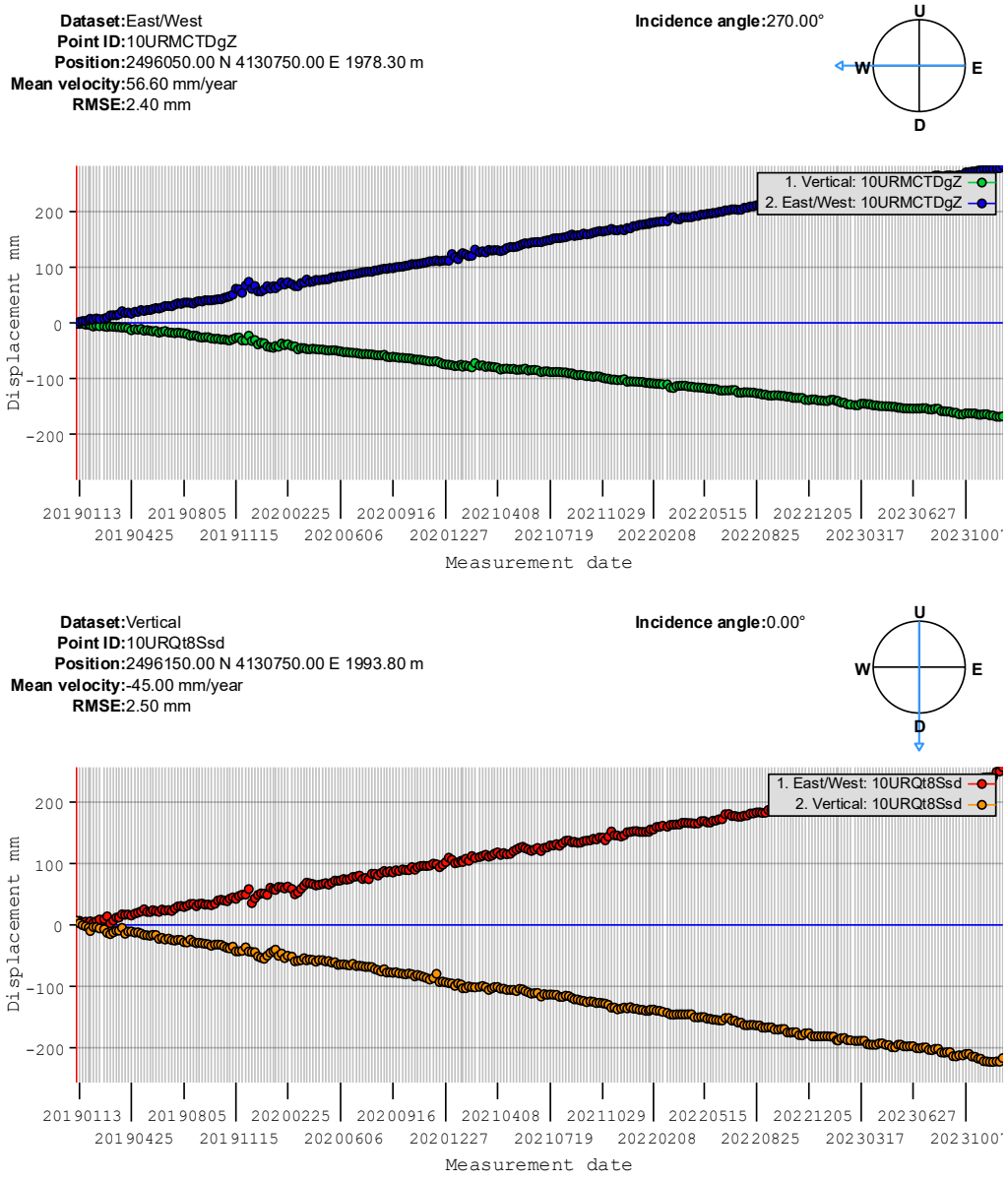

Figure 39. Representative EGMS Ortho displacement time series at Valprato Soana (source: Copernicus European Ground Motion Service, EGMS Explorer)

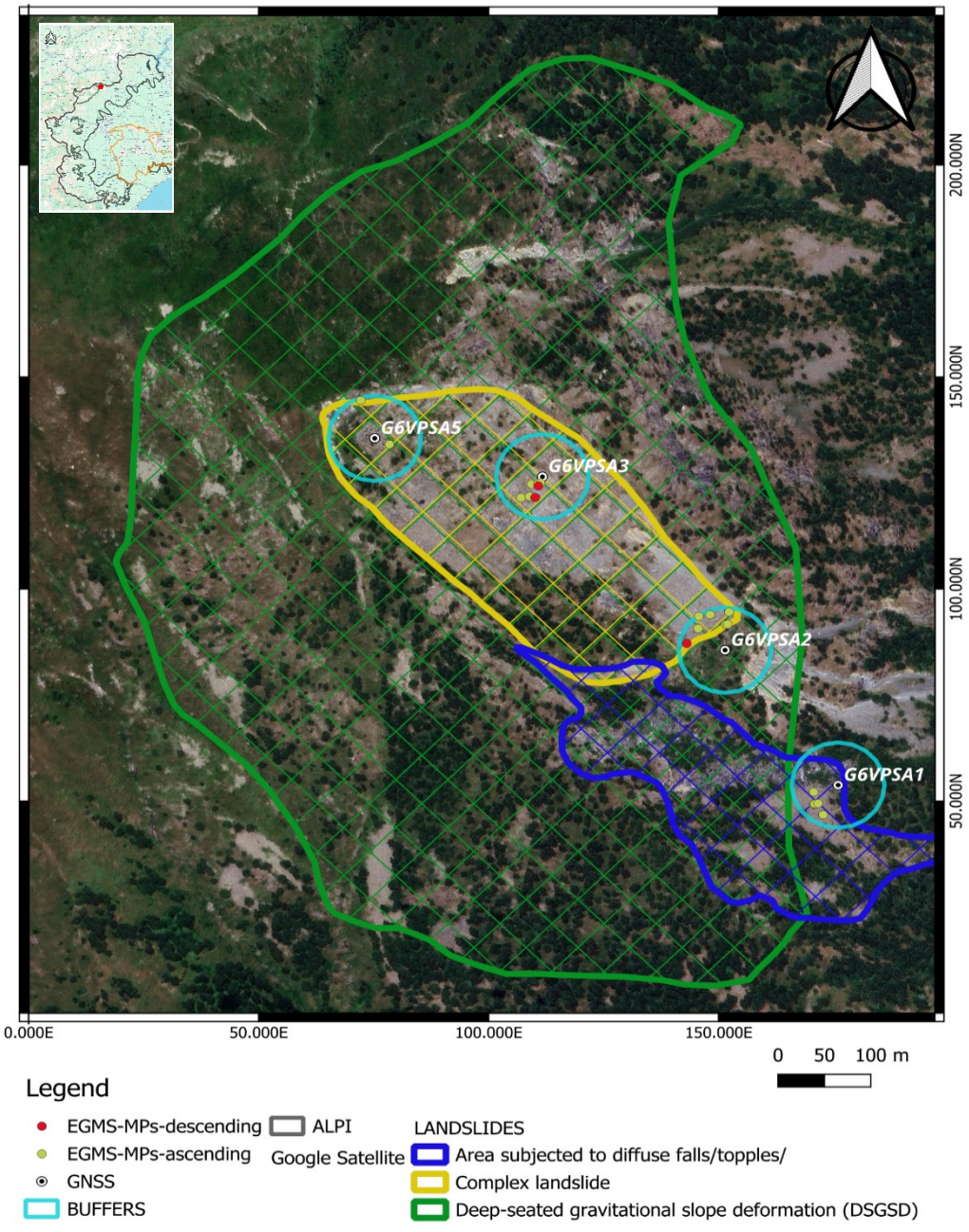

Figure 40. Spatial Distribution of GNSS Stations, EGMS Measurement Points, and Landslide Typologies in the Valprato Soana Case Study

A second very interesting exception is shown by the Sampeyre case in the analysis carried out for the ascending orbit, because here, the VSLOPE estimates are significantly lower than the mean velocities derived from GNSS measurements. According to ARPA documentation, the GNSS reference stations in this area have been relocated [Figure 41].

This relocation likely explains the observed discrepancy between EGMS-derived velocities and GNSS data, as the displacement time series is effectively interrupted or reset when stations are moved. Consequently, the GNSS averages are not directly comparable with the EGMS estimates over the same period [Figure 42].

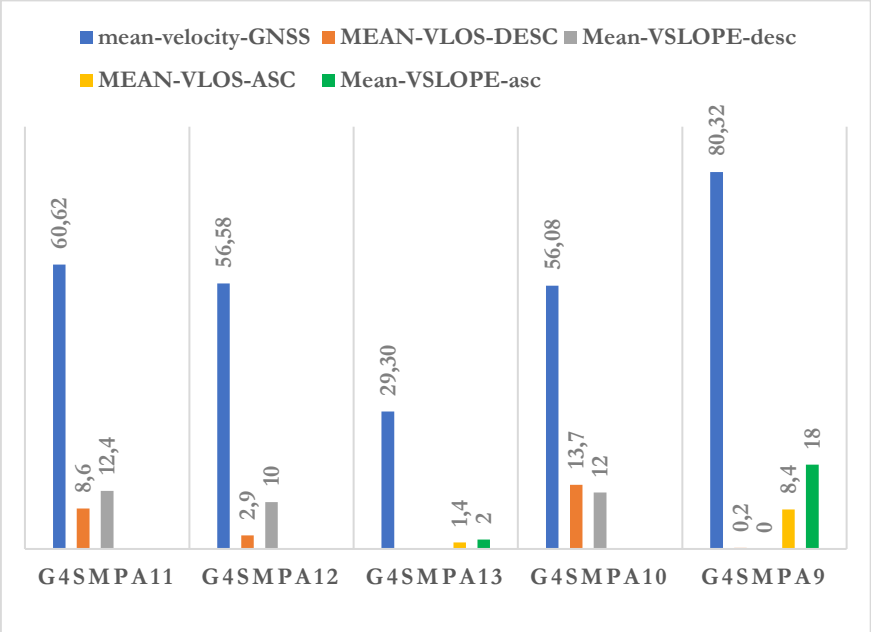

Figure 41. Comparison of GNSS Mean Velocity and EGMS Mean VLOS and VSLOPE at Selected Stations in Sampeyre

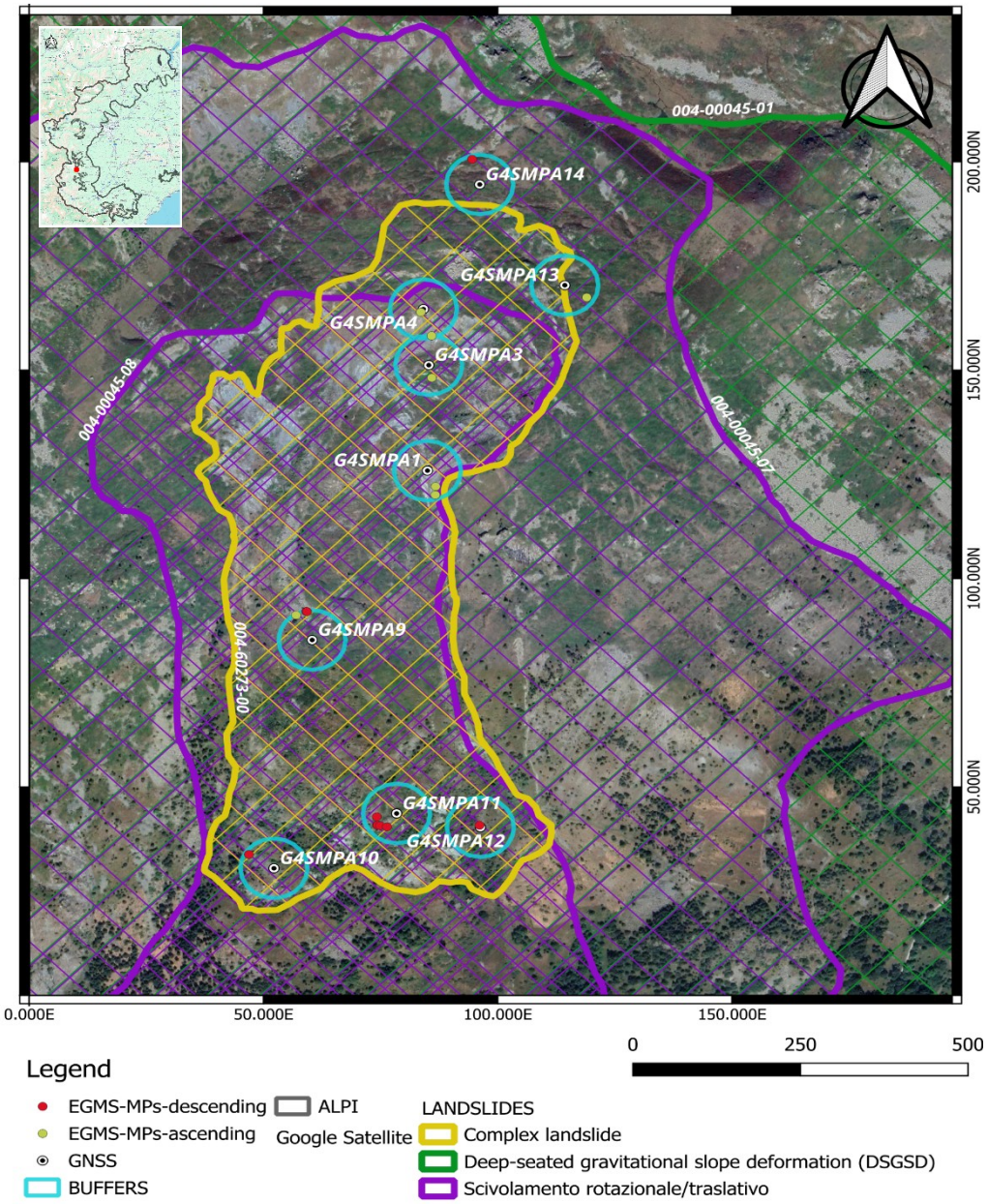

Figure 42. Spatial Distribution of GNSS Stations, EGMS Measurement Points, and Landslide Typologies in the Sampeyre Case Study

In the Paroldo case, the comparison between GNSS and EGMS-derived velocities shows a generally better agreement than in the Valprato Soana example, although most EGMS values still tend to underestimate the corresponding GNSS mean velocities [Figure 43].

Here the EGMS–GNSS comparison shows that the satellite data captures the general deformation pattern of the Paroldo landslide, identifying the same sectors as more or less active. The descending geometry is the most reliable, consistent with the higher descending visibility of the landslide, while ascending data are less robust at the landslide scale. In most cases EGMS underestimates GNSS velocity, which is expected because LOS measurements only capture one component of movement. However, at some benchmarks, especially after converting VLOS to VSLOPE, the agreement improves and becomes quite good [Figure 44].

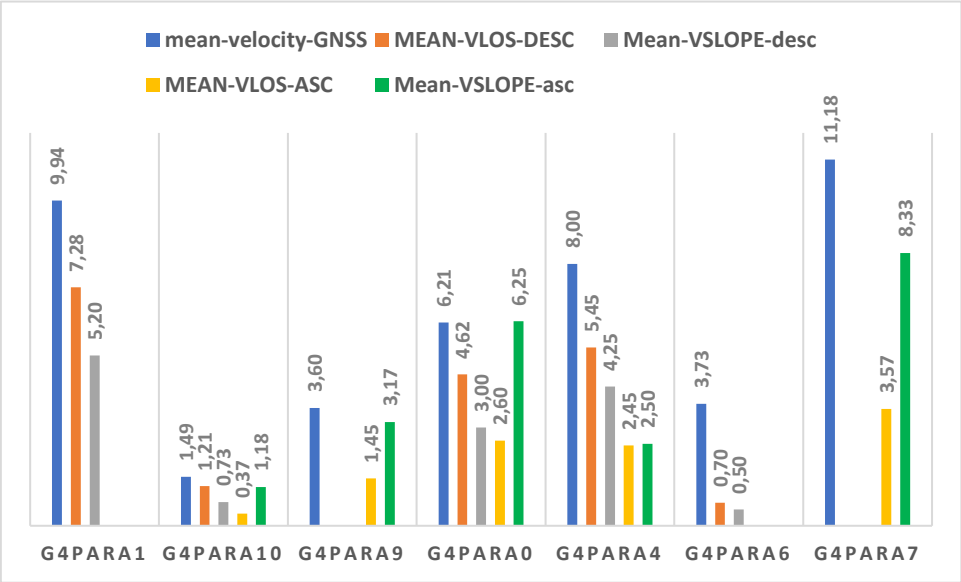

Figure 43. Comparison of GNSS Mean Velocity and EGMS Mean VLOS and VSLOPE at Selected Stations in Paroldo

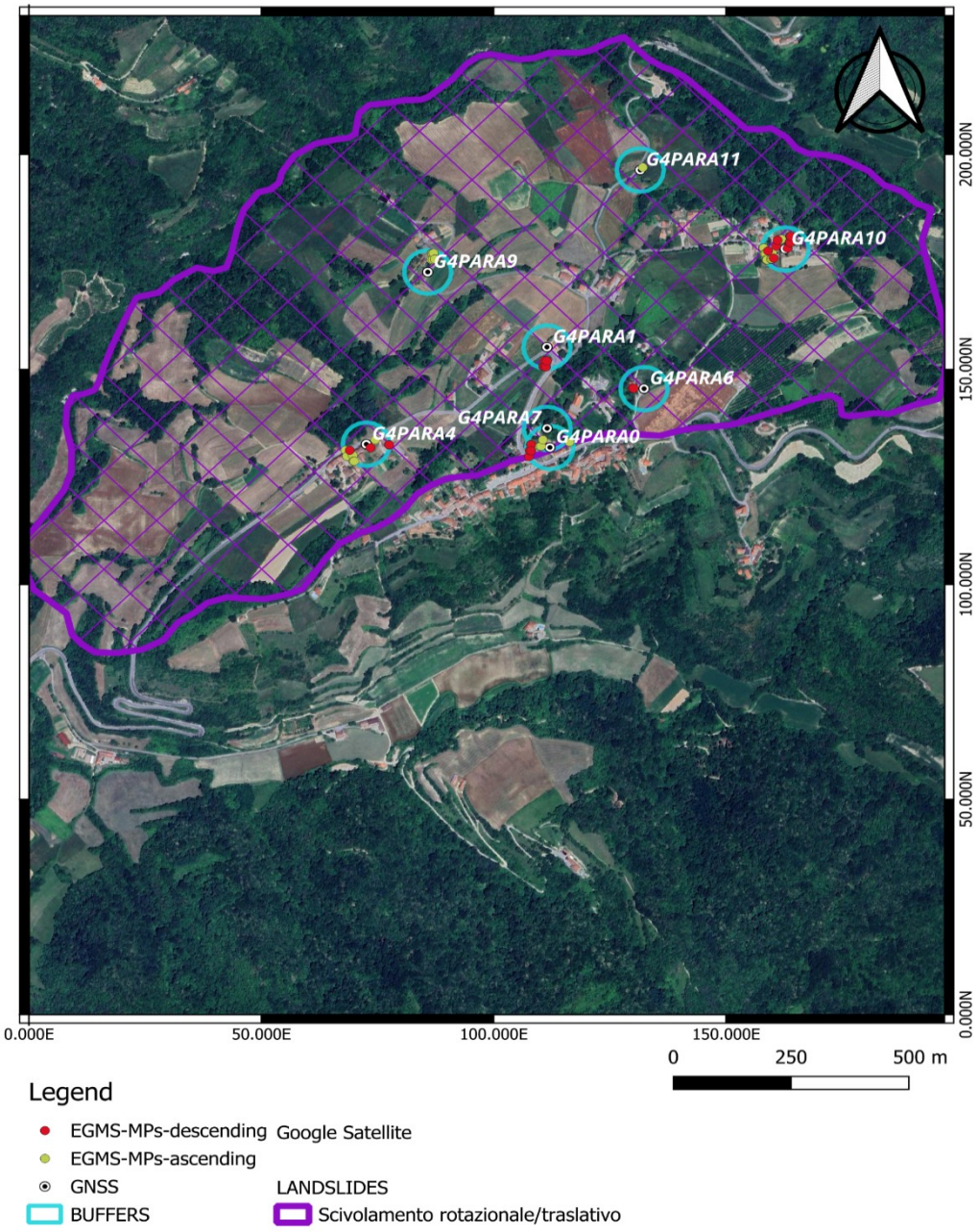

Figure 44. Spatial Distribution of GNSS Stations, EGMS Measurement Points, and Landslide Typologies in the Paroldo Case Study

The analysis of the Castelmagno case shows well that EGMS can detect the movement pattern quite consistently, even though the analysed stations are distributed across four different landslide typologies. In particular, in the cases where GNSS recorded very low or nearly zero velocities, EGMS also returned similarly low values, showing a good correspondence with the in-situ data [Figure 45].

A relatively good agreement is observed at the stations characterized by low to moderate GNSS velocities. At G4CSMA1, the descending EGMS values are very close to the GNSS mean velocity, with a mean descending VLOS of about 2.78 mm/year and a descending VSLOPE of 3.00 mm/year, compared with a GNSS value of 2.77 mm/year. A reasonable correspondence is also visible at G4CSMA8, where both ascending and descending values remain close to the GNSS mean velocity of 1.01 mm/year, and at G4CSMA3, where the ascending EGMS values are low and consistent with the very small GNSS velocity (0.25 mm/year). Another good agreement is found at G4CSMA6, where the ascending VSLOPE (4.37 mm/year) is very close to the GNSS mean velocity (4.53 mm/year), despite the lower descending values [Figure 46].

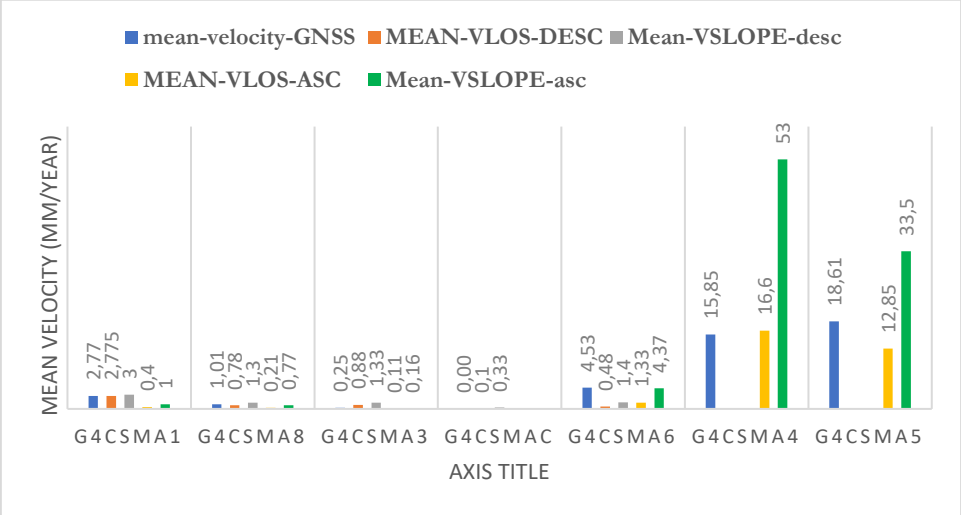

Figure 45. Comparison of GNSS Mean Velocity and EGMS Mean VLOS and VSLOPE at Selected Stations in Castelmagno

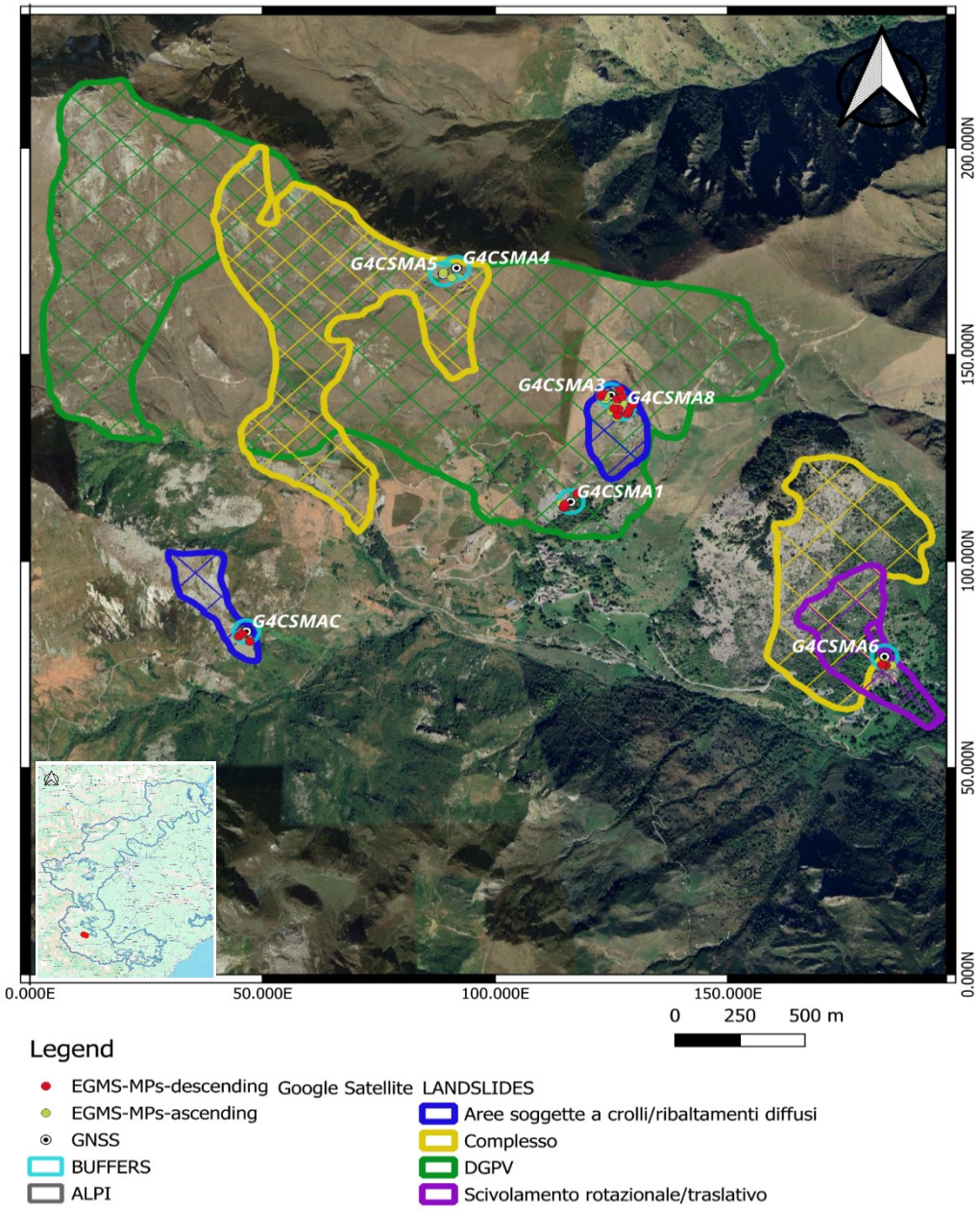

Figure 46. Spatial Distribution of GNSS Stations, EGMS Measurement Points, and Landslide Typologies in the Castelmagno Case Study

The Prunetto case is a strong example of how well EGMS can detect landslide movement. Even though the absolute values do not perfectly coincide with the GNSS measurements at every benchmark, the satellite data successfully separate the areas with very limited displacement from those showing greater activity. Points such as G4PRTC4, G4PRTC3, and G4PRTB10 display low velocities in both datasets, whereas the more active benchmarks, particularly G4PRTC5, G4PRTC6, and G4PRTC7, are also recognised by EGMS as the most mobile sectors. This suggests that EGMS is capable of reproducing the overall deformation pattern of the landslide and of identifying the relative differences in activity across the monitored area. In particular, the descending data show a closer match with the GNSS results, further supporting the reliability of EGMS in capturing the ongoing movement in this case [Figure 47], [Figure 48].

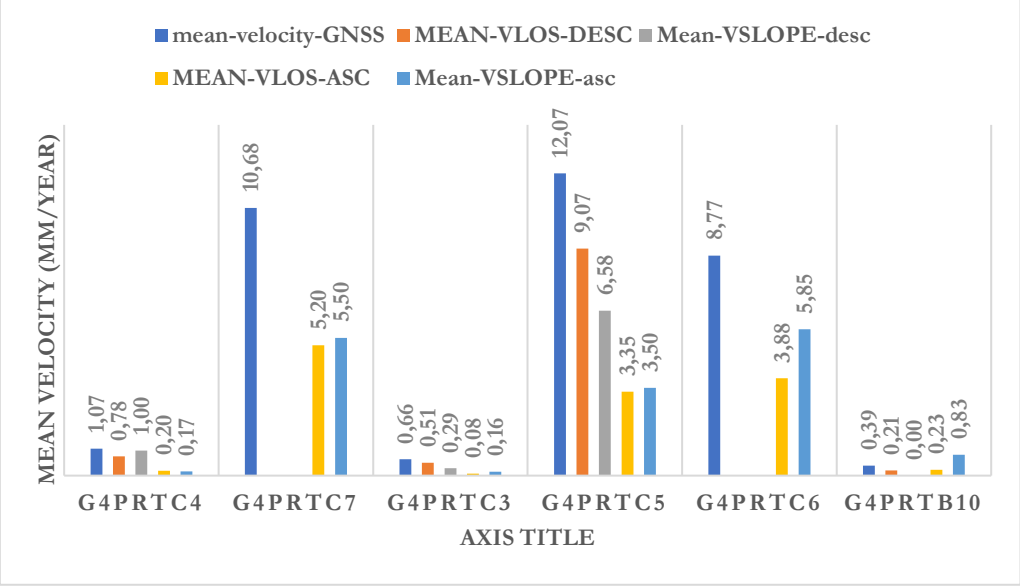

Figure 47. Comparison of GNSS Mean Velocity and EGMS Mean VLOS and VSLOPE at Selected Stations in Prunetto

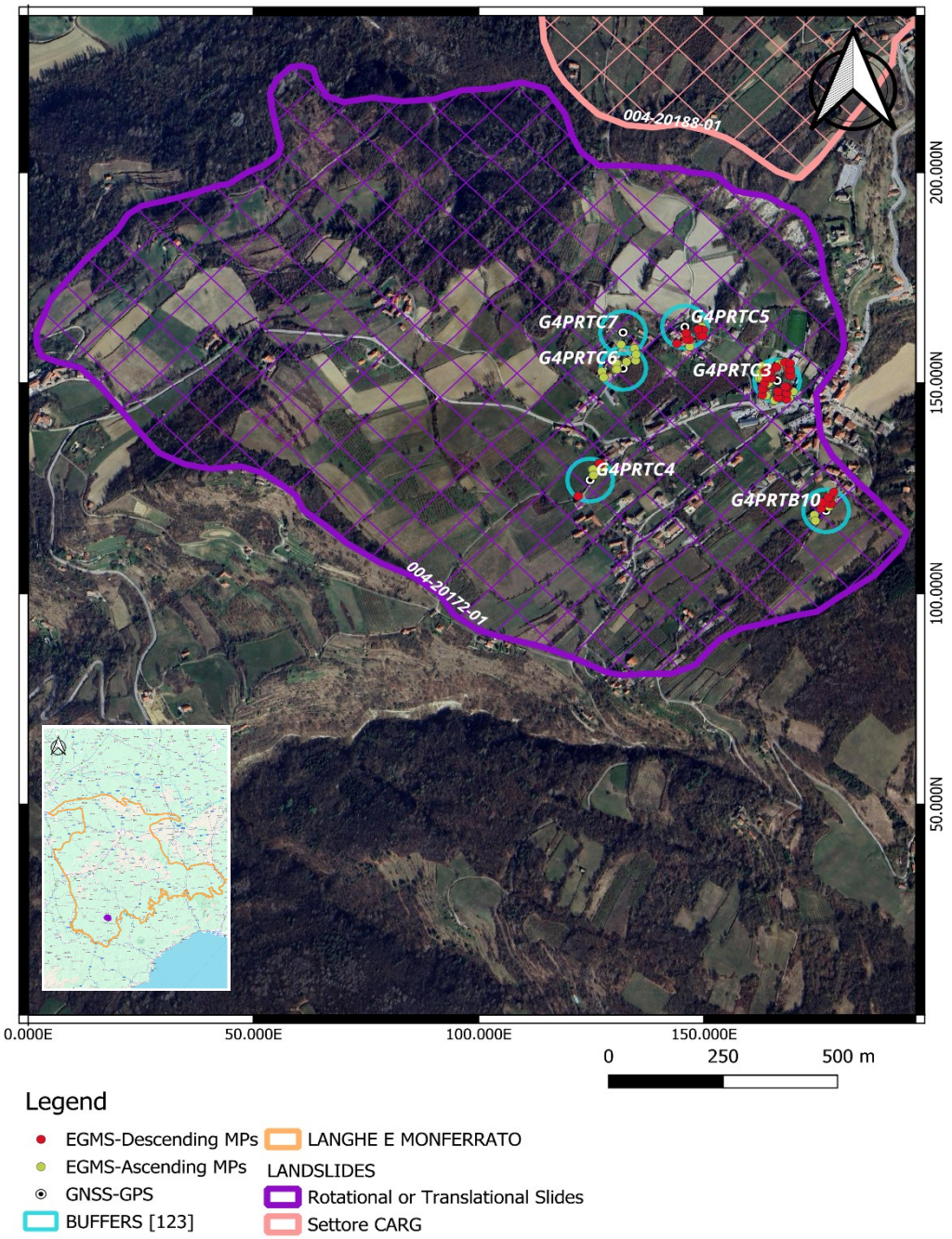

Figure 48. Spatial Distribution of GNSS Stations, EGMS Measurement Points, and Landslide Typologies in the Prunetto Case Study

5.6 COMPARISON BETWEEN EGMS AND OTHER INSAR DATASETS

The comparison between EGMS and the historical InSAR datasets was carried out for 62 selected landslides. The analysis focused on two main aspects: the number of measurement points available within each mapped landslide polygon and the mean deformation velocity recorded by each satellite mission. The number of points was considered in order to evaluate how well each dataset sampled the landslide, while the mean VLOS was used to compare the general deformation signal detected by the different missions. Since these datasets refer to different observation periods, the comparison cannot be interpreted as a direct validation. Instead, differences in the measured velocities may reflect temporal changes in landslide activity, while also being influenced by differences in acquisition geometry, wavelength, revisit time, and spatial coverage among the various SAR missions.

In this analysis I have used a chart in which for each acquisition geometry, the chart reports the available InSAR datasets along the Y axis in relation to their acquisition period along the X axis. The width of each bar represents the temporal interval covered by the corresponding dataset. The number shown inside each bar indicates the total number of measurement points (MPs) falling within the landslide polygon for that dataset. The mean velocity calculated for all MPs within the landslide polygon is represented by the color scale. The central part of the color scale, between about +2 and -2 mm/year, corresponds to movement values that are within the uncertainty range. Negative and positive values represent motion away from or toward the satellite, respectively [Figure 49].

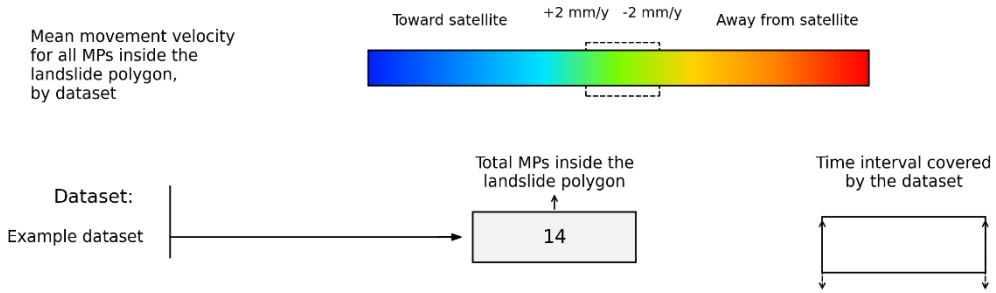

Figure 49. The legend of the graphs

Hear I have brought the analysis for the landslides that have been selected in perivious GNSS-EGMS comparison as the cases with the highest differences. One of the cases analysed in the previous section is the landslide located in Valprato Soana. In this case, two

GNSS reference points within the complex landslide sector, G6VPSA3 and G6VPSA5, were examined in greater detail. At this stage, it is useful to examine what the historical InSAR datasets indicate for the same landslide, in order to verify whether the deformation detected by EGMS is consistent with the previous satellite observations and to assess whether any relevant changes in activity may have occurred over time [Table 32].

In the ascending geometry, the historical datasets available for the Valprato Soana landslide, namely Radarsat (2003–2009), COSMO-SkyMed (2011–2014), Sentinel-1 (2014–2020), and EGMS (2019–2023), all detect relatively high mean VLOS values in absolute terms. This indicates that the landslide movement is consistently captured over time by different missions and suggests a persistent deformation pattern. In contrast, in the descending geometry, only Sentinel-1 and EGMS provide measurements, and both show much lower mean VLOS values than those observed in the ascending orbit. This means that the descending geometry captures only a smaller component of the actual movement [Figure 50], [Figure 51].

As the comparison between historical datasets and EGMS cannot be interpreted as a strict quantitative validation. Instead, it is more meaningful as a qualitative and multi-temporal assessment of whether the same landslide sector has been repeatedly identified as deforming by different SAR missions. In the case of Valprato Soana, the ascending datasets clearly support this interpretation, because despite their differences, they all detect a strong deformation signal with the same general sign and with relatively high absolute magnitudes.

Table 32. number of MPs and Mean VLOS of InSAR datasets for landslide 001-02042-04

INSAR Dataset	Mean-VLOS mm/year	Number-PS
ERS_ASC	-	-
ERS_DESC	-	-
RSAT_ASC	-52,30	22
RSAT_DESC	-	-
ENVISAT_ASC	-	-
ENVISAT_DESC	-	-
COSMO-ASC	-18,93	439
COSMO-DESC	-	-
SENTINEL-ASC	-59,41	98
SENTINEL-DESC	8,82	38
EGMS-ASC-088	-56,12	278
EGMS-DESC-066	3,70	186

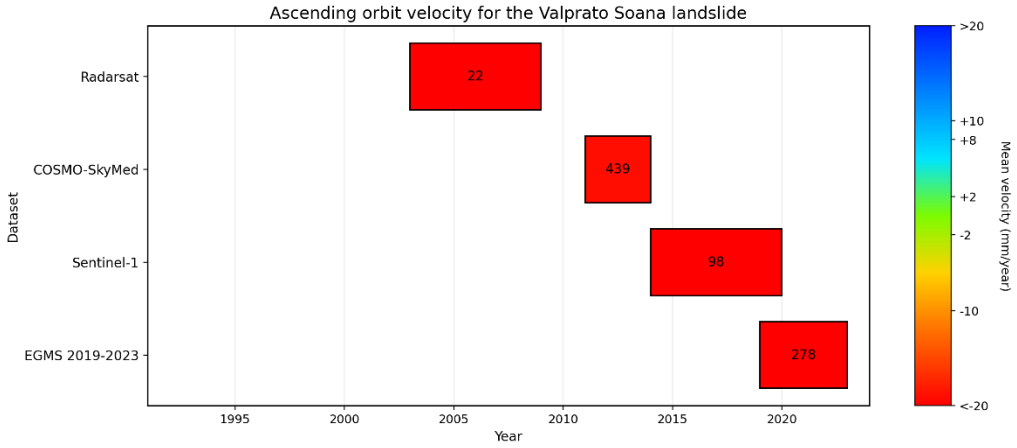

Figure 50. Mean VLOS of Ascending InSAR datasets for landslide 001-02042-04

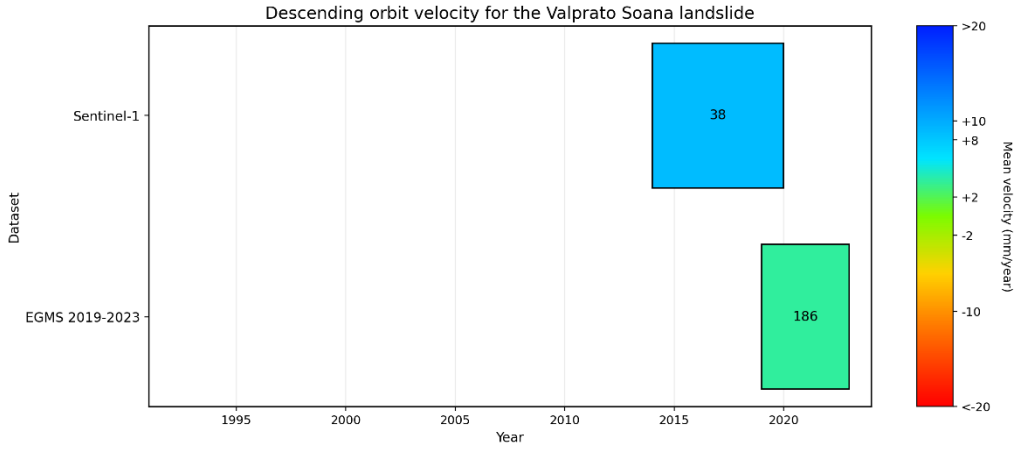

Figure 51. Mean VLOS of Descending InSAR datasets for landslide 001-02042-04

The comparison between EGMS and the historical InSAR datasets for the selected landslide in the Sampeyre Comune shows a deformation pattern that remains coherent through time. In the ascending geometry, both Radarsat and EGMS record negative mean VLOS values, indicating that the landslide movement has been detected in the same general direction in both observation periods. EGMS shows a more negative mean value than Radarsat, which may suggest stronger recent deformation, although part of this difference can also be related to the different observation periods and acquisition characteristics of the two datasets [Table 33].

The descending geometry confirms the same general behaviour. Radarsat, COSMO-SkyMed, and EGMS all show negative mean VLOS values, indicating persistent movement away from the satellite. In particular, the agreement between COSMO-SkyMed and EGMS is relatively good, and both datasets provide a much larger number of measurement points than Radarsat, making their estimates more spatially representative of the landslide. Overall, these results suggest that the deformation detected by EGMS is consistent with previous satellite observations and reflects a long-term active condition of the slope. Differences in velocity magnitude should be interpreted carefully, because the datasets belong to different periods and were acquired by SAR missions with different wavelength and revisit characteristics [Figure 52], [Figure 53].

Table 33. number of MPs and Mean VLOS of InSAR datasets for landslide 004-60273-00

INSAR Dataset	Mean-VLOS mm/year	Number-MPs
ERS_ASC		
ERS_DESC		
RSAT_ASC	-11,10157895	38
RSAT_DESC	-7,17	23
ENVISAT_ASC		
ENVISAT_DESC		
COSMO-ASC		
COSMO-DESC	-9,229879518	415
SENTINEL-ASC		
SENTINEL-DESC		
EGMS-ASC-088	-16,093952	463
EGMS-DESC-066	-9,540596	537

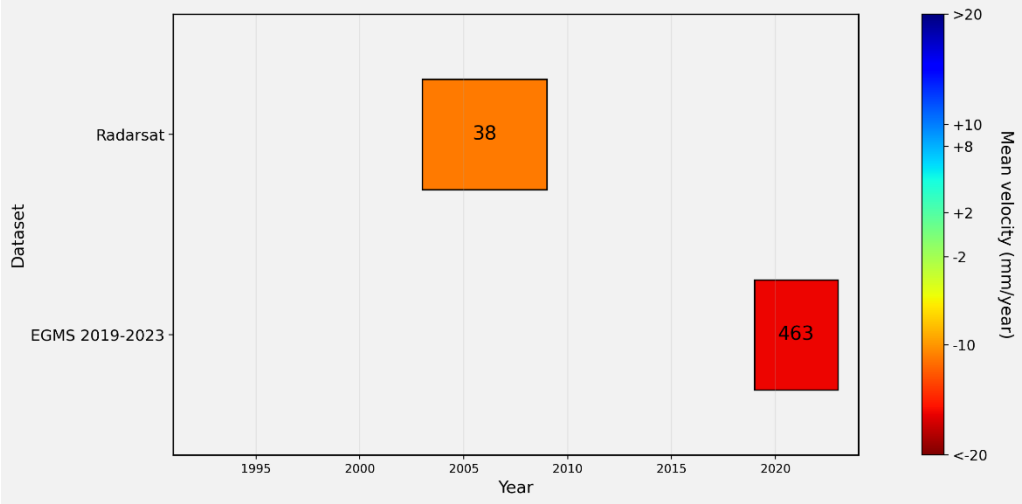

Figure 52. Mean VLOS of Ascending InSAR datasets for landslide 004-60273-00

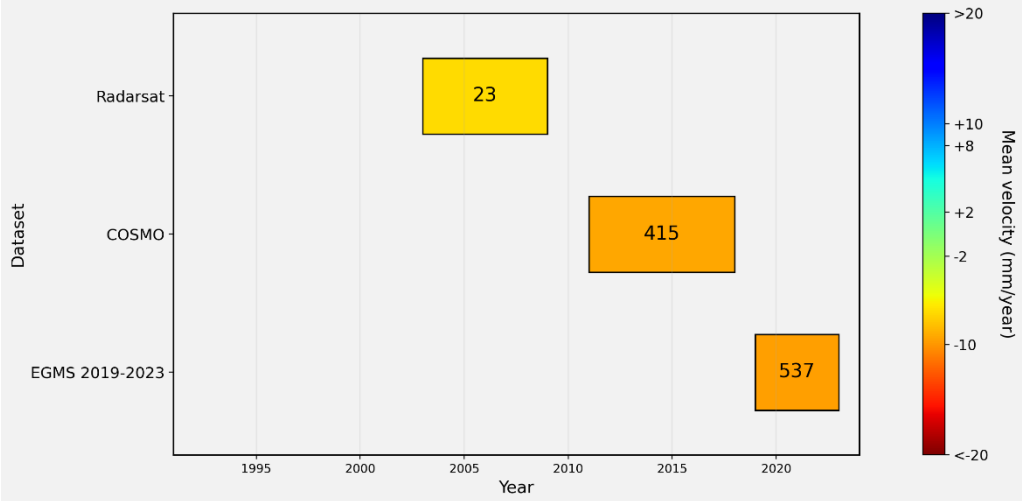

Figure 53. Mean VLOS of Descending InSAR datasets for landslide 001-02042-04

The comparison between EGMS and the historical InSAR datasets for the Paroldo landslide shows a generally coherent and low-magnitude deformation pattern through time. In the ascending geometry, ERS, Radarsat, ENVISAT, and EGMS all record mean VLOS values close to zero and slightly positive, suggesting that the landslide has remained active only at a modest rate over the different observation periods. In the descending geometry, Radarsat, ENVISAT, and EGMS all show negative values, with slightly greater absolute magnitudes than in the ascending orbit. This indicates that the descending geometry may better capture the main component of movement [Table 34].

Although the differences between the datasets should be interpreted carefully because they refer to different time intervals and different SAR missions, the overall agreement suggests that the deformation detected by EGMS is coherent with the historical InSAR observations. Therefore, the Paroldo case can be interpreted as a landslide characterised by persistent but weak deformation, with no clear evidence of major changes in activity state through time. [Figure 54], [Figure 55].

Table 34. number of MPs and Mean VLOS of InSAR datasets for landslide 004-20283-01

ERS_ASC	1,56	6
ERS_DESC	-	-
RSAT_ASC	0,95	36
RSAT_DESC	-2,95	36
ENVISAT_ASC	0,97	10
ENVISAT_DESC	-1,72	42
COSMO-ASC	-	-
COSMO-DESC	-	-
SENTINEL-ASC	-	-
SENTINEL-DESC	-	-
EGMS-ASC-088	0,20	327
EGMS-DESC-066	-4,67	306

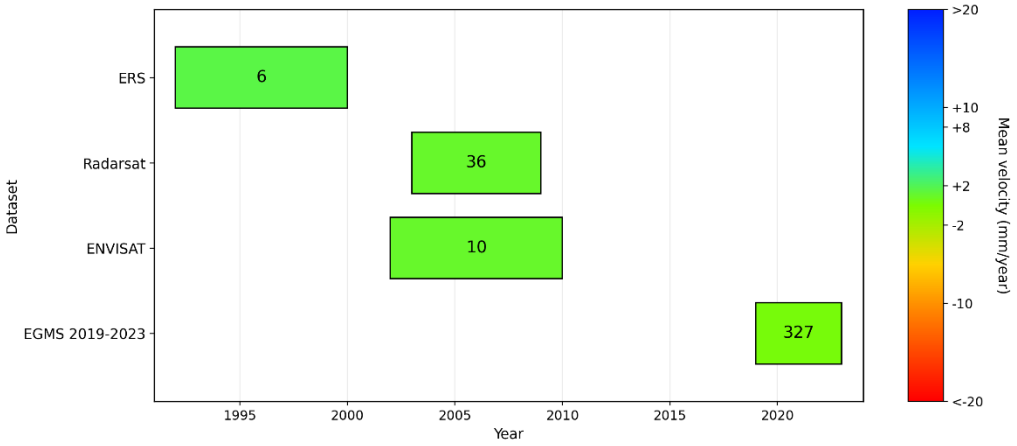

Figure 54. Mean VLOS of Ascending InSAR datasets for landslide 004-20283-01

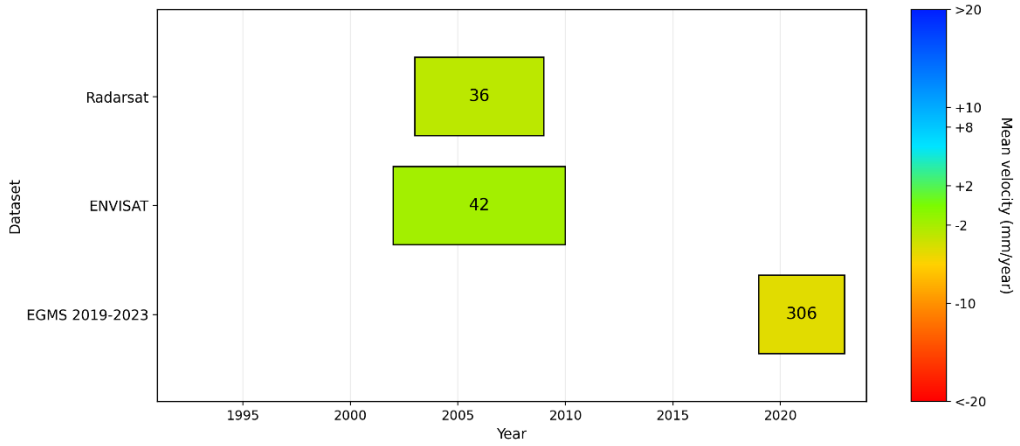

Figure 55. Mean VLOS of Descending InSAR datasets for landslide 004-20283-01

Within the Castelmagno landslide, located in the Alpine region and classified in SIFraP as a complex landslide (code 004-00061-04), the two charts show that both the historical InSAR data and the EGMS product detect deformation with consistently negative mean VLOS values. In the ascending geometry, only Radarsat and EGMS provide usable measurements. Radarsat shows a mean VLOS of about -3.0 mm/year, while EGMS gives a slightly more negative value of about -4.0 mm/year. This indicates that the landslide was already detectable in the historical period and that the recent EGMS observations confirm the persistence of movement. The much larger number of EGMS measurement points compared with Radarsat also suggests a more spatially representative estimate in the recent period [Table 35].

The descending chart shows the same general behaviour, but with stronger negative values. Radarsat records a mean VLOS of about -6.5 mm/year, while EGMS reaches about -6.9 mm/year. This close agreement between the historical and recent datasets indicates continuity of deformation over time, without major differences in the overall magnitude of the movement. The descending geometry therefore appears to capture the slope motion more effectively than the ascending one, since it provides both higher absolute velocities and a higher number of measurement points. Overall, the two charts suggest that Castelmagno is characterized by persistent slow movement, clearly visible in both observation periods, with the descending datasets offering the most robust representation of the landslide kinematics [Figure 56], [Figure 57].

Table 35. number of MPs and Mean VLOS of InSAR datasets for landslide 004-00061-04

INSAR Dataset	Mean-VLOS mm/year	Number-PS
ERS_ASC	-	-
ERS_DESC	-	-
RSAT_ASC	-3,02	60
RSAT_DESC	-6,50	92
ENVISAT_ASC	-	-
ENVISAT_DESC	-	-
COSMO-ASC	-	-
COSMO-DESC	-	-
SENTINEL-ASC	-	-
SENTINEL-DESC	-	-
EGMS-ASC-088	-4,04	906
EGMS-DESC-066	-6,94	1316

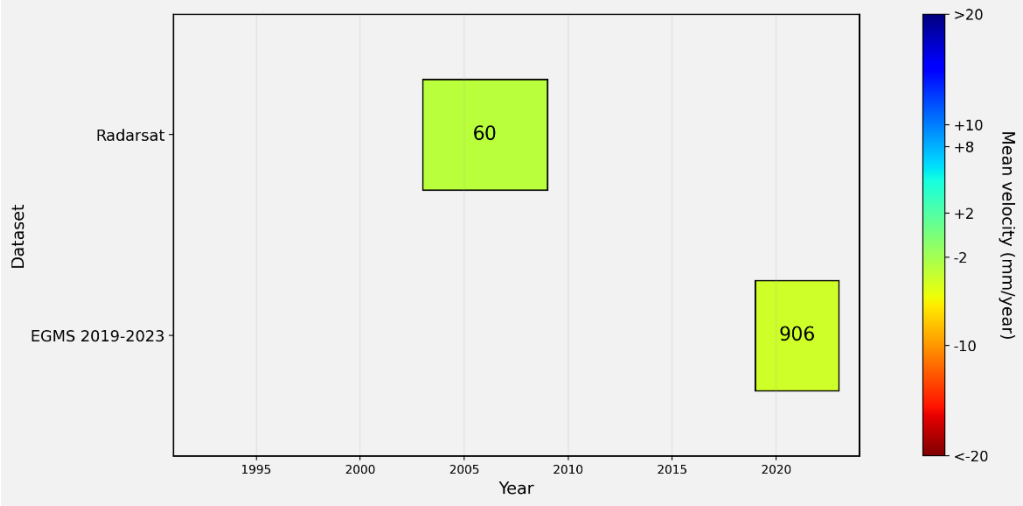

Figure 56. Mean VLOS of Ascending InSAR datasets for landslide 004-00061-04

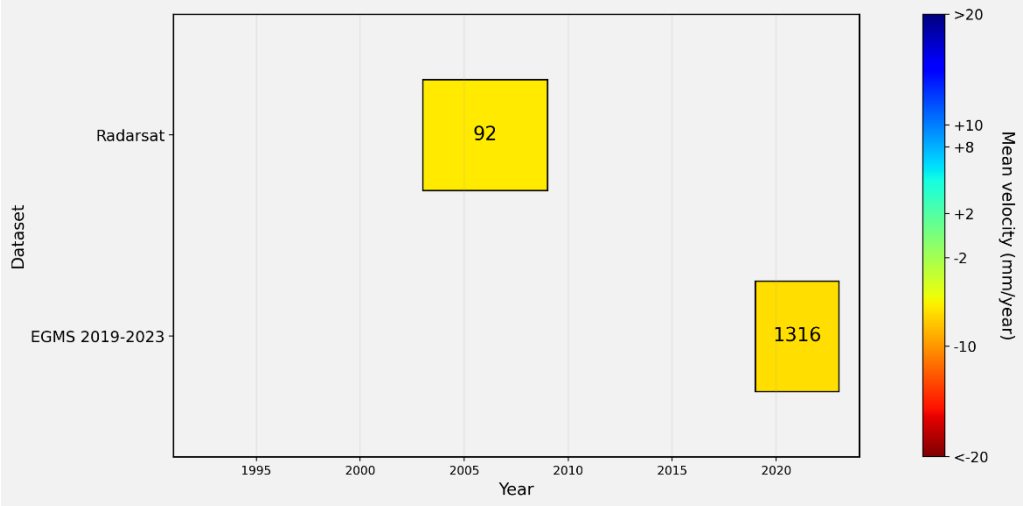

Figure 57. Mean VLOS of Descending InSAR datasets for landslide 004-00061-04

5.7 TIME-SERIES COMPARISON BETWEEN EGMS AND GNSS

The comparison of cumulative displacement time series derived from EGMS MPs within the buffers around the GNSS benchmarks at Valprato Soana provides an additional perspective on landslide movement trend through time. In this case, the main advantage of EGMS lies in its much denser temporal sampling compared with manual GNSS surveys. Because the satellite observations are acquired at much shorter intervals, they allow a more continuous reconstruction of deformation and make it easier to recognise short-term fluctuations, temporary accelerations, and changes in movement rate that may be associated with external triggering factors, such as periods of heavy precipitation. By contrast, GNSS measurements, although more accurate at the benchmark location, are available only at discrete survey dates and therefore cannot describe the intermediate evolution of displacement with the same level of detail. For this reason, the EGMS time series are particularly useful for understanding the temporal behaviour of the landslide, even where the absolute magnitude of the projected displacement must be interpreted with caution.

The time-series comparison further confirms the interpretation proposed in the previous section, showing that the projection of LOS displacement along the slope, especially for the ascending orbit, is the main reason for the observed mismatch with GNSS. In particular, the stronger increase of the ascending slope-parallel series relative to both GNSS and LOS measurements indicates that the discrepancy is introduced mainly during the slope-projection step rather than by poor quality of the EGMS signal itself.

At G6VPSA1, the ascending EGMS time series along the line of sight of satellite shows a clear and progressive increase in displacement through time, confirming that the satellite is able to detect ongoing movement in the sector around the benchmark. Although the agreement with GNSS is not exact, the temporal trend is coherent and persistent. The EGMS series also shows short-term fluctuations that are not visible in the GNSS record, highlighting the added value of the denser satellite sampling for describing the evolution of deformation between field campaigns [Figure 58].

G6VPSA2 shows the best overall correspondence between GNSS and EGMS. Both ascending and descending time series indicate a progressive accumulation of displacement, confirming persistent motion in the monitored sector. The ascending series follows the GNSS trend more closely, whereas the descending one remains weaker and less representative. This case therefore provides a positive example of the capability of EGMS to reproduce the temporal behaviour of the landslide and to complement GNSS observations by showing the continuity of movement through time [Figure 59], [Figure 60].

At G6VPSA3, the time-series comparison is consistent with the interpretation already discussed in the previous section. The ascending EGMS series shows a strong, coherent, and nearly linear increase in cumulative displacement, confirming that the satellite captures a real and persistent deformation signal. At the same time, its stronger increase relative to GNSS supports the idea that the main discrepancy is introduced during the LOS-to-slope projection step rather than by poor quality of the EGMS measurements. The descending series, by contrast, shows a much weaker response and underestimates the displacement observed by GNSS. Even so, both time series confirm the continuity of movement and demonstrate the usefulness of EGMS for tracking the temporal evolution of deformation [Figure 61], [Figure 62].

A similar pattern is observed at G6VPSA5, where the ascending EGMS series also shows a regular cumulative increase through time. Although the absolute values differ from GNSS, the overall trend confirms that the benchmark is located in a persistently moving sector of the landslide. In this case, the absence of representative descending measurements limits a two-geometry comparison, but the ascending time series still provides useful information on the evolution of displacement and again illustrates the advantage of EGMS in capturing intermediate variations between GNSS campaigns [Figure 63].

Overall, the Valprato Soana example highlights that the main strength of EGMS time series is not only their ability to detect displacement, but also their capacity to describe its temporal evolution in much greater detail than campaign-based ground monitoring. Even where local geometry and slope projection influence the quantitative agreement with GNSS, the short interval between satellite acquisitions makes it possible to identify periods of more active deformation, temporary changes in movement rate, and possible acceleration of movement, probably correlated with heavy precipitation occurring during the monitoring period.

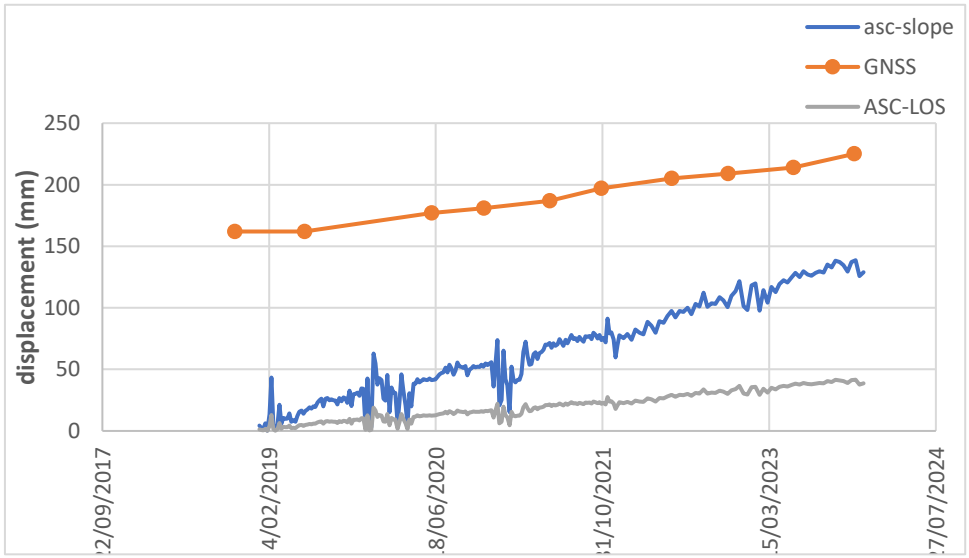

Figure 58. Time-series comparison between GNSS and ascending EGMS displacement at benchmark G6VPSA1, Valprato Soan

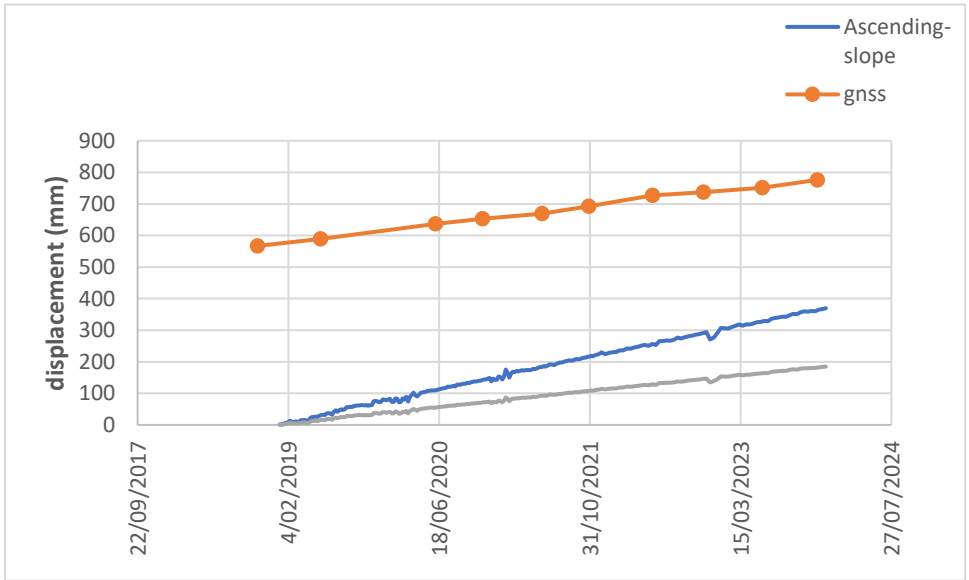

Figure 59. Time-series comparison between GNSS and ascending EGMS displacement at benchmark G6VPSA2, Valprato Soan

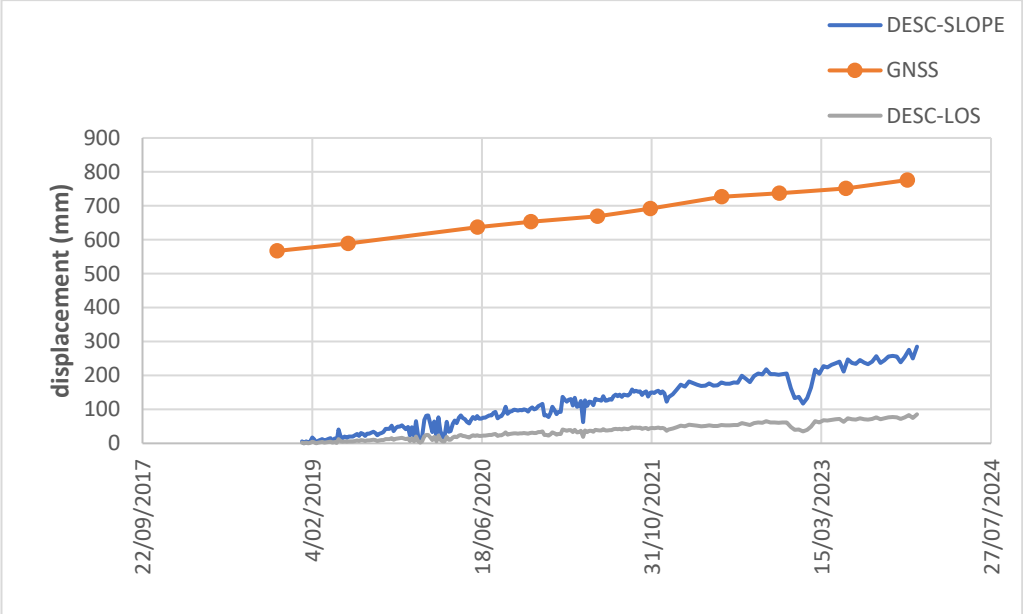

Figure 60. Time-series comparison between GNSS and descending EGMS displacement at benchmark G6VPSA2, Valprato Soan

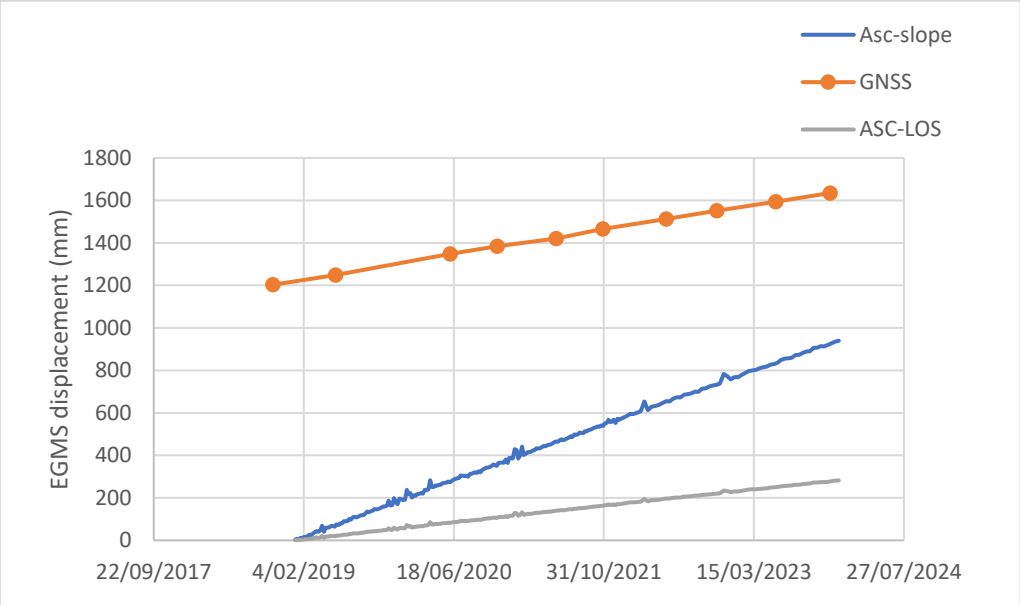

Figure 61. Time-series comparison between GNSS and ascending EGMS displacement at benchmark G6VPSA3, Valprato Soan

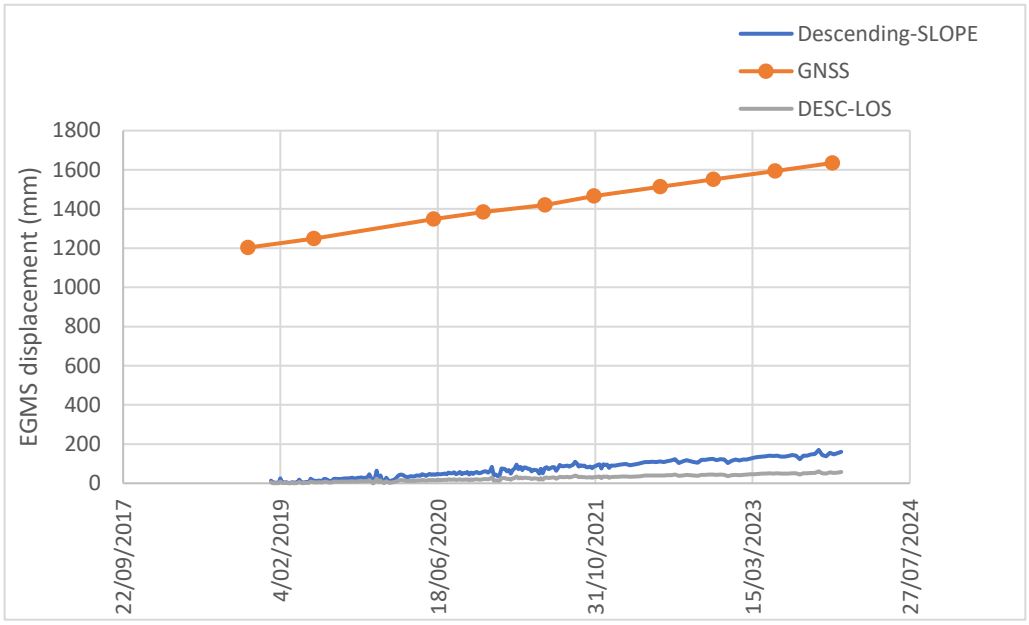

Figure 62. Time-series comparison between GNSS and descending EGMS displacement at benchmark G6VPSA3, Valprato Soan

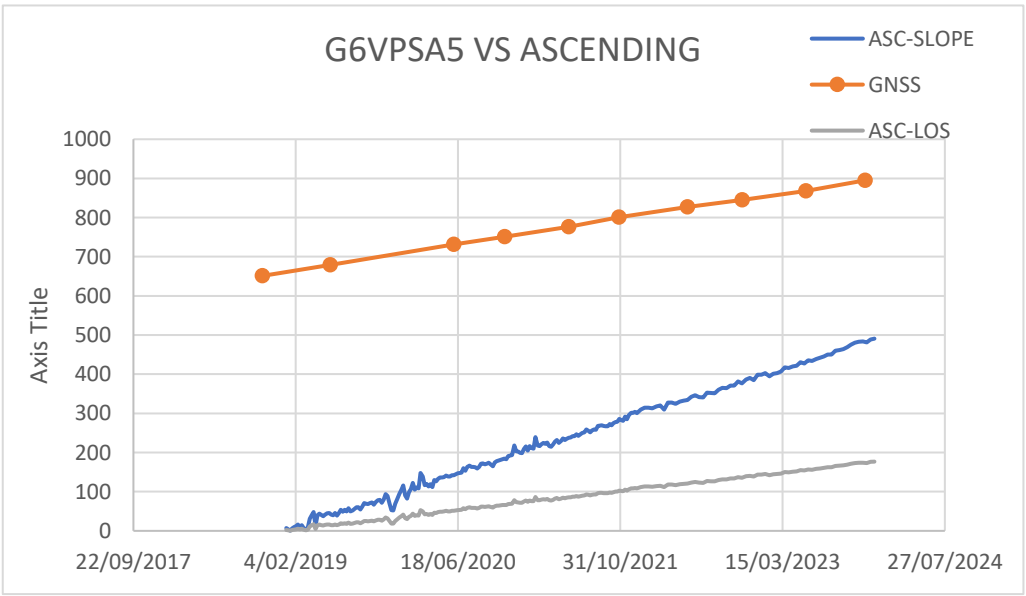

Figure 63. Time-series comparison between GNSS and ascending EGMS displacement at benchmark G6VPSA5, Valprato Soan

6.SUMMARY OF RESULTS AND CONCLUSIONS

This thesis assessed the usefulness of the European Ground Motion Service for landslide monitoring in the Piemonte Region by combining regional inventory analysis, comparison with GNSS measurements, and comparison with historical multi-temporal InSAR datasets. The objective was not only to verify whether EGMS detects deformation inside mapped landslides, but also to understand how reliable and meaningful this information is when interpreted in a regional landslide-monitoring framework.

At the regional scale, the results show that EGMS represents an important source of information for landslide analysis, although its coverage is not uniform across the whole region. In most sub-areas, the largest proportion of landslides containing measurement points is associated with a limited number of dominant geometries, especially ascending orbit 088 and descending orbit 066. Even so, the distribution of the covered landslides by state of activity generally remains consistent with the distribution reported in the PAI inventory. This means that, although the service does not observe all landslides equally well, it still provides a meaningful sample of the regional landslide framework.

The analysis by typology also shows that EGMS performs better for some landslide classes than for others. In general, the service is more effective in relation to landslides characterised by slow or progressive deformation, while its performance is weaker for faster processes. This is particularly clear in the Alpine sector, where deep-seated gravitational slope deformations and other slow-moving types are well represented, whereas rapid flows remain much less covered. This result confirms that EGMS is especially suitable for the study of slow-moving landslides, which are also the most compatible with the temporal and kinematic characteristics of InSAR measurements.

The kinematic analysis based on mean VLOS shows that most mapped landslides containing EGMS measurement points are characterised by low average LOS motion during the 2019–2023 period. In all sub-areas, the frequency distributions are strongly concentrated around 0 mm/year, with most values falling within approximately ±2 mm/year. This indicates that the regional dataset is dominated by landslides showing either very slow motion or velocities close to the uncertainty range of the measurements. However, the Alps display a wider distribution and more extreme values than the other sub-areas, indicating a greater variability of deformation and the presence of a limited number of landslides with stronger motion signals. This point is important because it shows that EGMS is useful not only for describing the general low-motion background of the regional inventory, but also for highlighting the smaller subset of cases characterised by more pronounced deformation.

Another significant result is that detectable motion is not restricted to landslides classified as active. In several sectors, dormant landslides also exceed the selected absolute mean VLOS thresholds, and a limited number of stabilised landslides show values greater than 3 mm/year. This does not automatically imply reclassification, but it suggests that some polygons currently mapped as dormant or stabilised may deserve renewed attention, especially where the detected motion is supported by a sufficient number of measurement points. In this sense, EGMS proves useful as a screening tool for identifying landslides that may require more detailed investigation.

The comparison with GNSS provides a more detailed assessment of EGMS reliability. After the selection of the subset suitable for validation, the analysis was carried out on 123 buffers distributed within 62 landslides. The general result is that mean EGMS VLOS tends to underestimate GNSS mean velocity. This is expected, because the satellite records only the component of motion projected along the line of sight, while GNSS provides a more direct measurement of surface displacement. The difference becomes more evident at higher velocities, where the EGMS values no longer increase proportionally to the GNSS ones.

The use of VSLOPE partly improves the physical meaning of the comparison, because it projects the LOS velocity along the slope direction. However, the results show that this step does not always improve the agreement. In some cases, it provides more realistic values, while in others it amplifies the mismatch. This is clearly shown by the Valprato Soana case, where the ascending VSLOPE strongly exceeds the corresponding GNSS velocity at some stations. The detailed analysis suggests that this is related to unfavourable local geometry, low C-index values, complex landslide behaviour, and the limitations of the slope-projection step itself. By contrast, other cases such as Paroldo, Castelmagno, and especially Prunetto show that EGMS can reproduce the general deformation pattern of the landslide reasonably well, particularly in descending geometry and where the geomorphological setting is more regular.

The time-series comparison further highlights one of the main advantages of EGMS. Even when the absolute agreement with GNSS is not perfect, EGMS provides a much denser temporal description of landslide behaviour than campaign-based ground measurements. This makes it possible to observe intermediate fluctuations, short-term changes in movement rate, and possible acceleration phases that are much more difficult to recognise from sparse GNSS surveys alone. For this reason, the value of EGMS is not limited to mean velocity comparison, but also lies in its ability to describe the temporal evolution of deformation in much greater detail.

The comparison with historical InSAR datasets also highlights the importance of EGMS within a broader multi-temporal perspective. Since the historical and recent datasets belong

to different observation periods and are also influenced by differences in acquisition geometry, wavelength, revisit time, and spatial coverage, the comparison cannot be interpreted as a direct validation. Rather, it helps to assess whether the recent deformation detected by EGMS is consistent with the longer-term behaviour of the same landslides. In several cases, the EGMS results are coherent with the signals observed by older satellite missions. Castelmagno is a clear example of this, showing a deformation pattern that remains in good agreement with the historical Radarsat data, especially in the descending geometry. Similar continuity is also visible in other selected landslides, indicating that EGMS can be interpreted as the most recent part of a longer deformation history rather than as an isolated source of information.

Overall, the results of this thesis show that EGMS is a useful and valuable tool for regional landslide monitoring in Piemonte. Its main strengths are the wide spatial coverage, the consistency of the product, the possibility of analysing large numbers of landslides within a common framework, and the dense temporal sampling of the displacement time series. At the same time, the study also highlights its main limitations. EGMS coverage is not uniform, LOS measurements systematically underestimate real displacement, the VSLOPE transformation is sensitive to topography and local geometry, and the reliability of the results decreases where only a few measurement points are available or where the landslide behaviour is particularly complex.

In conclusion, EGMS should be considered a complementary tool rather than a substitute for in situ monitoring. Its real strength lies in its capacity to support regional-scale interpretation, to identify landslides or sectors that deserve further attention, and to provide deformation information where direct monitoring is not available. When combined with landslide inventories, GNSS measurements, and historical InSAR datasets, EGMS becomes a strong component of an integrated monitoring strategy and offers a valuable contribution to regional landslide assessment in Piemonte.

REFERENCES

Abrahamson, N. A., & Bommer, J. J. (2005). Probability and uncertainty in seismic hazard analysis. *Earthquake spectra*, *21*(2), 603-607.

Autorità di Bacino Distrettuale del Fiume Po. (2023). Adozione della deliberazione n. 7/2023: Adozione della variante al "Piano stralcio per l'Assetto idrogeologico" (PAI) del bacino idrografico del fiume Po [Comunicato].

Bonì, R., Pilla, G., & Meisina, C. (2016). Methodology for detection and interpretation of ground motion areas with the A-DInSAR time series analysis. *Remote Sensing*, *8*(8), 686.

Bonì, R., Bordoni, M., Colombo, A., Lanteri, L., & Meisina, C. (2018). Landslide state of activity maps by combining multi-temporal A-DInSAR (LAMBDA). *Remote sensing of environment*, *217*, 172-190.

Bonì, R., Bordoni, M., Vivaldi, V., Troisi, C., Tararbra, M., Lanteri, L., ... & Meisina, C. (2020). Assessment of the Sentinel-1 based ground motion data feasibility for large scale landslide monitoring. *Landslides*, *17*(10), 2287-2299.

Bordoni, M., Vivaldi, V., Ciabatta, L., Brocca, L., & Meisina, C. (2023). Temporal prediction of shallow landslides exploiting soil saturation degree derived by ERA5-Land products. Bulletin of Engineering Geology and the Environment, 82(8), 308.

Canadian Space Agency [2024] "RADARSAT Program Overview", *Technical Report,* Canadian Space Agency, Ottawa, Canada.

Cianflone, Giuseppe, Salvatore Larosa, Lisa Beccaro, Antonio Viscomi, Cristiano Tolomei, Giovanna Chiodo, Tiziana La Pietra et al. "A revised landslide inventory of the Calabria Region (Italy)." *Journal of Maps* 21, no. 1 (2025): 2421292.

Confuorto, P., Casagli, N., Casu, F., De Luca, C., Del Soldato, M., Festa, D., ... & Raspini, F. (2023). Sentinel-1 P-SBAS data for the update of the state of activity of national landslide inventory maps. *Landslides*, *20*(5), 1083-1097.

Crosetto, M., Crippa, B., Mróz, M., Cuevas-González, M., & Shahbazi, S. (2025). Applications based on EGMS products: A review. *Remote Sensing Applications: Society and Environment*, *37*, 101452.

Cruden, D. M. (1993). Cruden, dm, varnes, dj, 1996, landslide types and processes, transportation research board, us national academy of sciences, special report, 247: 36-75. Landslides Eng. Pract, 24, 20-47.

Cuervas-Mons, J., Dominguez-Cuesta, M. J., & Jimenez-Sanchez, M. (2024). Potential and limitations of the new European ground motion service in landslides at a local scale. *Applied Sciences*, *14*(17), 7796.

Del Soldato, M., Confuorto, P., Bianchini, S., Sbarra, P., & Casagli, N. (2021). Review of works combining GNSS and InSAR in Europe. *Remote Sensing*, *13*(9), 1684.

ISPRA [2025] "Inventario dei Fenomeni Franosi in Italia (IFFI)", *Institutional Study,* Istituto Superiore per la Protezione e la Ricerca Ambientale, Italy.

ISPRA. [2025] Dissesto idrogeologico in Italia: pericolosità e indicatori di rischio – Edizione 2024 (Rapporti 415/2025).

Meisina, C. (2006). Characterisation of weathered clayey soils responsible for shallow landslides. Natural Hazards and Earth System Sciences, 6(5), 825-838.

Monserrat, O., Barra, A., Béjar-Pizarro, M., Rivera, J. S., Galve, J. P., Guardiola, C., ... & Luzi, G. (2024). ADATools: free and easy-to-use tools for semi-automatically extracting and analysing multitemporal interferometric displacement maps. *The International Archives of the Photogrammetry, Remote Sensing and Spatial Information Sciences*, *48*, 351-356.

Nikolakopoulos, K. G., Kyriou, A., Koukouvelas, I. K., Tomaras, N., & Lyros, E. (2023). UAV, GNSS, and InSAR data analyses for landslide monitoring in a mountainous village in western Greece. Remote Sensing, 15(11), 2870.

Notti, D., Herrera, G., Bianchini, S., Meisina, C., García-Davalillo, J. C., & Zucca, F. (2014). A methodology for improving landslide PSI data analysis. *International Journal of Remote Sensing*, *35*(6), 2186-2214.

Novellino, A., Cigna, F., Brahmi, M., Sowter, A., Bateson, L., & Marsh, S. (2017). Assessing the feasibility of a national InSAR ground deformation map of Great Britain with Sentinel-1. *Geosciences*, *7*(2), 19.

Pedretti, L., Bordoni, M., Vivaldi, V., Figini, S., Parnigoni, M., Grossi, A., ... & Meisina, C. (2023). InterpolatiON of InSAR Time series for the dEtection of ground deforMatiOn eVEnts (ONtheMOVE): application to slow-moving landslides. Landslides, 20(9), 1797-1813.

Regione Piemonte. (2024). Sistema Informativo Frane in Piemonte (SIFraP) [Dataset].

Solari, L., Del Soldato, M., Raspini, F., Barra, A., Bianchini, S., Confuorto, P., ... & Crosetto, M. (2020). Review of satellite interferometry for landslide detection in Italy. *Remote Sensing*, *12*(8), 1351.

Vradi, A., Sala, J., Solari, L., & Balasis-Levinsen, J. (2023). Validating the European ground motion service: an assessment of measurement point density. *The International Archives of the Photogrammetry, Remote Sensing and Spatial Information Sciences*, *48*, 247-252.